

*SURFACE PHOTOMETRY  
OF THE SHELL GALAXY  
NGC 2865*

*David Lee Wing*

*A thesis submitted in partial fulfillment of the  
requirements for the degree of  
Master of Science*

*Saint Mary's University  
Halifax, Nova Scotia  
July 1990*

© 1990 David L. Wing



## NOTICE

The quality of this microform is heavily dependent upon the quality of the original thesis submitted for microfilming. Every effort has been made to ensure the highest quality of reproduction possible.

If pages are missing, contact the university which granted the degree.

Some pages may have indistinct print especially if the original pages were typed with a poor typewriter ribbon or if the university sent us an inferior photocopy.

Reproduction in full or in part of this microform is governed by the Canadian Copyright Act, R.S.C. 1970, c. C-30, and subsequent amendments.

## AVIS

La qualité de cette microforme dépend grandement de la qualité de la thèse soumise au microfilmage. Nous avons tout fait pour assurer une qualité supérieure de reproduction.

S'il manque des pages, veuillez communiquer avec l'université qui a conféré le grade.

La qualité d'impression de certaines pages peut laisser à désirer, surtout si les pages originales ont été dactylographiées à l'aide d'un ruban usé ou si l'université nous a fait parvenir une photocopie de qualité inférieure.

La reproduction, même partielle, de cette microforme est soumise à la Loi canadienne sur le droit d'auteur, SRC 1970, c. C-30, et ses amendements subséquents.

ISBN 0-315-60441-7

## TABLE OF CONTENTS

The Examining Committee	iii
Acknowledgements	iv
Abstract	v
List of Tables	vi
List of Figures	vii

### I. Introduction

a) Galaxies with Shells	1
b) Theories of Shell Formation	2
c) Usefulness of Multicolour Surface Photometry	4
d) The Shell Galaxy NGC 2865	5
e) The Purpose of this Study	9

### II. Data Reduction

a) Observations	12
b) Detector Linearity	16
c) Preprocessing of the Galaxy Frames	19
d) Determination of the Sky Level	23
e) Isophote Fitting	24
f) Testing the Algorithms	28
g) Reduction of the Standard Star Photometry	37
h) Calibration of NGC 2865 Imagery	48
i) Plate Scale and Chip Orientation	52

### **III. Results**

a) Average Parameter Values	53
b) Departures from Perfectly Elliptical Isophotes	69
c) Comparison with Other Work	70

### **IV. Discussion**

a) Surface Brightness Profile Fits	81
b) Deviations from the Standard Brightness Profile	83
c) Isophotal Shapes and Orientations	84
d) Galaxy Colours and their Gradients	88

<b>V. Summary and Conclusions</b>	91
-----------------------------------	----

References	96
------------	----

Curriculum Vitae	100
------------------	-----

**The Examining Committee**

*David G. Turner*

---

**Dr. D.G. Turner  
Associate Professor of Astronomy  
Saint Mary's University**

*Jay A. Welch*

---

**Dr. G. A. Welch (Thesis Supervisor)  
Associate Professor of Astronomy  
Saint Mary's University**

*W. Long*

---

**Dr. W. Long  
Professor of Physics  
Saint Mary's University**

*T. Hasegawa*

---

**Dr. T. Hasegawa  
Department of Astronomy  
Saint Mary's University**

## Acknowledgements

I wish to thank the many people who made my two year visit to Halifax and Dartmouth a very pleasant and educational one. If it were not for their efforts, I am sure I would have found life here very difficult. I am glad to have had the opportunity to live in the Maritimes.

I wish to thank George Mitchell for allowing me the opportunity to study at Saint Mary's University, and also David Turner for exposing me to his unique teaching style (not to mention providing me with the motivation (?) to finish this thesis early). I also want to thank Tatsuhiko Hasegawa (Hase) for many helpful explanations and for being on the examining committee, and Mario Pedreros for obtaining the data from which this research is based. I want to thank also Dr. Lonc for being on the defense committee.

I wish to thank Gary Welch for being my thesis supervisor and for suggesting a very fascinating thesis topic. His patience and insight helped me improve this thesis many fold. Many thanks go to Cameron Reed for several enlightening explanations concerning quantum mechanics, and for many entertaining discussions over dinner. I greatly appreciate the hospitality of Randall Brooks during my stay in Halifax, and the help he gave me with the preparation of this thesis.

I must also thank all the members of the Halifax chapter of the *Royal Astronomical Society of Canada*, particularly Mary Lou Whitehorne, for their encouragement and many interesting talks. To my fellow classmates, who were able to tolerate me for so long, and who also gave me a glimpse into eastern canadian life, I also thank. I especially want to thank Lee Siow Wang (李小姐) for her help, patience, and endless encouragement during the last year.

## Abstract

### Surface Photometry of the Shell Galaxy NGC 2865

David L. Wing

July 1990

This thesis presents independently calibrated CCD surface photometry derived from 12 images of the shell galaxy NGC 2865 in the B, V, and R passbands. Short exposures were used to permit accurate sky subtraction. Mean isophotes were derived for each passband over the radial distance range 3" - 60". The isophotes are presented in the form of their best-fit (least-squares) ellipse parameters. The parameters for the best-fit de Vaucouleurs surface brightness law were determined for the mean profile in each passband and deviations of the actual surface brightness profile from the  $r^{1/4}$  law are discussed in terms of the galaxy's shell structure. From the best-fit ellipse parameters, the amplitudes of the  $\cos(4\theta)$  component of the isophotes could be measured. It was found that they do not show the boxiness often observed in a galaxy which had experienced a recent merger. On the contrary, a peak amplitude of about +1 percent ( $2\sigma$ ) over the interval of 25" - 40" suggests only the presence of a weak disk. If the disk is real it indicates that NGC 2865 is an S0, rather than an elliptical, galaxy. Also, both (B - V) and (B - R) colour gradients were measured and show that the galaxy becomes bluer with increasing radius. This may be explained in terms of a radial metallicity gradient in the sense that the metallicity decreases by about a factor of two per decade increase in distance.

## List of Tables

Table		
II-1	Observations of NGC 2865 _____	13
II-2	CCD/Telescope Parameters _____	14
II-3	Observations of the Standard Stars _____	15
II-4	CCD Linearity Correction Data _____	17
II-5	Reduction of the Standard Stars _____	38
III-1	B Surface Photometry of NGC 2865 _____	55
III-2	V Surface Photometry of NGC 2865 _____	57
III-3	R Surface Photometry of NGC 2865 _____	59
III-4	(B - V) and (B - R) Colours of NGC 2865 _____	66
V-1	Characteristics of NGC 2865 Derived in this Study _____	92

## List of Figures

Figure		
I-1	Photograph of NGC 2865 _____	6
II-1	Graph of the correction factor $k$ _____	18
II-2	Cross-section of a CCD image _____	21
II-3	Model galaxy contour containing a positive $a_4$ component _____	27
II-4	Model galaxy contour containing a negative $a_4$ component _____	29
II-5	Model galaxy surface brightness residuals _____	31
II-6	Plot of the model galaxy ellipticities and values derived by the ellipse fitting program _____	32
II-7	Plot of the model galaxy position angles and values derived by the ellipse fitting program _____	33
II-8	Plot of the normalized $a_4$ component for model galaxy _____	34
II-9	Instrumental $v$ magnitudes plotted against airmass for the standard stars _____	41
II-10	Instrumental $(b - v)$ colours plotted against airmass for the standard stars _____	42
II-11	Instrumental $(v - r)$ colours plotted against airmass for the standard stars _____	43
II-12	Plot of $V - v_0$ against $(b - v)_0$ for the standard stars _____	45
II-13	Plot of $(B - V)$ against $(b - v)_0$ for the standard stars _____	46
II-14	Plot of $(V - R)$ against $(v - r)_0$ for the standard stars _____	47
III-1	B, V, and R mean surface brightness profiles for NGC 2865 _____	61
III-2	B, V, and R mean isophotal position angle profiles for NGC 2865 _____	62
III-3	B, V, and R mean isophotal ellipticity profiles for NGC 2865 _____	63

III-4	B, V, and R mean normalized $a_4$ profiles for NGC 2865	64
III-5	(B - V) and (B - R) colour profiles for NGC 2865	68
III-6	Residuals between Jedrzejewski's surface photometry and the mean values found in this study	71
III-7	Residuals between Jedrzejewski's isophote ellipticities and the mean values found in this study	72
III-8	Residuals between Jedrzejewski's isophote position angles and the mean values found in this study	73
III-9	Residuals between Jedrzejewski's $a_4$ terms and the mean values found in this study	74
III-10	Residuals between Jedrzejewski's (B - R) colours and the mean colours found in this study	75
IV-1	Residuals between the best-fit de Vaucouleurs law and the mean B, V, and R surface brightness profiles	85

# I. INTRODUCTION

## *a) Galaxies with Shells*

Elliptical galaxies which appear to have large concentric shells of very low surface brightness in their outer halo have been known to exist for over two decades (Arp 1966; Vorontsov-Velyaminov 1959). Malin and Carter (1981, 1983) and Schweizer (1983) have noted that about 10% of normal elliptical galaxies exhibit sharp-edged, concentric features at various radii. These features have been termed "shells" by Malin and Carter and "ripples" by Schweizer. NGC 1344 is perhaps the best example of a galaxy with low surface brightness shells (Malin and Carter 1980; Carter, Allen, and Malin 1982). The shells were revealed by application of a photographic amplification technique (Malin 1978) on deep plates from the UK Schmidt telescope. Use of another technique, the unsharp masking procedure (Malin 1977), also showed the presence of inner ripples or shells that appear to be a continuation of the outer ones. The observational data on shells are scarce, however, mainly because the shells are faint, and because they are superimposed on the comparatively bright background of an elliptical galaxy.

Shells have been detected around both normal (for example NGC 3923 and NGC 1344) and abnormal (NGC 5128, NGC 7070A) elliptical galaxies, but are not seen around spiral galaxies and very rarely around S0 galaxies. They appear to occur preferentially around galaxies in the field. The shells are believed to be three-dimensional structures because of the fact that no galaxy has been found having thin, pointed shells, which would be expected if they were intrinsically planar. They do not completely surround the parent galaxy, but rather are seen as concentric arcs which are usually aligned with the major

axis of the galaxy. Shells are staggered or interleaved so that the next outermost shell is on the opposite side of the galaxy and the shell separation increases with distance. They are found over a wide range of radii that can extend to very large distances from the galaxy. Their total number has been observed to be as large as 20.

### *b) Theories of Shell Formation*

Very different explanations for the origins of these features have been proposed. A model in which shells are composed of stars that were formed in a shock wave resulting from a galactic wind was first proposed by Fabian, Nulsen, and Stewart (1980). Later, Williams and Christiansen (1985) considered the effects of a wind-driven blastwave associated with an active phase in the early history of the galaxy. In their model an expanding shell is created as the original interstellar medium of the galaxy is driven out at supersonic speeds. As the shell cools, primarily by radiation, the compression across the shock-wave front will be very large causing the shell to become thin in the direction of motion. The nonthermal continuum from the still active galaxy nucleus keeps the material in the shell at about  $10^4$  K. Once the activity in the nucleus ceases, the material cools until fragmentation occurs at a temperature of about  $10^2$  K and stars begin to form. These stars then decouple from the blast wave and will begin to follow radial bound orbits. After  $\sim 10^7$  years supernovae from the massive stars reheat the expanding blast wave, which will again cool radiatively resulting in a second episode of star formation. This allows multiple shell structures to be built up.

Quinn (1982, 1984), on the other hand, proposed that these shells are caused by the capture and eventual breakup of a low-mass disk galaxy or per-

haps a dwarf spheroidal galaxy by a much more massive elliptical galaxy. Disk systems consisting of 5000 test particles and having masses 10 to 100 times smaller than the elliptical galaxy were used in his N-body simulations. It was found that low-orbital-momentum encounters cause a wrapping of the disk system in phase space in the gravitational potential well of the elliptical galaxy. The stars end up oscillating within the elliptical galaxy's potential well, producing sharp crests at the radii of turnaround, but the galaxy which falls in must have small internal random motions in order for the shells to remain sharp. The maximum and minimum energy of the stars in the disk of the small galaxy set a limit to the maximum and minimum radius between which shells may form. In time, the number of shells should increase. However, the shells will merge into each other and become less distinct, and the shell spacings should decrease at smaller radii. This model of phase wrapping can explain quite naturally the shell properties of being interleaved, being aligned and concentric, and appearing only as arcs.

In this model, Quinn shows that the spatial distribution of the shells may be used to estimate the form of the potential well of the galaxy, and he uses the distribution of shells around NGC 3923 to infer the existence of a moderately massive dark component. Quinn also finds that the central potential is less concentrated in several galaxies than is predicted by an  $r^{1/4}$  surface brightness law under the assumption of a constant mass-to-light ratio. This result depends crucially on the difficult task of finding all the shells in the galaxy.

Thus, shells offer a tool for probing the intrinsic structure of some elliptical galaxies. The number of shells present in a galaxy can be used to date the encounter under the assumption that all the shells are the result of that encounter.

### *c) Usefulness of Multicolour Surface Photometry*

The colours of the shells, and their geometric properties such as their spacings, may be useful in deciding which model discussed above is likely to be correct. For instance, if an elliptical galaxy tidally rips apart a disk galaxy, causing the debris to form shells, then the colours of these shells should be identical and approximately the same colour as the disk galaxy that has fallen in (Quinn 1984, Hernquist and Quinn 1986, 1987a,b). On the other hand, if the blast wave models are correct then the shells might have a range of ages. Their colours should depend on the elapsed time since they were formed and also on the initial mass function of the stars in the shells. This, in turn, depends on the physical conditions present during each episode of star formation. In this case, the colours of the stars would have to be very blue since the stability of the shells would be less than one freefall time (Fabian *et al.* 1980).

Kundt and Krause (1985) investigated a variation of the galactic wind scenario in which an active galactic nucleus creates a wind that forms gas-rich filamentary shells. Stars formed in these gas shells would again have to be very blue because of the short dissipation time of the shells. This explanation seems unlikely, though, as the orbits of the stars would need to be fairly eccentric and would have to fall into thin shells. A series of explosive events, required to form the inner and outer shells, seems also unlikely as most shell galaxies do not have active galactic nuclei.

Multicolour surface photometry by Carter *et al.* (1982) and Fort *et al.* (1986) have shown that some shells are bluer than the parent galaxy. The shells appear to have the colour of a disk galaxy, thus favoring the theory that

they may have been accreted from either a low-mass disk galaxy or perhaps a dwarf spheroidal galaxy.

The location of shells may tell us something about the shape of elliptical galaxies. Dupraz and Combes (1985,1986) suggest, by statistical arguments, that when shells are short arcs bisected by the major axis, the galaxy is likely to be prolate and edge-on. If the shells are aligned with the major axis, then the galaxy is probably oblate and edge-on, and if the shells appear randomly distributed in azimuth and the elliptical galaxy is nearly round, then it is likely to be oblate and face-on.

#### *d) The Shell Galaxy NGC 2865*

NGC 2865 is located in the constellation Hydra at R.A.  $9^{\text{h}} 21^{\text{m}}24$ , Dec.  $-22^{\circ} 56'8$  (1950). Its galactic longitude and latitude are  $l = 252^{\circ}05$  and  $b = 18^{\circ}94$ . In the *Second Reference Catalogue of Bright Galaxies* (de Vaucouleurs, de Vaucouleurs, and Corwin 1976) it is listed as an E3 galaxy with a total (asymptotic)  $B_T$  magnitude of  $12^{\text{m}}35 \pm 0^{\text{m}}09$ . Its  $(B - V)_T$  and  $(U - B)_T$  colours, uncorrected for foreground extinction are  $0^{\text{m}}92 \pm 0^{\text{m}}05$  and  $0^{\text{m}}35 \pm 0^{\text{m}}06$  respectively. These colours, corrected for foreground extinction, are listed as  $0^{\text{m}}79 \pm 0^{\text{m}}05$  and  $0^{\text{m}}27 \pm 0^{\text{m}}06$  respectively. The redshift velocity, corrected for solar motion, is  $V_o = 2443 \pm 75 \text{ km s}^{-1}$  which implies a distance of 24 Mpc ( $H_o = 100 \text{ km s}^{-1} \text{ Mpc}^{-1}$ ) and a K correction of  $0^{\text{m}}04$  for the effect of redshift on the B magnitude. In the catalogue the galactic extinction is estimated to be  $0^{\text{m}}46$  (cosecant law), so that the corrected total  $B_T$  magnitude is  $11^{\text{m}}85$ .

In deep photographs (for example Malin and Carter 1983 (Figure 5), reproduced here in Figure I - 1) the galaxy has a chaotic outer structure that

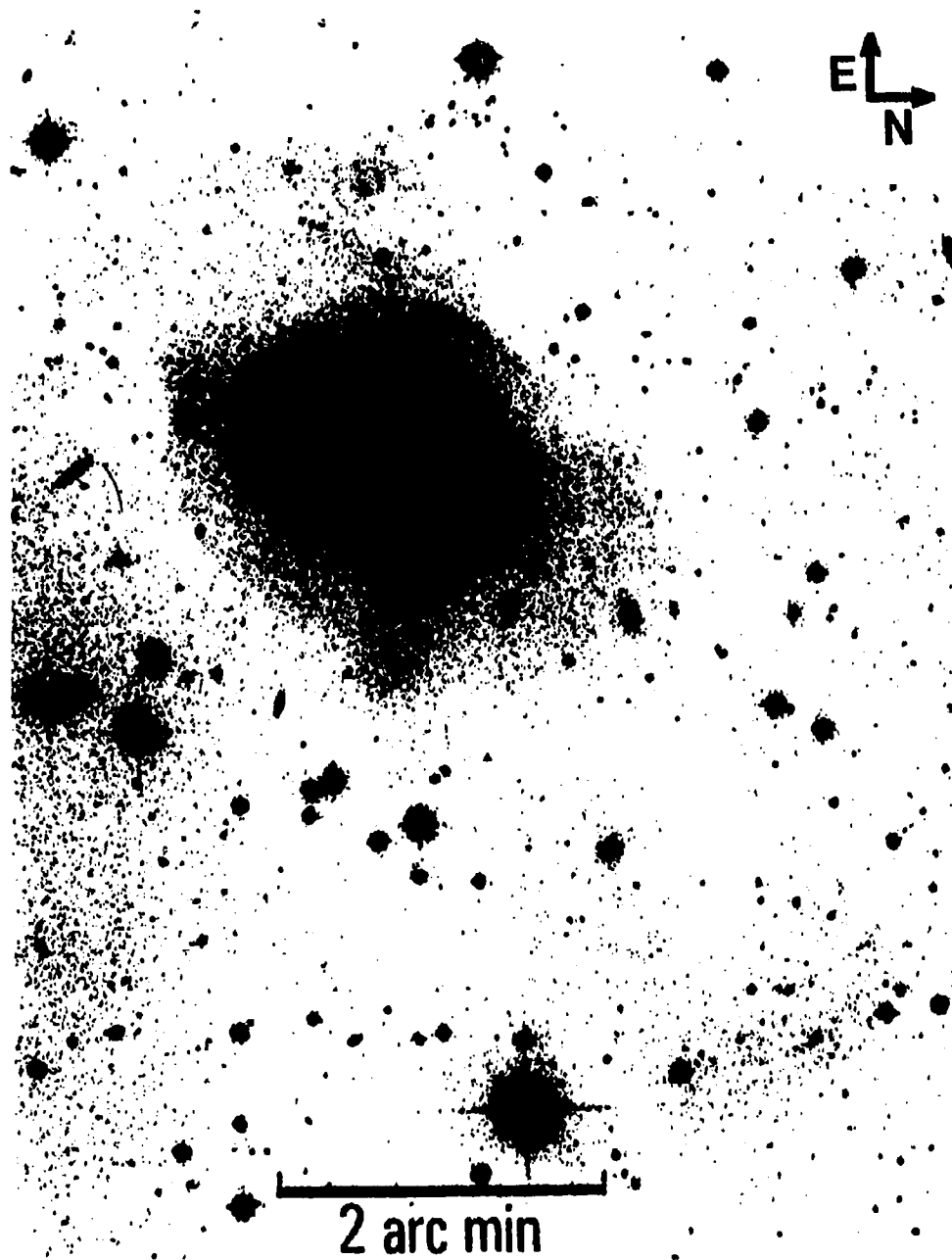


Figure I - 1. A long exposure photograph of the shell galaxy NGC 2865 (reproduced from Malin and Carter (1983), Figure 5). A bright shell can be seen immediately to the east of the galaxy whereas to the west a jet-like feature is present. Note the small diffuse loop extending  $\sim 1'$  to the south-west and a much larger and fainter loop extending  $\sim 4'$  to the north-west.

shows as many as three outer shells together with a tail (or a jet) extending outward to the west. A faint diffuse loop to the north-west can be seen together with sharp-edged shells to the east. Malin and Carter (1983) include NGC 2865 in their *Catalog of Elliptical Galaxies With Shells*, which lists 137 elliptical galaxies south of  $-17^\circ$  declination which exhibit shell or ripple features at large radii.

Evidence for a recent merger includes a somewhat blue colour for an elliptical galaxy. Sandage and Visvanathan (1978a, b) made photometric observations of a sample of 405 elliptical and S0 galaxies and provided transformations from their  $ubV$  passbands to the Johnson system. Their data, corrected for foreground extinction and K factor, indicate that  $\langle U - B \rangle = 0^m54$  for a sample of 53 field elliptical galaxies compared to their observed  $(U - B)$  of  $0^m48$  for NGC 2865. The bluer colour for NGC 2865 may be due to a recently accreted small galaxy. Although NGC 2865 is not listed in the *General Catalog of HI Observations of Galaxies* (Huchtmeier and Richter 1989), a substantial amount of neutral hydrogen [ $3.2 \times 10^9 \cdot (50/H_0)^2 \cdot M_\odot$ ] was observed in this galaxy by Carter and Wellington (1987). This material is thought to have been donated during the accretion process.

Fort *et al.* (1986) published CCD surface photometry of two of the shells and the jet-like structure in NGC 2865. Their photometry was transformed to the Johnson B, V, and R passbands, and to a passband intermediate between Johnson R and I which they call RL. They found the colours of the shells, corrected for galactic reddening, to range in  $(B - V)$  between  $0^m72 \pm 0^m11$  and  $0^m53 \pm 0^m13$  and in  $(V - R)$  from  $0^m77 \pm 0^m08$  to  $0^m84 \pm 0^m09$ . The colour of the tail, also corrected for galactic reddening, was found to have  $(B - V) =$

$0^m75 \pm 0^m09$  and  $(V - R) = 0^m80 \pm 0^m07$ . This indicates that the shells appear to be slightly bluer than the main body of the galaxy which has  $(B - V) = 0^m79$  (Second Reference Catalogue). Their  $(B - V)$  colours are similar to the colours of Sb or Sc galaxies which typically lie in the range of  $0^m5$  to  $0^m8$  (de Vaucouleurs 1977). They estimate the luminosity of the shell system to be in the range of  $2.4 - 4.8 \times 10^9 \cdot L_{\odot}$ , which contributes between 11% and 22% of the mass of NGC 2865 under the assumption of a mass-to-light ratio of 5 for the shells. As for the jet-like feature, they found it to have a colour similar to but slightly redder than the shells, although the errors were large.

Fort *et al.* also attempted to calculate the dynamical age of the shell system using the model of Quinn (1984). Based on the number of separate shell features they could identify and on the gravitational potential of the parent galaxy, they estimated an age on the order of  $10^9$  yrs under the assumption that the shell system was formed as the result of a radial collision.

Jedrzejewski (1987) obtained CCD surface photometry of NGC 2865 in the B and R passbands. Synthesized aperture photometry measurements for the well-studied galaxies in his programme were used in conjunction with published aperture photometry to calculate the extinction and zero-point constants needed to normalize the observations to the photometric system. Based on the best-fit relation, all observations were then placed on a uniform scale. He fit the isophotes of the galaxy to ellipses out to a distance of 100 arcsecs from the galaxy centre and presented his results in the form of the best fit least-squares ellipse parameters as a function of radius. Although Jedrzejewski does not discuss his surface photometry results for NGC 2865, his work does appear to be the only published photometry for the galaxy to date.

Wilkinson *et al.* (1987) surveyed a subset of the Malin and Carter (1983) catalogue of shell galaxies and attempted to observe NGC 2865 with the VLA. At a wavelength of 20 cm and resolution of about 15" they failed to detect the galaxy above a limiting flux of 0.36 mJy ( $3\sigma$ ).

Thronson *et al.* (1987) used the *Infrared Astronomical Satellite* (IRAS) database to survey early-type (elliptical and S0) galaxies that exhibit shell structure. By combining satellite scans, they estimated the following IR fluxes for NGC 2865:  $F_{12\mu\text{m}} \leq 75$  mJy,  $F_{25\mu\text{m}} \leq 50$  mJy,  $F_{60\mu\text{m}} = 250 \pm 25$  mJy,  $F_{100\mu\text{m}} = 450 \pm 130$  mJy. In terms of its IR fluxes, NGC 2865 appears to be similar to normal S0 type galaxies rather than to an elliptical galaxy.

#### *e) Purpose of this Study*

This study set out to obtain accurate CCD surface photometry of NGC 2865 in the B, V, and R passbands in an effort to improve upon the available data. The photometry reported here should be a significant improvement over Jedrzejewski's results because it has been independently calibrated using aperture photometry on standard stars observed during the same night as the galaxy. Also, to ensure that the sky intensity on each image could be reliably determined, short-integration images of the galaxy were used.

Mean isophotes were derived for each passband over the radial distance range of  $\sim 3 - 60$  arcsecs which are presented in the form of their best-fit (least-squares) ellipse parameters. This ellipse-fitting technique was chosen not only because it increases the surface brightness signal-to-noise ratio but also because it produces a set of ellipse parameters (contour intensity, ellipticity, and position angle) as a function of radius. Ellipticity changes and position-

angle twisting seen in the isophotes of elliptical galaxies can be explained as the result of the projection of triaxial figures, though it can not be used to determine the triaxial shape of elliptical galaxies unambiguously.

Although Fort *et al.* (1986) looked at the colours and structure of only two of the shells and the tail of NGC 2865, they did not examine the galaxy's overall surface brightness. Accurate surface photometry is needed to determine the characteristics of the underlying galaxy. If the presence of shells is the result of unusual activity occurring within the parent galaxy, then that activity may be reflected in its surface brightness distribution.

The parameters for the best-fit de Vaucouleurs surface brightness law were determined for the mean profile of NGC 2865 in each passband. Deviations of this mean surface brightness profile from the standard  $r^{1/4}$  law are discussed in terms of the galaxy's shell structure.

Nieto and Bender (1989) suggest that boxy isophotes in elliptical galaxies may be the result of a merging process. If the shells of NGC 2865 are the result of a merger with another galaxy, then one might expect to see a deviation of the isophotes from being almost perfectly elliptical to having a slightly boxy shape. On the other hand, Kormendy and Djorgovski (1989) point out that accreted material captured by a parent galaxy should continue to trickle in long after the merger process is complete. In this case, pointed isophotes would form after the merger if enough material is accreted to form an observable disk.

The departure of the isophotes from perfect ellipticity is usually expressed in terms of the coefficients of a Fourier decomposition. In such a decomposition, the amplitude of the  $\cos(4\theta)$  component is most sensitive to devia-

tions from pure ellipticity due to boxy or pointed isophotes. Therefore, the amplitude of the  $\cos(4\theta)$  component of the isophotes has been measured to determine whether or not the isophotes are boxy or pointed.

## II. DATA REDUCTION

### *a) Observations*

A total of twelve images of NGC 2865 were obtained over a two hour period on the night of January 24/25, 1987 on the 1 metre Swope Telescope at Cerro Las Campanas, Chile, by Dr. Mario Pedreros. The observations were taken during a photometric night, with the FWHM of stars typically being 1".9 (B), 1".6 (V), and 1".4 (R). A journal of observations of the galaxy is given in Table II - 1.

The RCA 53612 CCD chip used to obtain the data consisted of 320 x 512 pixels each 30 x 30  $\mu\text{m}$  in size. The scale was  $\sim 0.87''$  pixel<sup>-1</sup> so that the projected size of the field on the sky was approximately 4'.6 x 7'.4. Four frames in each of the B and V passbands and in the Gunn r passband were taken with integration times ranging from 60 sec to 210 sec. Each frame also includes an overscanned region of 32 columns which was used to determine the DC offset of the electronics. As mentioned before, short integrations were used to ensure that the sky intensity in each frame could be reliably determined, and also so that the galaxy nucleus would not saturate the CCD. The most important parameters describing the CCD/telescope combination are listed in Table II - 2.

To measure extinction and calibrate the surface photometry of the galaxy in the Johnson B and V passbands and in the Cousins R passband, six stars from Landolt's (1973, 1983) standard star lists were also observed three times throughout the same night. A journal of observations of the standard stars is given in Table II - 3.

Table II - 1: Observations of NGC 2865

Frame no.	Exposure Time (sec)	Filter <sup>1</sup>	Sidereal Time (mid-exposure)	Airmass (X)
LCO588	60	B	9:28	1.006
LCO589	210	B	9:40	1.008
LCO590	180	B	9:44	1.010
LCO591	180	B	9:49	1.011
LCO592	60	r	9:55	1.014
LCO593	100	r	9:58	1.016
LCO594	100	r	10:00	1.017
LCO595	60	r	10:03	1.018
LCO596	60	V	10:06	1.020
LCO597	90	V	10:08	1.022
LCO598	90	V	10:10	1.024
LCO599	60	V	10:12	1.025

<sup>1</sup> Johnson B and V, and Gunn r filters

Table II - 2: CCD/Telescope parameters

---

---

CCD chip: RCA 53612

Format: 320 x 512 pixels

Pixel size: 30 $\mu$ m x 30  $\mu$ m

Pixel size at Cassegrain focus of Swope: 0.862" x 0.862"

Frame size at Cassegrain focus of Swope: 4.6' x 7.4'

Readout noise:  $\sim 30 e^-$

System gain: 0.28 ADU/ $e^-$  = 3.6  $e^-$  /ADU

Dark current (average):  $\sim 0.04 e^- \text{ pixel}^{-1} \text{ s}^{-1}$  = 136  $e^- \text{ pixel}^{-1} \text{ hr}^{-1}$

Linearity: ratio of observed pixel count to true pixel count varies by a factor of  $\sim 4 - 5$  over the true pixel count range of  $\sim 10^2 - 10^4$

Cosmetic details: 1 row spanning the length of the frame having significantly low sensitivity - row no. 188, with rows 187 and 189 also being slightly affected.

---

Table II - 3: Observations of the Standard Stars

Frame #	Field # <sup>1</sup>	Exposure Time <sup>2</sup> (sec)	Filter <sup>3</sup>	Sidereal Time (mid-exposure)	Airmass (X)
RIB495	95	7	r	4:41	1.161
VIB498	95	7	V	4:48	1.164
BIC501	95	20	B	4:55	1.167
RIB509	99	5	r	4:59	1.566
VIC512	99	8	V	5:08	1.534
BIC515	99	14	B	5:15	1.510
VIB537	95	5	V	6:08	1.553
RIB540	95	5	r	6:17	1.585
BIB543	95	15	B	6:24	1.614
VIB548	99	5	V	7:23	1.156
RIB551	99	5	r	7:30	1.153
BIB554	99	10	B	7:39	1.149
VIB565	95	5	V	8:19	2.703
RIB568	95	5	r	8:27	2.835
BIB571	95	20	B	8:36	2.993
VIC600	99	3	V	10:49	1.463
RIB603	99	5	r	10:59	1.496
BIB606	99	8	B	11:09	1.531

<sup>1</sup> Field #95 contains the standard stars #301 and #302.

<sup>1</sup> Field #99 contains the standard stars #267, #366, #367, and #362.

<sup>2</sup> Average of 3 frames.

<sup>3</sup> Johnson B and V, and Gunn r filters

### *b) Detector Linearity*

Today, most standard surface photometry of galaxies is done using CCDs. This is due primarily to a high quantum efficiency reaching a peak of ~80%, a wide dynamic range of over  $10^3$ , a linearity that is accurate typically to about  $10^{-3}$ , and a spectral response covering 4000Å to 11,000Å (Okamura 1988). Many older CCD chips, however, suffer from a low-level charge transfer inefficiency which manifests itself as a non-linear response in chip sensitivity at low light levels.

The RCA-CCD used at Cerro Las Campanas during these observations was found to have a significant non-linear response in sensitivity almost throughout its entire range. Since this non-uniformity was not restricted to low light levels, the problem was not believed to be associated with a low-level charge transfer inefficiency in the chip. Therefore, exposing the chip to a short pre-flash before each image was taken would not have removed this effect. Therefore, to remove this effect an empirical correction factor  $k$ , was defined by

$$k = \frac{\log_{10}(\text{Observed pixel count})}{\log_{10}(\text{True pixel count})} .$$

Data necessary to construct a correction curve were supplied by Dr. Ian Thompson of the Carnegie Institution of Washington and are given in Table II - 4. The calibration is based on tests conducted with the CCD over several months, and appears quite stable over that time period.

A plot of the correction factor  $k$  against the observed pixel count is shown in Figure II - 1, where the correction factor is normalized to be unity for a

Table II - 4: CCD Linearity Correction Data

Log(Observed count)	Correction Factor (k)
1.43	0.775
1.73	0.794
2.09	0.849
2.20	0.872
2.41	0.914
2.53	0.936
2.71	0.961
2.73	0.963
2.85	0.980
2.85	0.983
3.03	1.000
3.04	1.000
3.05	1.000
3.16	1.012
3.16	1.015
3.20	1.015
3.26	1.020
3.34	1.026
3.36	1.025
3.47	1.036
3.65	1.044
3.78	1.051
3.96	1.062
4.08	1.062
4.26	1.065
4.38	1.059
4.43	1.062
4.45	1.060

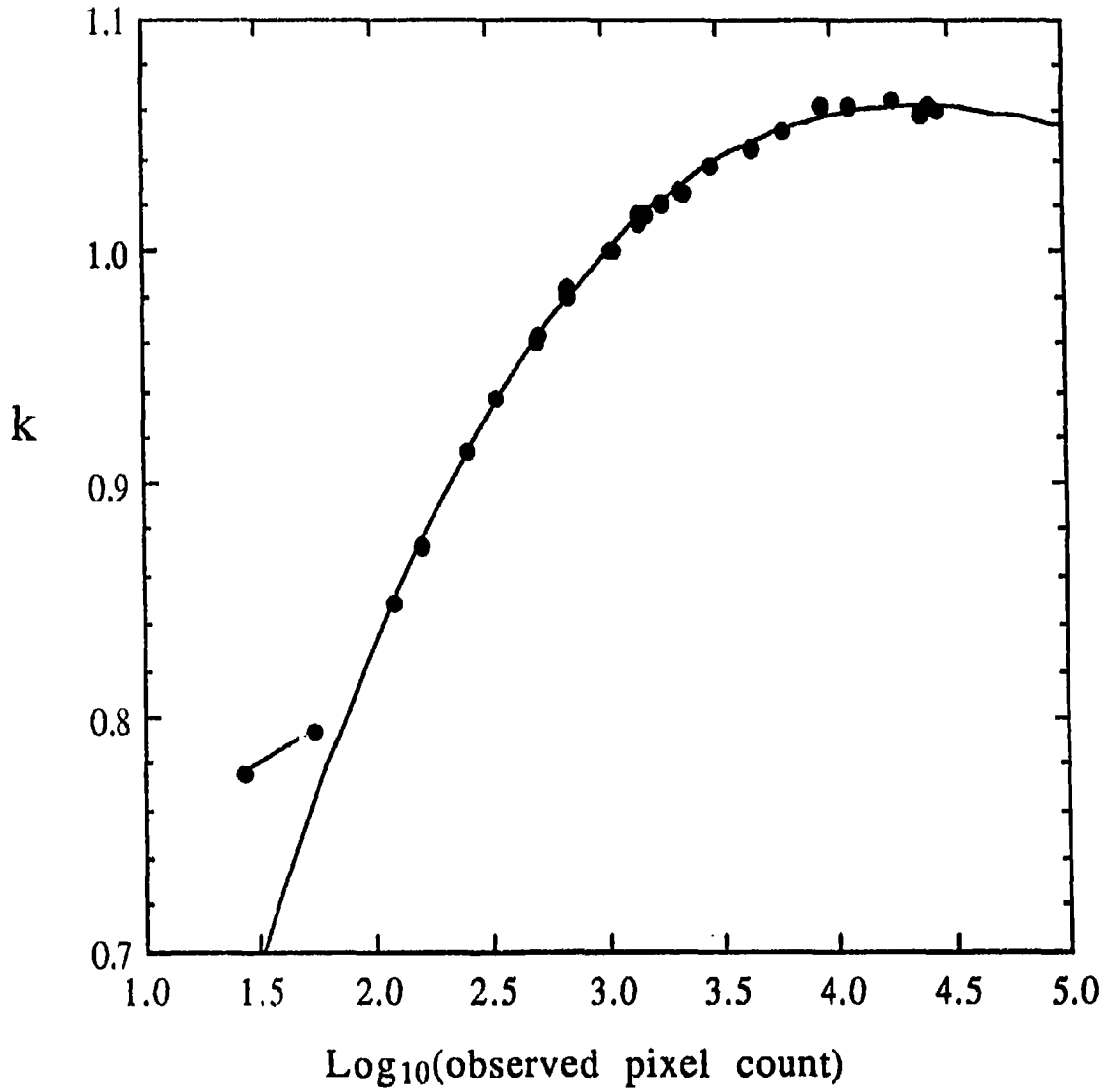


Figure II - 1. Plot of the correction factor  $k$  as a function of the logarithm of the observed pixel count. A straight line was fit to the two data points having the lowest count values while a third order polynomial was fit to the remaining points.

pixel count of 1000. A third-order polynomial was fit by the method of least-squares to all the data points except the first two, which correspond to raw pixel counts of less than 100. These first two points were fitted separately with a straight line. Thus, the equation for the true pixel counts can be expressed as

$$\text{True pixel count} = (\text{Observed pixel count})^{1/k},$$

where the coefficients of the best-fit polynomials are

$$k = 2.12 \times 10^{-2} + 6.02 \times 10^{-1} N - 1.12 \times 10^{-1} N^2 + 6.57 \times 10^{-3} N^3, \quad \text{for } N \geq 1.90, \text{ and}$$

$$k = 6.84 \times 10^{-1} + 6.33 \times 10^{-2} N, \quad \text{for } N < 1.90,$$

where  $N = \log_{10}(\text{observed pixel count})$ .

All the data frames taken with this CCD chip, as well as the mean dark and flat-field frames, were corrected for this non-linearity effect before any pre-processing was begun. The correction was applied by dividing the logarithm of each raw pixel count by the correction factor derived from the curve fit and then computing the antilogarithm of the quotient.

### *c) Preprocessing of the Galaxy Frames*

The procedure for preprocessing CCD images often varies among CCD camera systems and even among investigators. Okamura (1988) gives a good review of the factors that affect the performance of CCD detectors, and outlines the basic CCD preprocessing techniques used to convert a “raw” data frame into an appropriate form for analysis. The procedures outlined in his

paper were essentially followed in the preprocessing of all the galaxy frames used here.

First, a DC offset value equal to the mean of 7500 pixels in the over-scanned region of each image was subtracted from that image. This offset component is indicated in Figure II - 2 which is a diagram showing a cross-section of a typical raw CCD image. The horizontal axis in the diagram represents the column number of the chip and the vertical axis shows the average ADU counts across five columns and 11 rows (through the middle of the galaxy) in the raw image.

A bias pattern was then removed in each frame by subtracting, pixel by pixel, a high signal-to-noise average of eight zero-exposure frames (the mean bias frame). The structure found in this mean bias frame was generally on the order of  $\pm 0.2$  analog-to-digital units (ADU) superimposed on a mean value of about 0.5 ADU. However, the ADU row averages beginning from row 1 to about row 10 jumped from a high of about 200 down to a low of about -5. Beyond row 10, the row averages approached the 0.5 ADU level. The pixel to pixel variations in the mean bias frame were on the order of 1.6 ADU rms.

Next, a mean dark frame was created by adding two individual dark frames amounting to a total of 900 seconds. This frame was then scaled to each galaxy frame according to its exposure time, and subtracted from the data frame. Upon examination, the mean dark frame showed a bright region in the lower left corner of the frame (coordinates 0,0). The ADU values in this corner reached values as high as about 100, but fell to a more typical value of about 0.9 in the center of the frame. At the opposite corner the mean pixel

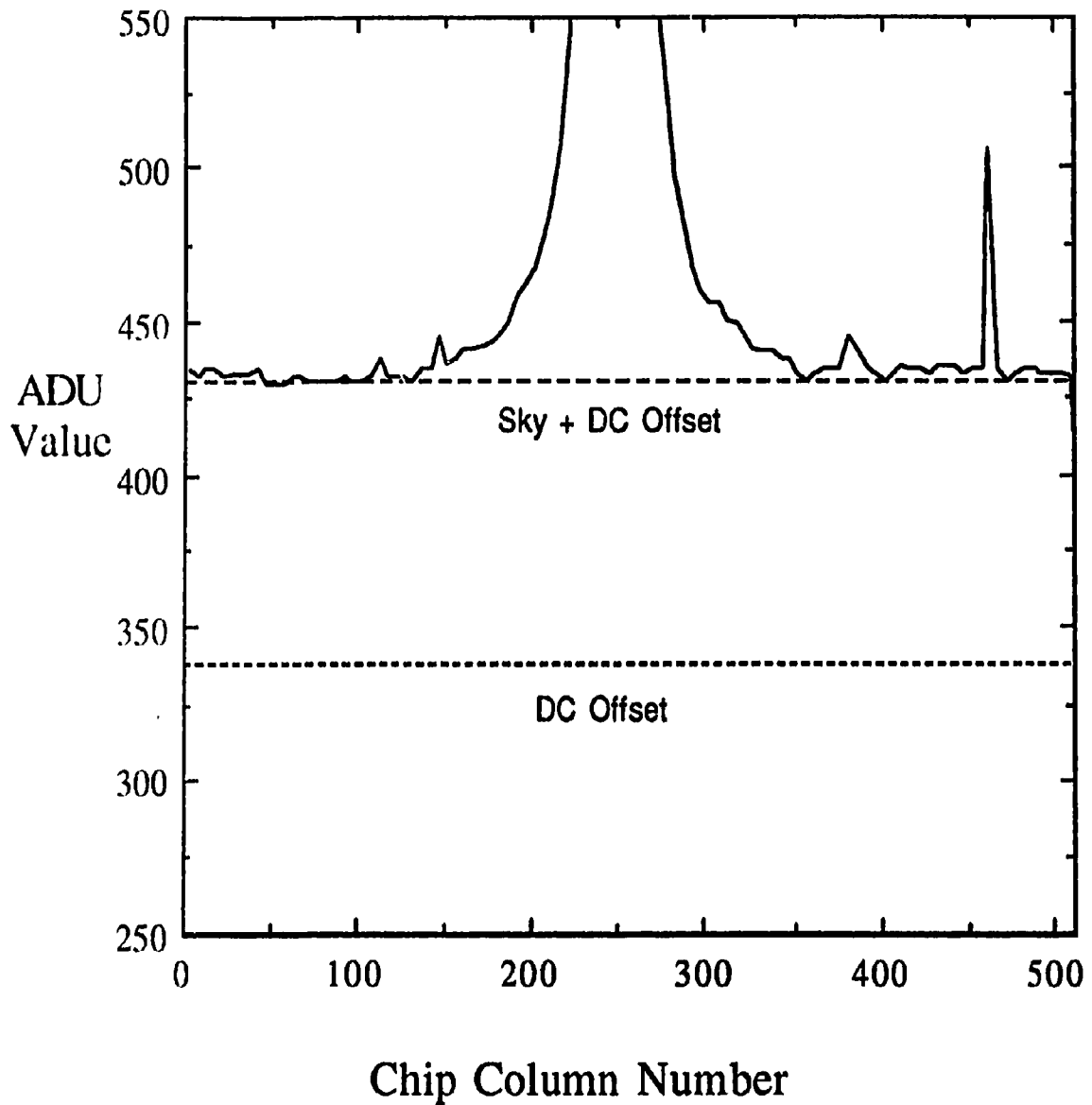


Figure II - 2. Cross-section of a typical, raw CCD image. The horizontal axis represents the column number (x axis) of the chip and the vertical axis shows the ADU counts averaged over five columns and 11 rows. The large peak in intensity centred around column #250 is due to the galaxy, whereas the smaller peak centred around column #450 is due to a star.

value fell to about 0.2 ADU. The pixel to pixel variations in the mean dark frame were on the order of 9 - 10 ADU rms.

Spatial nonuniformities in chip sensitivity, determined from the flat field images, were found to be about 14 percent across the frame (V passband) and were removed by flat-fielding each data frame. Inspection of the flat-field images revealed that some of these nonuniformities were clearly not associated with chip sensitivity. Dust within the telescope, located along the optical path, cast doughnut-shaped shadows onto the chip. To remove these nonuniformities in chip sensitivity and illumination, a mean flat-field frame image was created in each passband from an average of three exposures of an evenly illuminated white patch located on the inside wall of the observatory dome. After both the galaxy and flat-field frames were corrected for offset, bias, and dark counts, the galaxy frame was divided, pixel by pixel, by the flat-field frame. The pixel to pixel variation in the mean visual flat field image was on the order of 0.8 percent.

A small amount of fringing could be seen on the galaxy frames and was due primarily to the presence of strong night-sky emission lines. The fringing appeared strongest in the R passband with progressively weaker amounts in the V and B passband images and appeared only on one side of the frames. Since no fringing was visible near the galaxy, it was decided not to correct for this effect.

Cosmic ray events, which appear as single- or double-pixel events of very high charge, and some cosmetic defects in the chip, were also removed from the flattened data images. This was accomplished using a program that searched the data frame for pixel values that were more than about three stan-

dard deviations from the mean pixel value within a  $7 \times 7$  square region surrounding the pixel being examined. Such pixel values are replaced with the median pixel value of the surrounding  $7 \times 7$  pixel region.

Finally, cosmetic defects too large to be removed in the previous step (longer than three or four pixels in length) were dealt with. Small areas in the chip contain "hot" pixels which trap charge and consequently produce a large signal regardless of the level of illumination. Likewise, small areas of "cold" pixels are not efficient at trapping charge and therefore produce a low signal regardless of the level of illumination. These defects were removed interactively by replacing their value with the median value of a surrounding region chosen by the operator. More severe problems in the chip appeared as two to three adjacent rows that showed systematically higher/lower pixel values. These defective rows often extended about a quarter to a half of the length of the field, with the longest one extending the entire field length and passing near the galaxy centre. Linear interpolation was performed across the width of these shorter features to reduce their effects, but the defective row running through the galaxy was not altered. It was thought that the large intensity gradient in the inner region of the galaxy would have been adversely affected by using a linear interpolation.

#### *d) Determination of Sky Level*

In the images, the galaxy is oriented with its long axis only about  $20^\circ$  -  $30^\circ$  away from the long dimension of the CCD frame, so that the corners appear clear of any contribution from the galaxy's halo. To confirm this, the intensities along the borders of each frame were examined to determine at what radial distance the outskirts of the galaxy merged into the background sky

level. This was accomplished by displaying the mean ADU values of a small number of rows (or columns) as a function of their x (or y) coordinate for each frame. The contribution from the galaxy was considered negligible when it could no longer be distinguished from the typical background intensity. In some cases the outskirts of the galaxy extended to the frame border closest to the galaxy, though in no frame did the galaxy light extend to the frame borders furthest away from the galaxy. In all cases the frame corners were free of galaxy light.

In each frame small regions free of background stars were selected in the frame corners, and elsewhere along the border if the galaxy contamination was negligible. Typically, six regions were chosen comprising about 9 000 to 11 000 pixels. The pixel values contained in these regions were used to model the background sky intensity by fitting them to a 2-dimensional first-order polynomial (plane) by the method of least-squares. This sky level (see Figure II - 2) was then subtracted from the data frame to produce the final galaxy image frame.

#### *e) Isophote Fitting*

To analyse the intensity in a galaxy image along only the major and minor axes is very wasteful of the information contained in the rest of the image. A more useful method of presenting the surface photometry data is to fit the derived isophotal contours with a set of concentric ellipses. These are often found to be satisfactory approximations to the isophotes of most elliptical galaxies, as well as to the bulges of most disk galaxies (Carter 1987, Jedrzejewski 1987).

For each of the twelve galaxy frames, a set of ellipses was constructed according to the following procedure. A set of target intensity values was chosen that was expected to span the brightness range of the galaxy in a particular frame, at approximately equal radial increments. To accomplish this, the galaxy brightness profile was approximated using a  $r^{1/4}$  law, from which the brightness levels at equal increments of about two pixels were found.

Based on this set of target intensities, a contour image was formed by “turning on” or “turning off” each pixel in the preprocessed image. A simple criterion for turning an individual pixel on or off was chosen and was based on the values found in a  $3 \times 3$  square pixel cell surrounding the pixel under consideration. If at least two contiguous pixels in this cell had values greater than the target intensity value, and at least two contiguous pixels had values less than or equal to the target intensity value, then the central pixel was “turned on”. If either one of these conditions was not met then the central pixel was “turned off”. The position of a pixel that had been “turned on” was used later in the ellipse-fitting procedure. A pixel that had been “turned off” was given zero weight in this procedure, while a pixel that had been “turned on” was given a weight of unity.

Once the contour frame was made, it was cleaned to remove pixels “turned on” because of background stars or row defects not removed in the preprocessing steps. This was accomplished using an interactive program that displayed each of the individual contour images within a set. The operator can examine each contour, one by one, and “turn off” pixels not associated with the galaxy surface brightness distribution.

Once all the contour images within a set had been cleaned, ellipses could then be fitted to each one. There are five parameters needed to describe completely the position, size, shape, and orientation of a particular ellipse. These are the x and y coordinates of the centre, the ellipticity, position angle and semi-major axis length. The simplex method (Jacoby *et al.* 1972), with a least-squares goodness of fit criterion, was chosen as the computational method to determine these parameters. In addition, each ellipse has a mean isophotal intensity associated with it, which was determined by sampling the intensity values of the galaxy around the best-fit ellipse at one degree intervals. The four pixels surrounding each sampling point were used to interpolate the intensity values at that sampling point along the ellipse.

This type of fit provides not only the brightness profile of the galaxy but also isophote ellipticities and position angles as functions of the semimajor axis, which are important in the study of its structure.

The departures of the isophotes from perfect ellipticity are usually characterized in terms of the Fourier amplitudes  $a_i$  and  $b_i$  in the series

$$\Delta r(\theta) = \sum_{i=0}^{\infty} [a_i \cos(i\theta) + b_i \sin(i\theta)] ,$$

where  $\Delta r(\theta)$  is the radial displacement of the actual isophote from the best-fit ellipse at position angle  $\theta$ . Of most interest is the  $a_4$  amplitude. If positive, it indicates "pointed" isophotes, suggesting the presence of a highly inclined disk oriented along the long axis of the galaxy. Figure II - 3 shows the outline of a perfectly elliptical contour (solid dots) together with the same contour having a +10%  $a_4$  component (open circles). The contour with the  $a_4$  com-

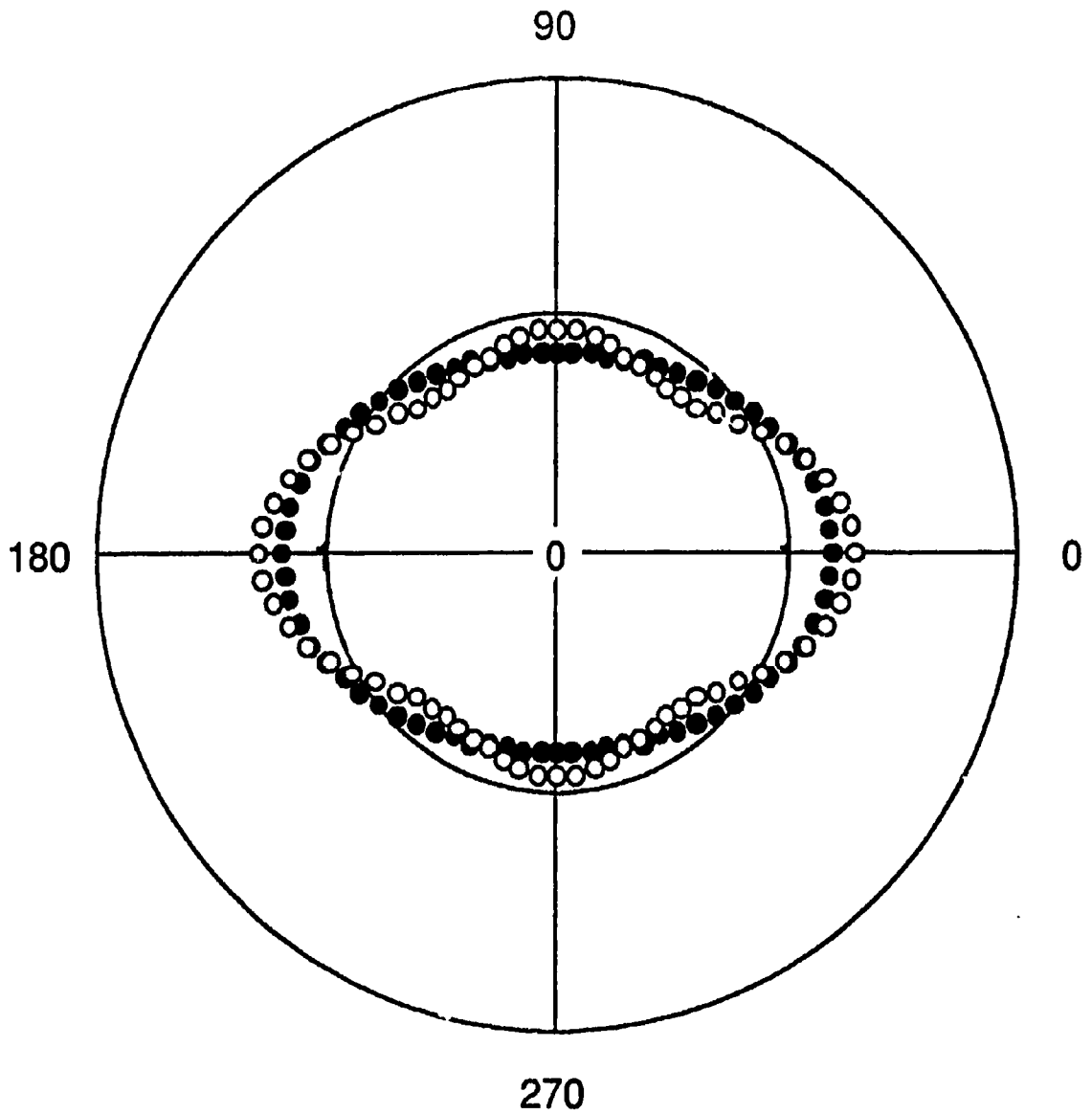


Figure II - 3. A diagram of a “pointy” contour. The solid dots represent a contour having unit area and the same ellipticity as an E3 galaxy. The open circles show the same contour having a 10 percent positive  $a_4$  component added to it.

ponent extends to a greater distance along the major axis, but at  $45^\circ$  from the major axis it extends a smaller distance, than the perfectly elliptical contour. This gives the contour its “pointy” appearance. If, on the other hand, the  $a_4$  component is negative, it indicates that the galaxy has “boxy” isophotes. Figure II - 4 shows the outline of a perfectly elliptical contour (solid dots) together with the same contour having a -10%  $a_4$  component (open circles). The contour with the  $a_4$  component extends to a smaller distance along the major axis, but at  $45^\circ$  from the major axis it extends a greater distance, than the perfectly elliptical contour. This gives the contour its “boxy” appearance.

The value of  $a_4$  for each contour was computed using the following procedure. First, the distances from the center of the best-fit ellipse to each of the “turned on” pixels were averaged into  $5^\circ$  bins. Then, within each bin, the average radius of the best-fit ellipse was determined and subtracted from the average pixel distance. This yielded a total of 72 mean residuals around the contour. By dividing the mean residual in each bin by the average radius of the best-fit ellipse within that bin, the residuals were transformed to values describing the deviations from an ellipse with a unit semi-major axis. Finally, these 72 normalized residuals were fitted by least-squares to the trigonometric series described above using the coefficients  $a_3$ ,  $b_3$ ,  $a_4$ , and  $b_4$ .

#### *f) Testing the Algorithms*

It is very difficult to determine the accuracy to which the intensity, ellipticity, position angle, and  $\cos(4\theta)$  coefficients of the isophotes can be measured. The reliability of such measurements may be strongly influenced by such things as the seeing during the observations, the changing signal-to-noise ratio that occurs from the center of the galaxy to its outer regions, and the type of

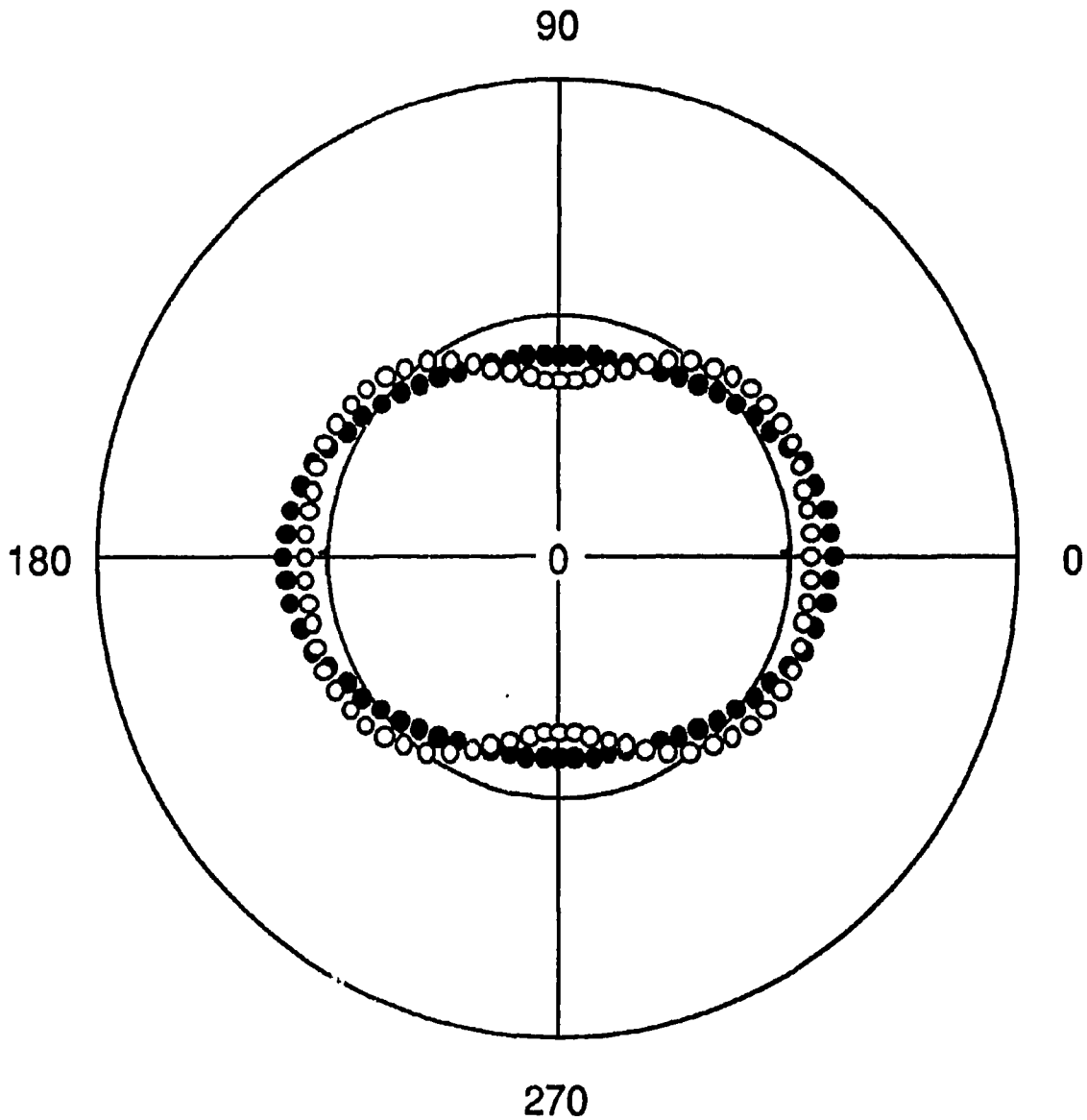


Figure II - 4. A diagram of a “boxy” contour. The solid dots represent a contour having unit area and the same ellipticity as an E3 galaxy. The open circles show the same contour having a 10 percent negative  $a_4$  component added to it.

algorithm used to find the best-fit ellipse. The first two effects cannot easily be controlled by the observer. The algorithm to find the the ellipse parameters, however, can be tested to determine its ability to extract the “correct” ellipse.

In order to estimate the reliability of the ellipse fitting program, a model galaxy was constructed with known geometrical and photometric parameters. The model was based on parameter values that had already been derived from a typical galaxy frame - LCO591. This was done so that it would resemble NGC 2865 as closely as possible. The observed surface brightness of the galaxy was fitted to a  $r^{1/4}$  law using a least squares criterion. From the best-fit  $r^{1/4}$  law the model intensities could be computed at any semi-major axis distance. The estimates of isophotal ellipticity and position angle as a function of semi-major axis were obtained by modeling the observed values with a series of low order polynomials that were spliced together . A look-up table was formed containing values for each parameter at one-pixel increments. This was used to construct an ideal artificial galaxy frame, to which a noise level having  $\sigma \approx 8.8$  was added. This was typical of the level present in the pre-processed observational frames.

The normal procedure for creating the contour images and determining the ellipse parameters was followed on this model galaxy frame. Figure II - 5 shows the radial dependence of the residuals between the model galaxy intensity distribution in the look-up table and the intensity values found by the program, and Figures II - 6 and 7 show the radial dependence of the derived model ellipticities and position angles together with the values found by the ellipse fitting algorithm. Figure II - 8 is a radial plot of the normalized  $a_4$

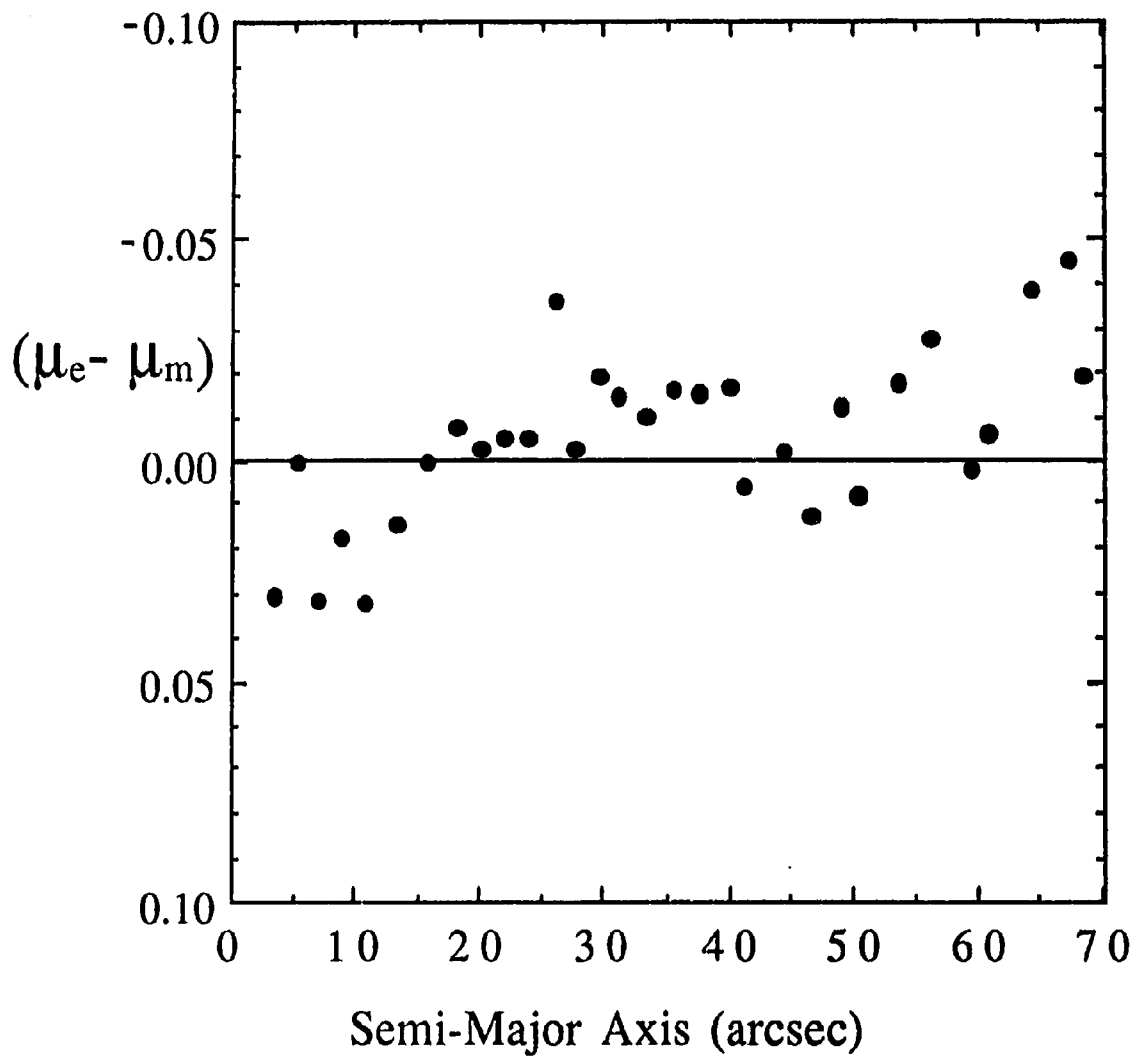


Figure II - 5. Surface brightness residuals computed by subtracting the actual model surface brightness  $\mu_m$  (in magnitudes per arcsec<sup>2</sup>) from  $\mu_e$ , the values estimated by the computer program.

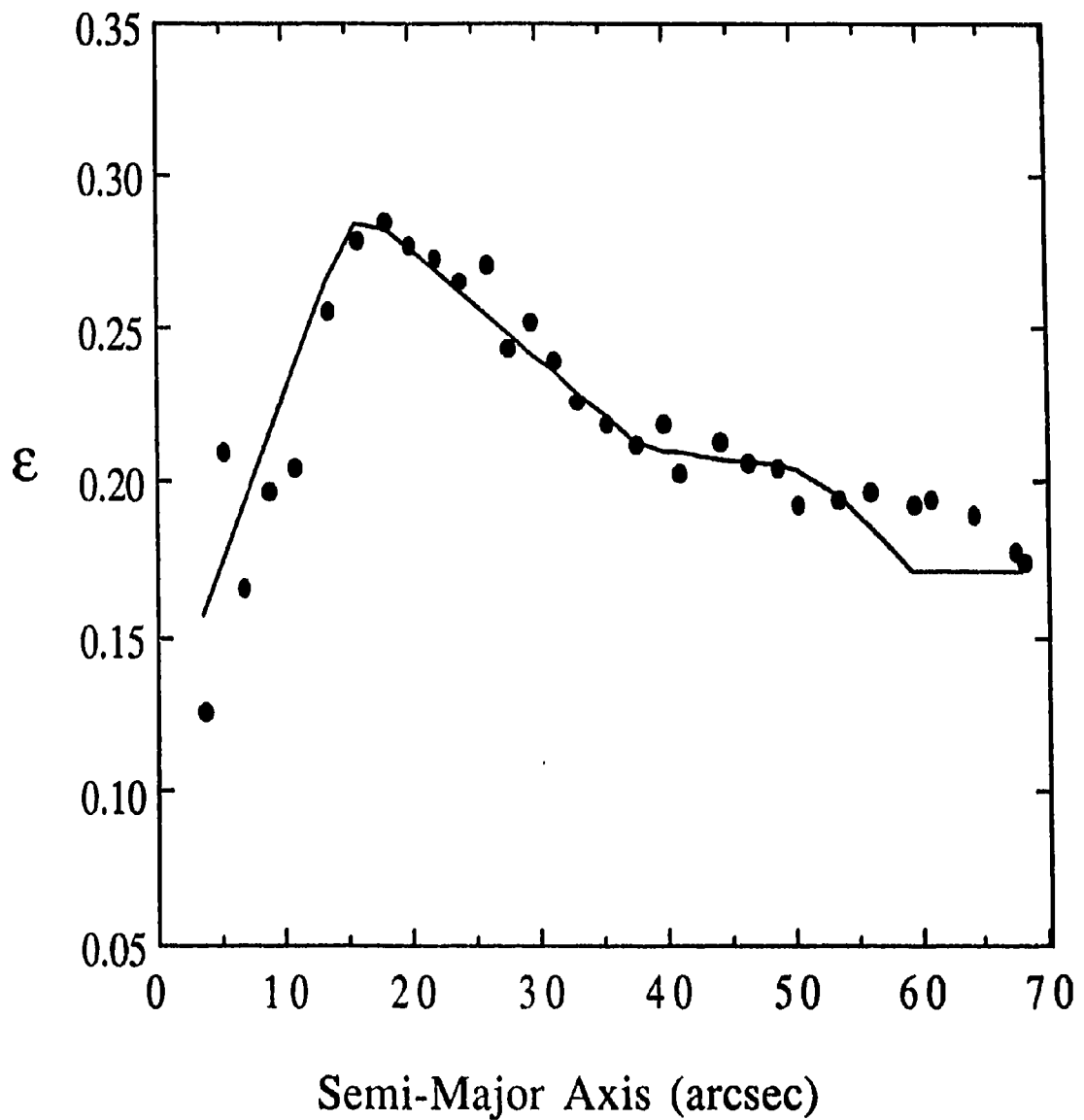


Figure II - 6. Comparison of the isophotal ellipticity  $\epsilon$  estimated by the ellipse fitting program (solid dots) with the actual model values (line).

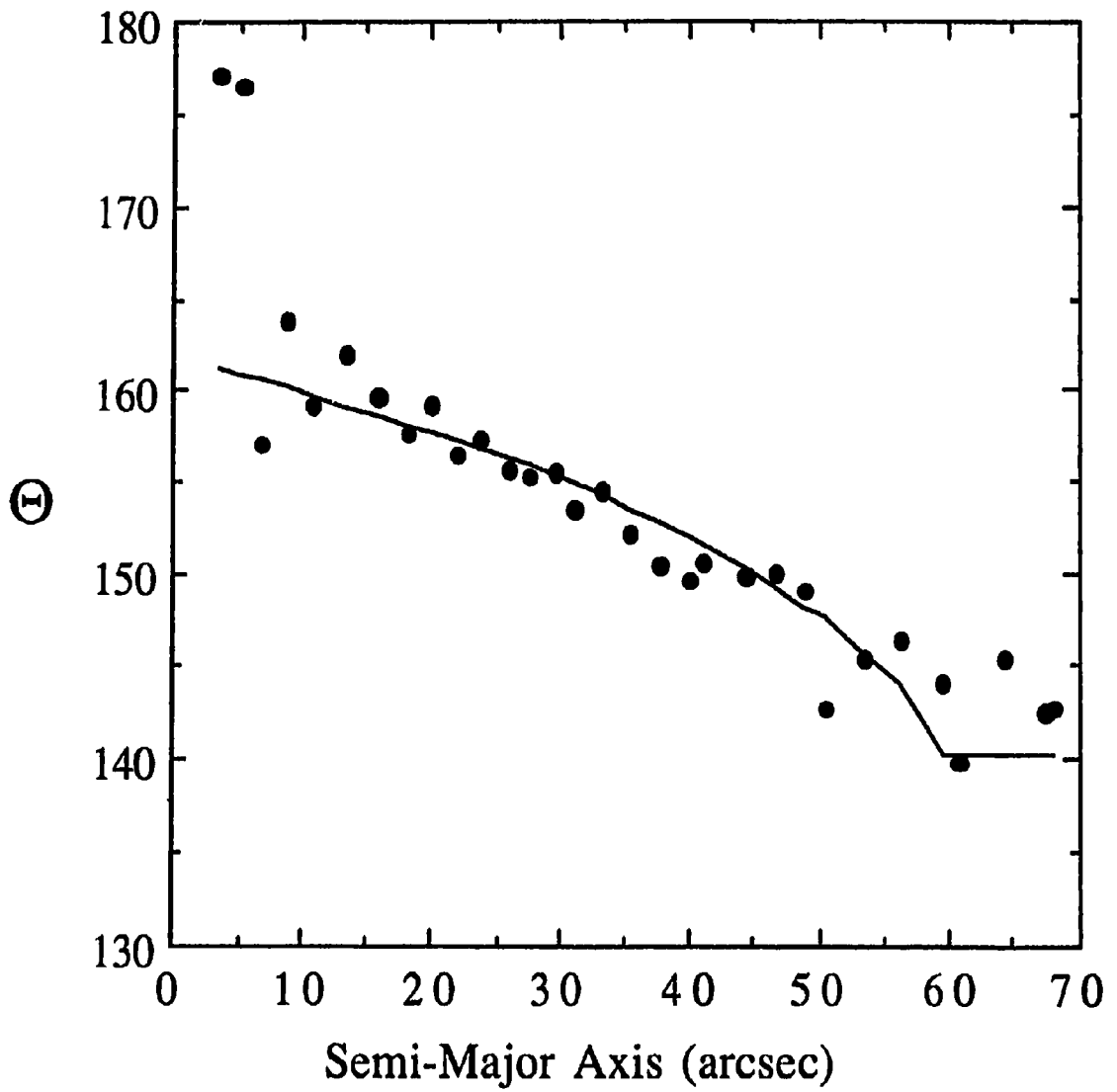


Figure II - 7. Comparison of the isophotal position angles  $\Theta$  found by the ellipse fitting program (solid dots) with the actual model position angles (line).

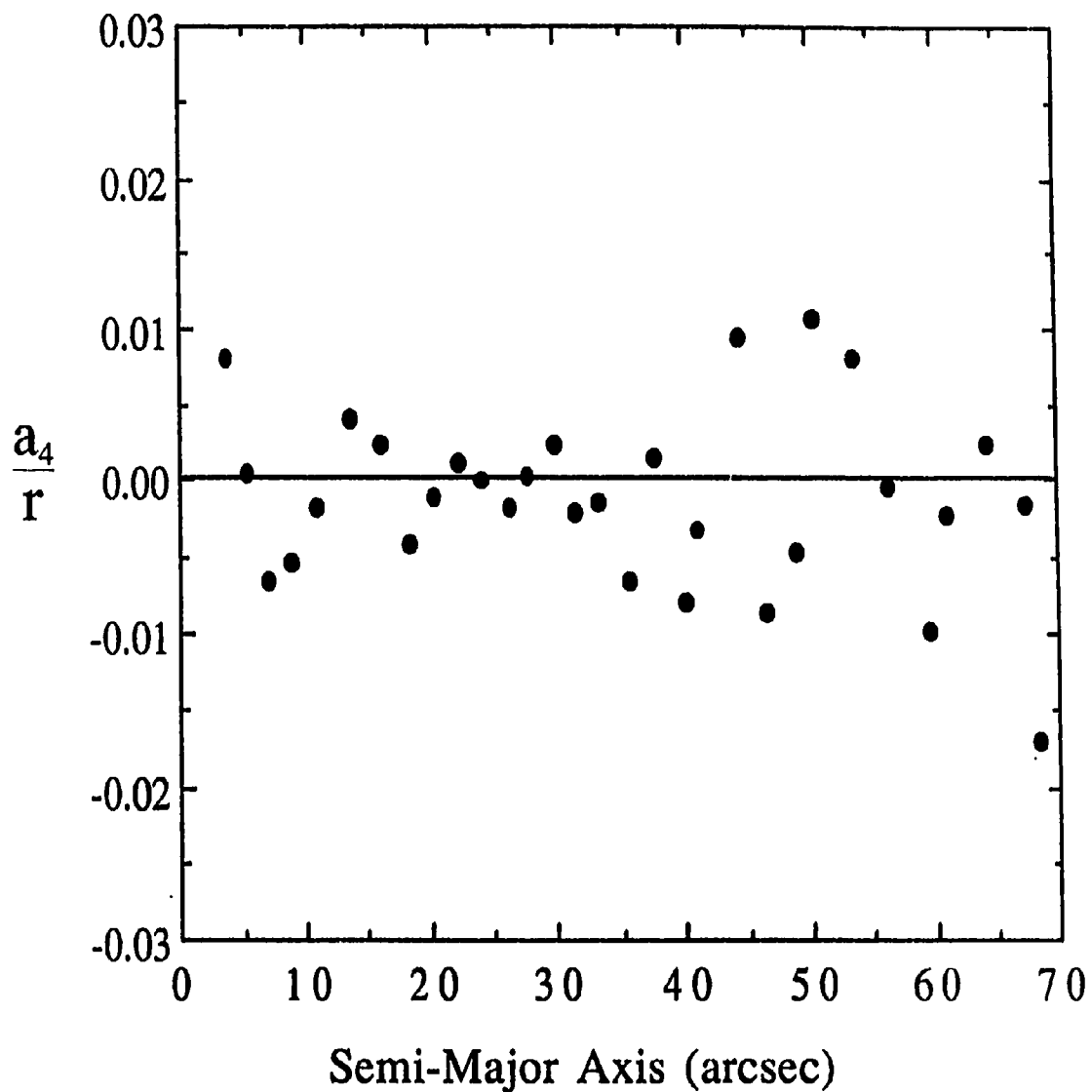


Figure II - 8. Plot of the normalized  $a_4$  residuals ( $a_4/r$ ) found for the model galaxy using the ellipse fitting program. Since the isophotes in the model galaxy were formed using perfect ellipses, the expected residuals should be zero.

components found by the computer program. Since the model galaxy was constructed using perfectly elliptical isophotes, the expected residuals in the  $a_4$  components should be zero.

The graphs show that the agreement is good between the actual and estimated ellipse parameter values. The rms residuals from the expected results for the model galaxy give a typical uncertainty for intensity measurements of  $\pm 0^m.02$ . For position angle, the values derived by the computer program are very close to the model values except very near the galaxy centre. The derived position angles of the two isophotes with the smallest semi-major axes ( $r < 6''$ ) both deviated by about  $15^\circ$  from the model values. The large discrepancy in position angle found for these two isophotes is most likely tied to their small ellipticities ( $\epsilon < 0.18$ ). The combination of small isophotes, composed of only a small number of pixels and having an almost circular shape, makes the position angle ill-defined. An rms residual of  $\pm 2.2$  for semi-major axes greater than  $6''$  applies when these two data points are omitted. This is comparable to the rms mean difference of  $\pm 2^\circ$  quoted in the studies by both Franx *et al.* (1989) and Jedrzejewski (1987). Naturally, it follows that larger uncertainties would be expected if NGC 2865 were more circular in overall appearance.

The bright asymmetric spike extending from the galaxy towards the northwest appeared to alter the shape of the isophotes significantly. Therefore, to assess the effect of the spike on the derived ellipse parameters, one contour set taken from a typical image frame had a section of its isophotal contours removed in the regions where the spike appeared to influence its shape. The ellipse fitting program was run on this contour set and it was found that the

ellipse parameters were not altered beyond the level of scatter already seen between the values found in the four frames of each passband.

There are two factors which may tend to cause the ellipticity of the isophotes to be underestimated near the galaxy core. At small radii, because of the low number of sample pixels in the image, the ellipticity is underestimated if the galaxy is flattened (Jedrzejewski 1987). In addition, seeing will also tend to cause the isophotes to become more circular at small radii, again resulting in the ellipticity being underestimated. In this study the smallest isophote that was fitted was twice as large as the estimated seeing; therefore, the underestimation of the ellipticity for small semi-axes due to seeing was not considered to be significant. The inner isophotes were treated no differently in the reductions. The rms residual for ellipticity was found to be  $\pm 0.015$ . Finally, the rms deviation of the normalized  $a_4$  term (Figure II - 8) about the expected value of zero was  $\pm 0.6$  percent, which is comparable to the rms residual of  $\pm 0.5$  percent quoted by Jedrzejewski (1987) for faint galaxies.

An improvement over the testing procedure done for this study would be to create several more model galaxies spanning a greater range of isophotal ellipse parameters. In this way more accurate estimates of where the ellipse fitting algorithm begins to have difficulty in determining each ellipse parameter, as a function of the others, can be made. Also, by creating model galaxies having isophotes of different ellipticities in their central regions and convolving them with an assumed seeing function, the effects of both seeing and sampling rate can be properly assessed. With this information, predictions of how well the algorithms will perform as functions of seeing and CCD/telescope combination can be made. Unfortunately, adequate time and resources were not available to carry out this additional testing.

The use of a model galaxy is limited to testing such things as the accuracy of the ellipse fitting procedure and the accuracy of the mean contour intensity value. A model galaxy, however, is not affected by the uncertainties in the pre-processing steps that lead up to a typical galaxy frame. For example, the tests done here do not give an indication of how well the background sky was subtracted which is very important in the faint outer regions of the galaxy. Also, the ellipse fitting algorithm does not have to contend with large asymmetries in surface brightness which are evident in the outer regions of NGC 2865 and which may greatly affect the derived ellipse parameter values.

*g) Reduction of Standard Star Photometry*

To calibrate the derived galaxy photometry, six stars from two fields (fields 95 and 99) of Landolt's (1973, 1983) standard star lists were observed three to four times during the same night that NGC 2865 was observed. To help simplify the photometric reduction procedure, each set of B, V, and r frames of a particular field was taken one after the other so that they would have similar air masses. The frames were pre-processed in the same way as the galaxy frames and aperture photometry was done using DAOPHOT (Stetson 1987). The stellar magnitude was found by plotting a curve of growth for each star and estimating its asymptotic magnitude by eye. At this point all instrumental magnitudes were scaled to a common exposure time arbitrarily chosen to be one second. The results are given in Table II - 5.

Only two of the standard stars, #301 and #302, were found to have a range of air masses large enough to estimate the extinction reliably. These two stars generated preliminary extinction coefficients of:

Table II - 5: Reduction of the Standard Stars

Star #301		B - V = 1.29				
V = 11.21		V - R = 0.692				
Air mass	$v_x$	$(b - v)_x$	$(v - r)_x$	$v_o$	$(b - v)_o$	$(v - r)_o$
1.164	14.420	0.851	0.914	14.214	0.782	-0.016
1.585	14.510	0.870	0.977	14.230	0.775	-0.003
2.835	14.725	0.949	1.131	14.224	0.780	-0.012

Star #302		B - V = 0.84			
V = 11.68					
Air mass	$v_x$	$(b - v)_x$	$(v - r)_x$	$v_o$	$(b - v)_o$
1.164	14.916	0.483	-0.142	14.710	0.388
1.585	14.984	0.517	-0.118	14.704	0.388
2.835	15.204	0.619	-0.066	14.703	0.388

Star #362		B - V = 1.14			
V = 10.80					
Air mass	$v_x$	$(b - v)_x$	$(v - r)_x$	$v_o$	$(b - v)_o$
1.153	14.013	0.720	-0.041	13.809	0.642
1.496	14.061	0.731	-0.017	13.797	0.629
1.534	14.076	0.729	-0.027	13.805	0.624

Table II - 5 continued.

Star #366		B - V = 0.16				
V = 11.50						
Air mass	$v_x$	$(b - v)_x$	$(v - r)_x$	$v_o$	$(b - v)_o$	
1.153	14.676	-0.046	-0.560	14.472	-0.176	
1.496	14.747	-0.014	-0.528	14.483	-0.183	
1.534	14.779	-0.008	-0.512	14.508	-0.181	

Star #367		B - V = 1.00				
V = 11.14		V - R = 0.531				
Air mass	$v_x$	$(b - v)_x$	$(v - r)_x$	$v_o$	$(b - v)_o$	$(v - r)_o$
1.153	14.332	0.654	-0.078	14.128	0.572	-0.138
1.496	14.393	0.642	-0.083	14.129	0.532	-0.157
1.534	14.409	0.644	-0.072	14.138	0.531	-0.149

Star #267		B - V = 0.58			
V = 12.30					
Air mass	$v_x$	$(b - v)_x$	$(v - r)_x$	$v_o$	$(b - v)_o$
1.153	15.676	0.171	-0.176	15.472	0.056
1.496	15.547	0.368	-0.265	15.283	0.233
1.534	15.570	0.357	-0.267	15.299	0.219

$$k_v = 0^m1767 \pm 0^m0034,$$

$$k_b = 0^m2471 \pm 0^m0074,$$

$$k_r = 0^m1199 \pm 0^m0086.$$

Because the three frames in each set must be taken sequentially at the telescope, the air mass of each frame was slightly different. With the above preliminary extinction coefficients, the instrumental magnitudes for individual frames were transformed to a common air mass, namely that for the red passband. Since these corrections for air mass were small (none were more than 0<sup>m</sup>.008), no colour terms were used in the transformations at this stage.

Once the observations in each set were reduced to a common air mass, the following procedure for photoelectric reductions was employed. First, using the data for stars #301 and #302, the first and second order terms in the extinction equations were determined. The results were:

$$k'_v = 0^m177 \pm 0.003,$$

$$k''_v = 0 \text{ (adopted),}$$

$$k'_{bv} = 0^m103 \pm 0^m010,$$

$$k''_{bv} = -0.056 \pm 0.010,$$

$$k'_{vr} = 0^m070 \pm 0^m02,$$

$$k''_{vr} = 0.133 \pm 0.07.$$

Figures II - 9, 10, and 11 show the variations in the instrumental v magnitude and in the instrumental (b - v) and (v - r) colours measured for stars #301 and #302 as a function of air mass. The resulting equations to convert the instrumental magnitudes to zero air mass become:

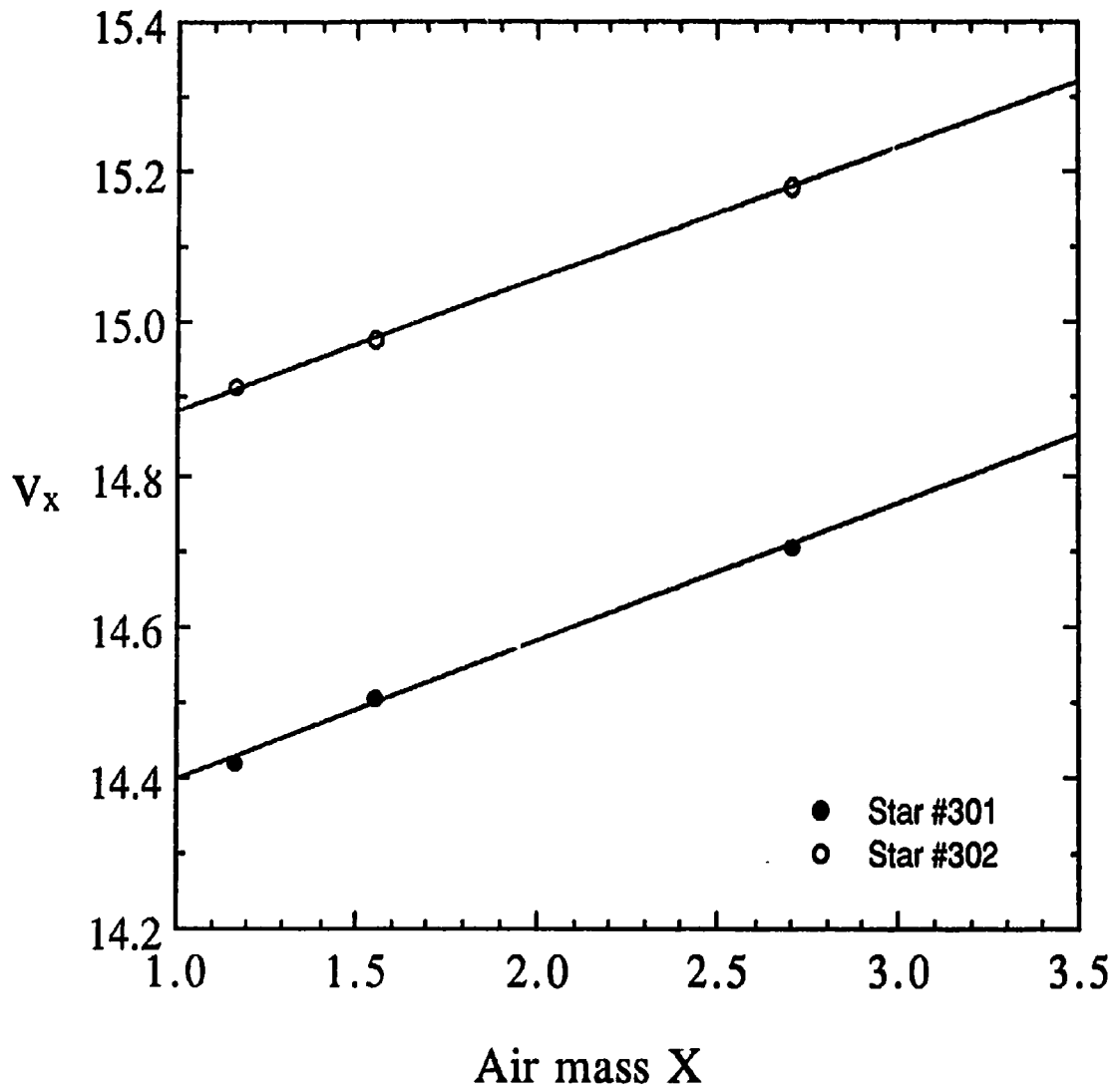


Figure II - 9. The instrumental magnitudes of stars #301 and #302, from Landolt's lists of standard stars, as a function of air mass. The lines are the least-squares fits to the data.

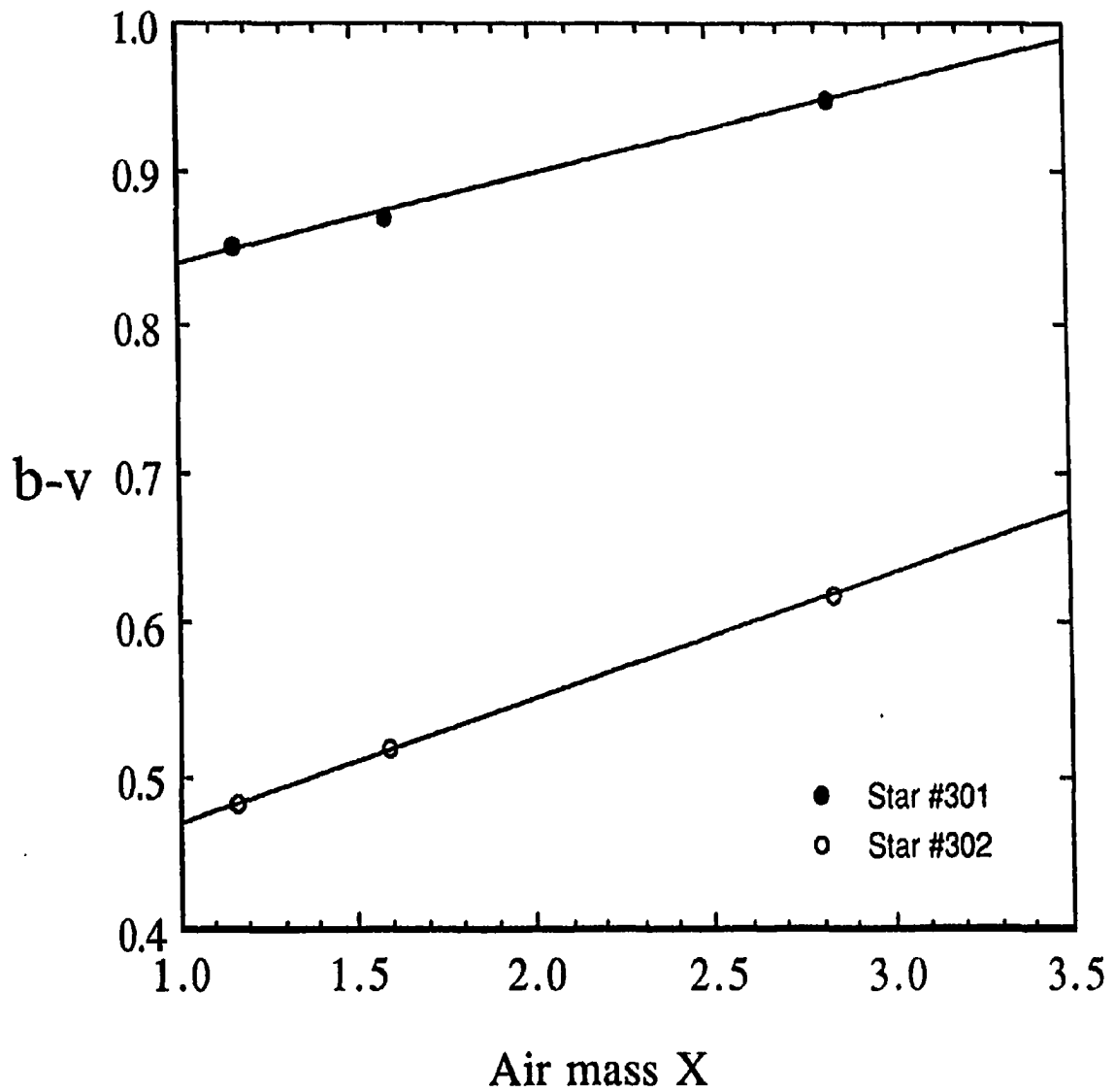


Figure II - 10. The instrumental (b - v) colours of stars #301 and #302, from Landolt's lists of standard stars, as a function of air mass. The lines are the least-squares fits to the data.

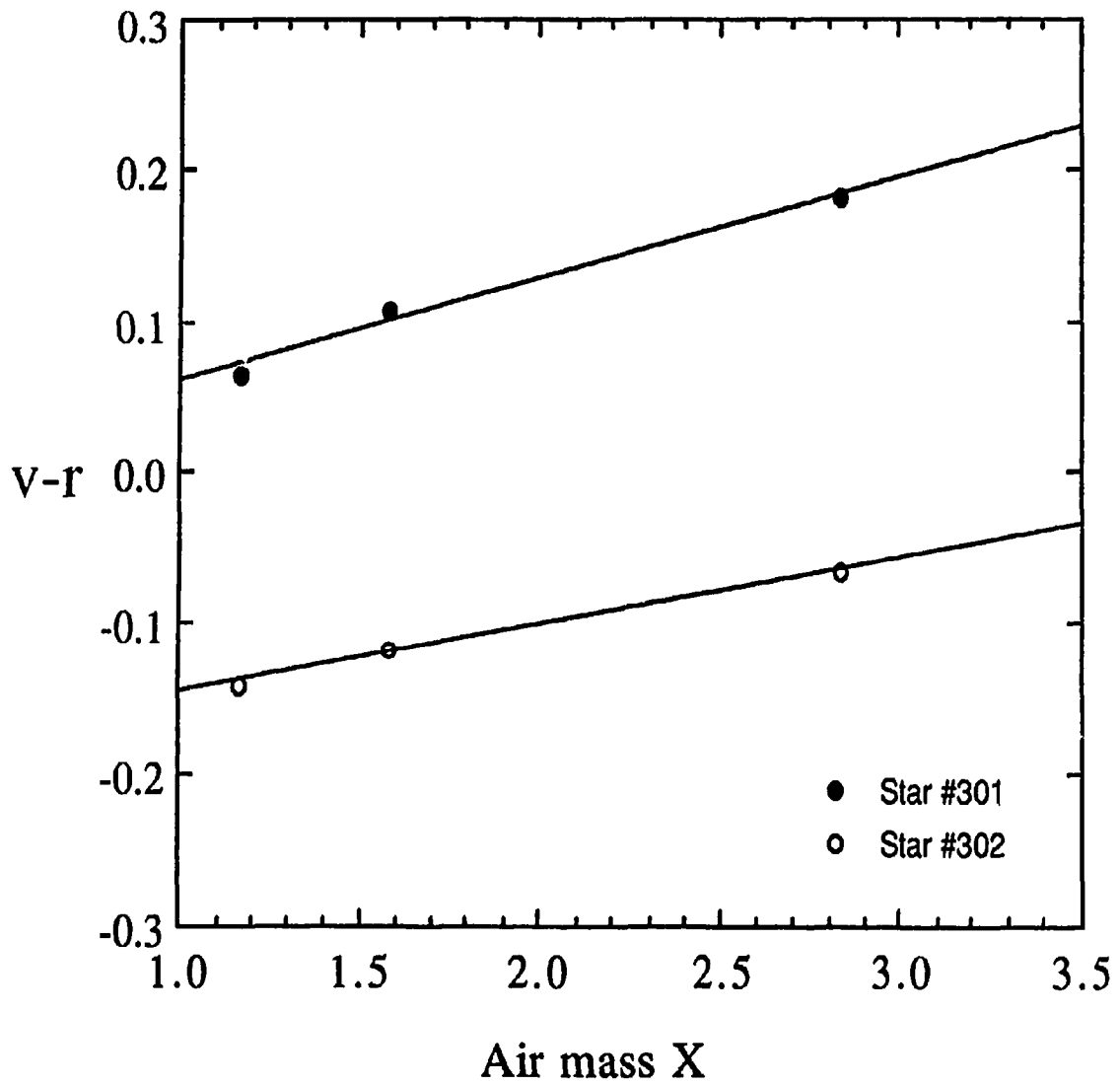


Figure II - 11. The instrumental (v - r) colours of stars #301 and #302, from Landolt's lists of standard stars, as a function of air mass. The lines are the least-squares fits to the data.

$$v_o = v_x - (0.177 X) ,$$

$$(b - v)_o = \frac{(b - v)_x - (0.103 X)}{(1 - 0.056 X)} ,$$

$$(v - r)_o = \frac{(v - r)_x - (0.070 X)}{(1 + 0.133 X)} ,$$

where quantities with a subscripted x are the observed values and the subscript o denotes extra-atmospheric quantities (zero air mass). Figures II - 12, 13, and 14 show the magnitudes and colours of all the standard stars plotted against their extinction-corrected instrumental colours.

Finally, the transformation equations to obtain Johnson B and V magnitudes, and Cousins R magnitudes, are:

$$V - v_o = -2^m.996 (\pm 0^m.007) - 0.019 (\pm 0.012) (b - v)_o,$$

$$\text{rms difference} = 0^m.015,$$

$$B - V = 0^m.375 (\pm 0^m.008) + 1.182 (\pm 0.014) (b - v)_o,$$

$$\text{rms difference} = 0^m.017,$$

$$V - R = 0^m.703 (\pm 0^m.006) + 1.16 (\pm 0.06) (v - r)_o,$$

$$\text{rms difference} = 0^m.008.$$

In the graphs for the transformation relations of  $V - v_o$  and  $B - V$ , one observation of star 267 in field 99 consistently deviated from the trend of the other observations. The reduction process for that one observation was rechecked but revealed no error in the analysis. Therefore, star 267 was omitted in determining the transformation equation coefficients. Of the remaining five

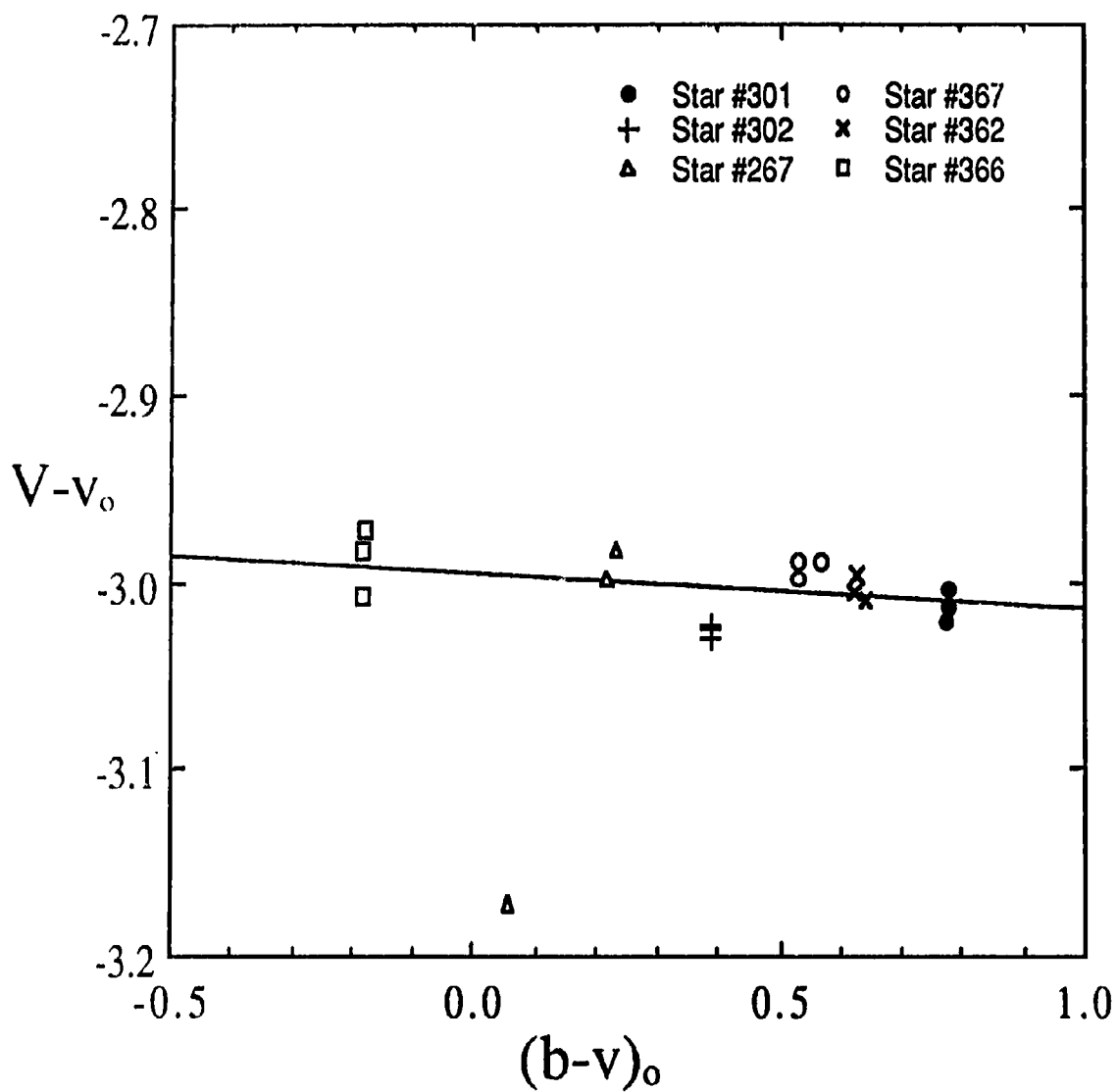


Figure II - 12. Plot of  $V - v_0$  against the extinction-corrected instrumental  $(b - v)_0$  colour for the 5 standard stars. The straight line represents the least-squares fit to the data.

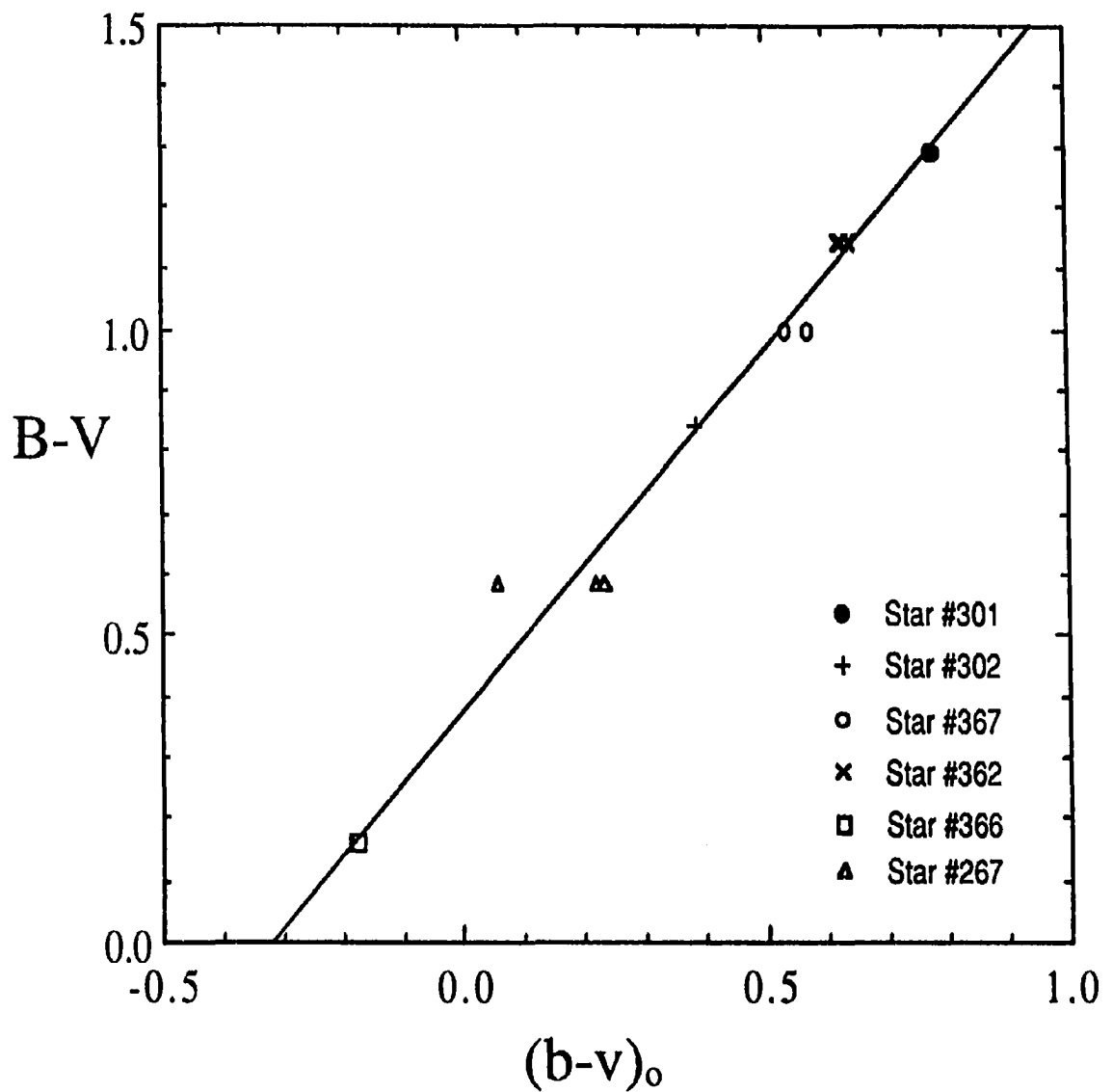


Figure II - 13. Plot of  $(B - V)$  against the extinction-corrected instrumental  $(b - v)_o$  colour for the 5 standard stars. The line represents the least-squares fit to the data.

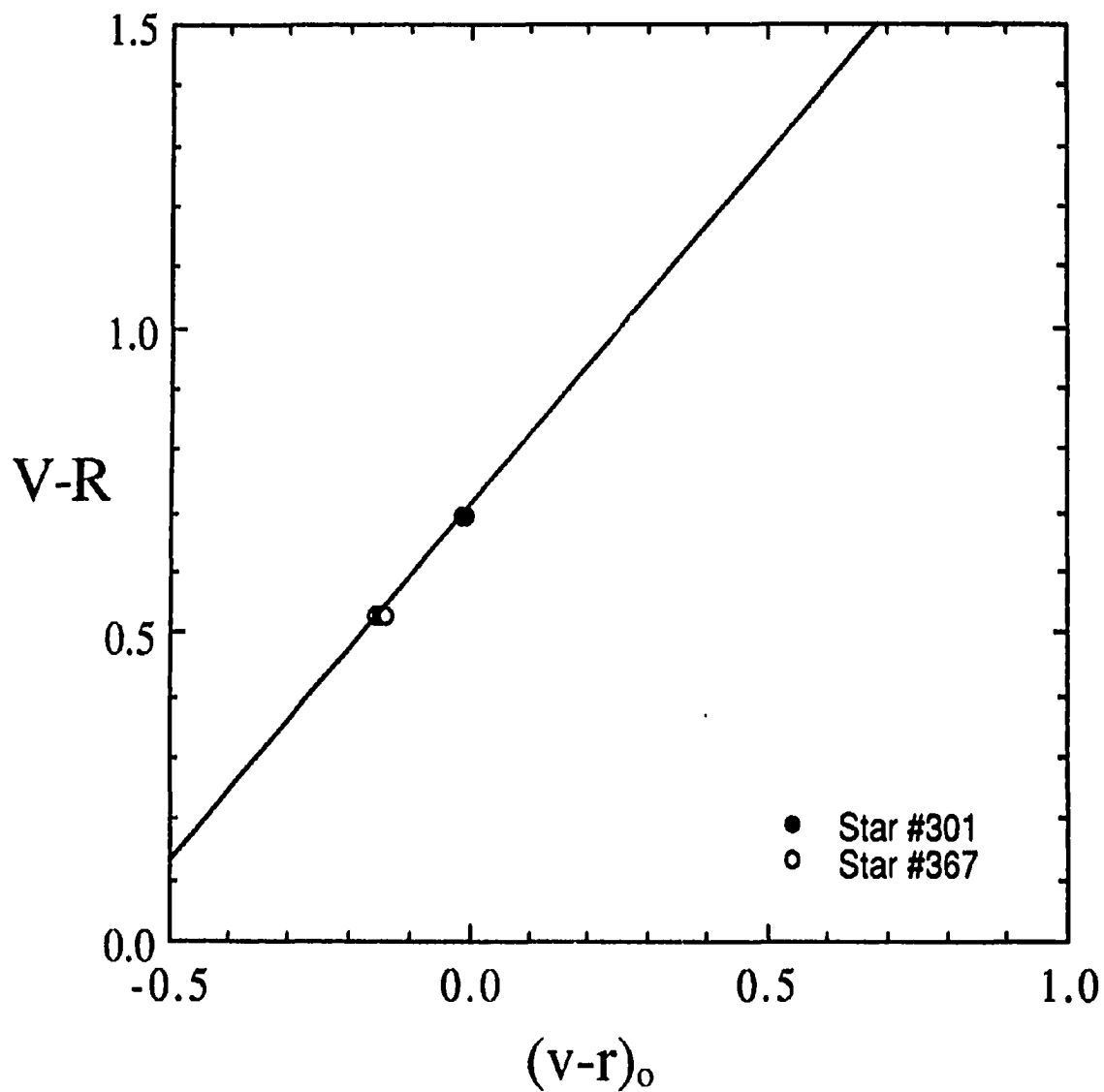


Figure II - 14. Plot of  $(V - R)$  against the extinction-corrected instrumental  $(v - r)$  colour for the 2 standard stars having  $R$  magnitudes listed by Landolt. The line represents the least-squares fit to the data.

stars, Landolt lists R magnitudes for only two, and their V - R colours differ by only 0<sup>m</sup>15. Because of this, the V - R equation coefficients are rather poorly determined.

#### *h) Calibration of NGC 2865 Imagery*

In applying the transformation equations to the galaxy frames, the pixel ADU values in the central region of the galaxy were integrated and treated in the same way as a stellar source. The region chosen was one enclosed by an isophote with a semi-major axis of about 32 pixels (~28") which corresponded to an area of 2460.8 pixel<sup>2</sup>. It contained a little over one half of the total galaxy light, under the assumption of an  $r^{1/4}$  intensity distribution. Reference frames were chosen to represent each of the B, V, and R passbands. Frames LCO590, LCO597, and LCO593 were selected as the reference frames because each appeared to be typical of the set of images taken in the same passband.

The integrated intensities and exposure times for the galaxy region described above in each of the three reference frames were: 937 466 ADU (180 sec), 760 017 ADU (90 sec), and 783 095 ADU (100 sec) respectively. The reference frames were then scaled to an exposure time of one second, the same exposure time that was used in the stellar photometry. The integrated intensities per second of time in the galaxy region were: 5 208.14 ADU (B), 8 444.63 ADU (V), and 7 830.95 ADU (R).

One bright star within the integration area was located about 8" from the galaxy nucleus. In order to estimate this star's contribution to the galaxy light, the galaxy's surface brightness was linearly interpolated across the star.

This was difficult owing to the rapidly changing intensity gradient near the galaxy's centre. It was estimated from the mean blue frame that the star contributes approximately 343 ADU per second (with about  $\pm 10\%$  uncertainty), which is a little less than 7 percent of the galaxy light within the contour or a little more than 3 percent of the total blue galaxy light. Since we only measured the galaxy light to determine its  $(b - v)_o$  colour, the small contribution from the star was not removed at this time.

The instrumental magnitudes from each of the reference frames within the galaxy region described above were computed using the formula

$$m_x = 25 - 2.5 \cdot \log_{10}(\text{ADU}),$$

where  $m_x$  is the instrumental magnitude for either the B, V, or R passband and the ADU values are given for an exposure time of one second.

These instrumental magnitudes were then transformed to a common air mass of  $X = 1.0156$  (the air mass of the R frame) using the preliminary extinction coefficients. The corrections were very small,  $-0^m001$  and  $0^m001$  for the V and B frames respectively. The instrumental magnitudes for the reference frames at an air mass of zero and  $X = 1.0156$  were:

$$v_x = 15^m183, \quad b_x = 15^m709, \quad r_x = 15^m265,$$

$$v_o = 15^m004, \quad b_o = 15^m451, \quad r_o = 15^m139,$$

so that

$$(b - v)_x = 0^m526, \quad (v - r)_x = -0^m082,$$

$$(b - v)_o = 0^m447, \quad (v - r)_o = -0^m135.$$

With the transformation equations, the transformed magnitudes for the reference frames become:

$$V = 12^m000, \quad B - V = 0^m903, \quad V - R = 0^m547.$$

Since we now know the B, V, and R magnitudes that correspond to a region of the galaxy for which the integrated ADU values are known, the calibrated surface brightness can be expressed as:

$$\mu_B = -2.5 \log_{10}(\text{ADU}) + 22^m195 \cdot \text{arcsec}^{-2},$$

$$\mu_V = -2.5 \log_{10}(\text{ADU}) + 21^m816 \cdot \text{arcsec}^{-2},$$

$$\mu_R = -2.5 \log_{10}(\text{ADU}) + 21^m188 \cdot \text{arcsec}^{-2}.$$

In these expressions the ADU values are given for a one second exposure time and  $\mu_B$ ,  $\mu_V$ , and  $\mu_R$  are the Johnson B and V, and Cousins R, magnitudes expressed in units of  $\text{mag} \cdot \text{arcsec}^{-2}$ . The first term on the right side of the expressions is equal to an instrumental magnitude such that one ADU produces a magnitude of zero. The second term is an offset that was computed by substituting into the above equations the ADU values and B, V, and R magnitudes determined for the galaxy contour region. An additional term of  $-0^m322$  is included in the offsets to convert the contour intensities from ADU per pixel to ADU per  $\text{arcsec}^2$ .

The remaining galaxy frames can now be calibrated by first correcting them to the same air mass as the reference frames using the preliminary extinction coefficients. Then, after these frames are scaled to a one second exposure time, the previous equations can be applied to them. The differences in air mass, however, between the reference frames and the other frames resulted in

changes in the derived surface brightness that were no more than 0<sup>m</sup>.003. Since this is much smaller than the uncertainty in estimating the contour intensities, these corrections were not applied.

Because the determination of both  $V - v_0$  and  $B - V$  depend on the  $(b - v)_0$  colour through the transformation equations, we should ideally determine  $(b - v)_0$  as a function of radial distance from the centre of the galaxy. However, this is a very lengthy procedure and it will be shown that the range of  $(b - v)_x$  expected in the galaxy will only have a small effect on the final  $(B - V)$  colours.

The ranges of  $(B - V)$  and  $(V - R)$  found for the galaxy in this study are about 0<sup>m</sup>.1 and 0<sup>m</sup>.05, respectively. It was assumed that instrumental  $(b - v)$  and  $(v - r)$  colours may be lower by about the same amounts, that is  $(b - v)_x$  and  $(v - r)_x$  might be as low as about 0<sup>m</sup>.43 and -0<sup>m</sup>.13, respectively. By following the same procedure as before, the expressions for the calibrated magnitudes become:

$$m_B = -2.5 \log_{10}(\text{ADU}) + 22^m.174 \cdot \text{arcsec}^{-2},$$

$$m_V = -2.5 \log_{10}(\text{ADU}) + 21^m.818 \cdot \text{arcsec}^{-2},$$

$$m_R = -2.5 \log_{10}(\text{ADU}) + 21^m.190 \cdot \text{arcsec}^{-2}.$$

The changes in the equation constants due to the changes in the galaxy colours are only -0<sup>m</sup>.021 in B, 0<sup>m</sup>.002 in V, and 0<sup>m</sup>.002 in R. It can be seen that internal variations in  $(b - v)_x$  and  $(v - r)_x$  expected for this galaxy produce a change in the equation constants of no more than about 0<sup>m</sup>.02. These small variations in galaxy colour were not corrected for in the reductions.

### *i) Plate Scale and Chip Orientation*

The pixel scale of the CCD and the orientation of the chip with respect to the sky were checked by measuring the positions of seven standard stars in two different star fields. Only stars #267, #362, #366, #367 in field 99, and stars #528, #526, and #529 in field 103 were considered in the analysis because they had the largest separations from each other.

The centres of the stellar images were found by fitting them to a 2-dimensional Gaussian function; their sky coordinates were taken from Landolt's (1973, 1983) papers. Landolt lists the right ascension coordinates of the stars to the nearest second of time, which caused the estimates of angular separation to be, in general, several times (1.5 to 3 times) larger than the uncertainty associated with their pixel distance measured in the images. Star #528 showed a chip orientation, when it was paired with any other star, that was over 2 degrees larger than the values obtained using other pairs of stars. Therefore, it was decided not to use this star in determining the chip's scale or orientation.

From the remaining six stars, five pairs were chosen having the largest separations. The separations between these stars ranged between about 261 and 427 pixels (227" to 368"). The weighted mean pixel scale from these five pairs was  $0.862 \text{ pixel}^{-1} \pm 0.003 \text{ pixel}^{-1}$  and the weighted mean difference in the orientation of the chip's x-axis with the true N-S direction,  $\Delta\theta$ , was  $-0.2 \pm 0.4$ . Since  $\Delta\theta$  was  $\approx 0^\circ$  to within the calculated uncertainty, no correction was applied to the ellipse position angles.

### III. RESULTS

#### *a) Average Parameter Values*

The isophotometry covers approximately the inner 60" ( $= 7.1 h^{-1} \cdot \text{kpc}$  with  $h = H_0 / (100 \text{ km} \cdot \text{s}^{-1} \cdot \text{Mpc}^{-1})$ ) of NGC 2865, extending roughly to the locations of the bright shells studied by Fort *et al.* (1986), and covering the base of the jet-like feature that extends westward from the galaxy centre.

In the V and R passbands the best fit ellipse parameters derived from the four frames were linearly interpolated to a common set of semi-major axis values. Then, the mean surface brightness was determined using the weighted mean ADU value computed from the four frames in each passband. For ellipticity, position angle, and  $a_4$  term, an equally weighted mean was computed.

In the B passband the surface brightness estimated from one of the frames appeared to be inconsistent with the values obtained from the other three blue frames. Frame LCO588 produced a surface brightness, over its entire semi-axis range, that was approximately 7 percent fainter than the mean of the other three frames. The preprocessing steps which could have led to such an apparent offset in the derived surface brightness were rechecked but showed nothing unusual compared with the other three blue frames. As well, the surface brightness profile for LCO588 appeared no different from the other blue frames. This frame, however, did have the shortest exposure time (60 s) which may indicate that the estimated exposure time was incorrect. If the offset in the intensity values was due to an error in the exposure time, then the error is between 5 to 6 seconds.

To be able to use the surface brightness data derived from this frame, it was decided to bring its profile in line with the mean of the other three frames. This was accomplished by multiplying its ADU values by the constant factor 1.07025. The remaining parameters for this frame were given equal weight in determining the mean values for this passband.

The average values for the surface brightness, isophotal position angle, ellipticity, and  $\cos(4\theta)$  amplitude are presented in Tables III - 1, 2, and 3 as a function of the semi-major axis. These are shown graphically in Figures III - 1, 2, 3, and 4 for all three passbands. For each parameter the rms differences between the values derived in each frame and the mean value derived from the four frames were computed and then averaged over all semi-major axis distances. These average rms differences are listed at the bottom of each table for each passband.

In their current form, it is not possible to compare directly our R or (B - R) surface brightness profiles with those of Jedrzejewski since the two sets were not calibrated on the same photometric system. However, Davis *et al.* (1985) derived a set of transformation equations that relate the Cousins and Johnson systems. By rearranging their equations, one obtains the following relationships:

$$(R_C - R_J) = 0.12 (B_J - R_C) + 0^m07,$$

$$(B - R)_J = 1.12 (B_J - R_C) + 0^m07,$$

where the subscripts J and C refer to the Johnson and Cousins systems, respectively. For a median  $(B_J - R_C)$  value of  $1^m45$  for NGC 2865, one finds  $(R_C - R_J)$  to be  $0^m24$ . Therefore, to convert between  $R_C$  and  $R_J$ , and between

Table III - 1: B Surface Photometry of NGC 2865

Semi-Major Axis Length (arcsec)	B Surface Brightness (mag·arcsec <sup>-2</sup> )	Ellipticity (1 - b/a)	Position Angle N thru E (deg)	Cos(4θ) Component (×100)
2.83 <sup>1</sup>	18.83	0.097	148.0	-3.7
3.94	19.35	0.132	162.1	0.4
5.28	19.81	0.158	168.6	1.3
6.93	20.23	0.182	165.1	0.2
8.43	20.56	0.203	162.5	0.1
10.25	20.85	0.240	159.9	0.0
11.74	20.05	0.253	159.7	-0.6
13.98	21.31	0.271	159.1	0.1
15.65	21.50	0.278	158.4	0.0
17.30	21.69	0.270	158.0	-0.4
18.97	21.87	0.271	157.2	-0.3
20.67	22.05	0.273	157.0	-0.5
22.47	22.23	0.276	157.3	0.1
23.79	22.36	0.274	157.0	0.7
25.51	22.52	0.266	156.2	0.7
27.18	22.67	0.262	156.2	0.4
28.47	22.79	0.252	155.4	0.8
29.15	22.86	0.240	154.1	1.1
31.23	23.03	0.229	155.2	1.0
32.95	23.15	0.221	153.5	0.9
34.67	23.26	0.220	153.3	1.1
36.19	23.36	0.218	153.0	1.2
38.68	23.50	0.219	152.7	0.3
40.67 <sup>2</sup>	23.60	0.215	150.5	0.3
42.77 <sup>2</sup>	23.76	0.208	151.4	0.1

Table III - 1, Continued

Semi-Major Axis Length (arcsec)	B Surface Brightness (mag·arcsec <sup>-2</sup> )	Ellipticity (1 - b/a)	Position Angle N thru E (deg)	Cos(4θ) Component (x100)
45.45 <sup>2</sup>	23.90	0.203	150.1	0.5
46.71 <sup>2</sup>	23.95	0.204	148.6	0.2
49.81 <sup>2</sup>	24.08	0.202	145.5	-0.5
52.23 <sup>2</sup>	24.16	0.191	144.3	0.1
54.43 <sup>2</sup>	24.26	0.184	143.1	-0.6
55.21 <sup>2</sup>	24.30	0.178	143.3	-0.4
61.01 <sup>1</sup>	24.51	0.176	151.0	2.9
Mean rms diff. in 4 data frames	± 0 <sup>m</sup> 02	± 0.009	± 1 <sup>o</sup> 6	± 0.6

<sup>1</sup> Ellipse parameters are the average of 2 data frames

<sup>2</sup> Ellipse parameters are the average of 3 data frames

Table III - 2: V Surface Photometry of NGC 2865

Semi-Major Axis Length (arcsec)	V Surface Brightness (mag·arcsec <sup>-2</sup> )	Ellipticity (1 - b/a)	Position Angle N thru E (deg)	Cos(4θ) Component (×100)
3.94	18.49	0.100	161.7	0.3
5.28	18.90	0.175	164.7	0.4
6.93	19.32	0.181	163.1	-0.3
8.43	19.64	0.205	163.0	0.2
10.25	19.95	0.237	160.4	-0.1
11.74	20.15	0.252	158.7	0.0
13.98	20.40	0.283	159.6	0.1
15.65	20.60	0.276	157.9	-0.1
17.30	20.79	0.275	158.0	-0.3
18.97	20.97	0.276	157.3	-0.3
20.67	21.15	0.275	157.3	-0.3
22.47	21.35	0.268	156.2	0.0
23.79	21.48	0.263	156.1	0.3
25.51	21.63	0.259	156.1	0.6
27.18	21.79	0.250	156.2	1.0
28.47	21.91	0.236	155.6	1.0
29.15	21.98	0.230	155.2	0.9
31.23	22.15	0.223	155.0	1.5
32.95	22.27	0.222	154.6	1.5
34.67	22.37	0.226	154.7	1.2
36.19	22.47	0.228	154.4	0.9
38.68	22.63	0.224	152.3	0.7
40.67	22.77	0.209	151.8	0.4
42.77	22.88	0.209	152.3	1.3
45.45	23.04	0.204	152.0	0.8

Table III - 2. Continued

Semi-Major Axis Length (arcsec)	V Surface Brightness (mag·arcsec <sup>-2</sup> )	Ellipticity (1 - b/a)	Position Angle N thru E (deg)	Cos(4θ) Component (x100)
46.71	23.10	0.203	151.4	1.1
49.81	23.23	0.196	149.5	1.3
52.23	23.33	0.184	147.8	-0.2
54.43 <sup>1</sup>	23.40	0.180	148.8	0.2
55.21 <sup>1</sup>	23.42	0.179	149.2	0.5
Mean rms diff. in 4 frames	± 0 <sup>m</sup> .04	± 0.014	± 2°0	± 0.5

<sup>1</sup> Ellipse parameters are the average of only 2 data frames

Table III - 3: R Surface Photometry of NGC 2865

Semi-Major Axis Length (arcsec)	R Surface Brightness (mag·arcsec <sup>-2</sup> )	Ellipticity (1 - b/a)	Position Angle N thru E (deg)	Cos(4θ) Component (x100)
3.94 <sup>1</sup>	17.93	0.098	163.5	0.2
5.28	18.37	0.150	167.3	0.5
6.93	18.77	0.187	164.3	0.3
8.43	19.06	0.226	162.1	0.7
10.25	19.36	0.252	159.7	0.8
11.74	19.57	0.271	158.8	0.1
13.98	19.83	0.288	158.6	-0.1
15.65	20.03	0.285	158.3	-0.4
17.30	20.22	0.280	157.6	-0.5
18.97	20.41	0.276	158.0	-0.7
20.67	20.60	0.271	158.3	-0.6
22.47	20.78	0.270	157.7	-0.1
23.79	20.90	0.272	156.9	0.3
25.51	21.08	0.263	155.8	0.5
27.18	21.25	0.252	155.4	0.6
28.47	21.36	0.248	155.1	0.6
29.15	21.42	0.243	155.0	0.6
31.23	21.60	0.228	154.5	0.8
32.95	21.71	0.228	153.3	0.9
34.67	21.82	0.229	152.7	1.2
36.19	21.91	0.233	153.1	1.2
38.68	22.07	0.236	153.6	0.5
40.67	22.22	0.225	152.5	0.6
42.77	22.36	0.218	153.2	-0.3
45.45	22.51	0.215	152.4	0.3

Table III - 3. Continued

Semi-Major Axis Length (arcsec)	R Surface Brightness (mag·arcsec <sup>-2</sup> )	Ellipticity (1 - b/a)	Position Angle N thru E (deg)	Cos(4θ) Component (x100)
46.71	22.56	0.218	152.8	0.8
49.81	22.68	0.216	150.2	0.2
52.23	22.79	0.204	148.7	1.2
Mean rms diff. in 4 data frames	± 0 <sup>m</sup> 03	± 0.013	± 1 <sup>o</sup> 5	± 0.6

<sup>1</sup> Ellipse parameters are the average of 3 data frames

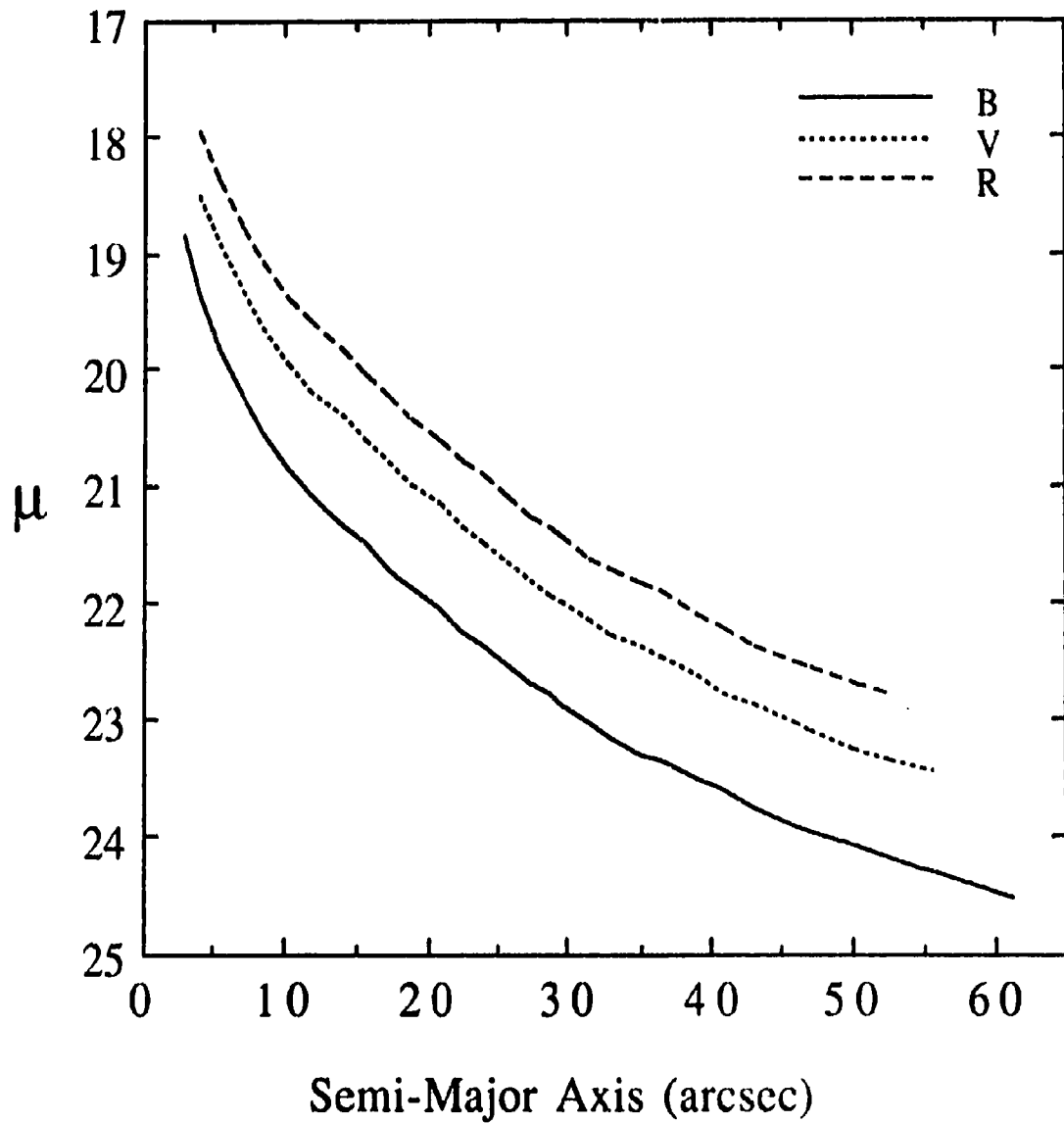


Figure III - 1. The mean apparent surface brightness  $\mu$  (in magnitude·arcsec<sup>2</sup>), of NGC 2865 in the B, V, and Cousins R passbands as a function of semi-major axis. The data are taken from Tables III - 1, 2, and 3.

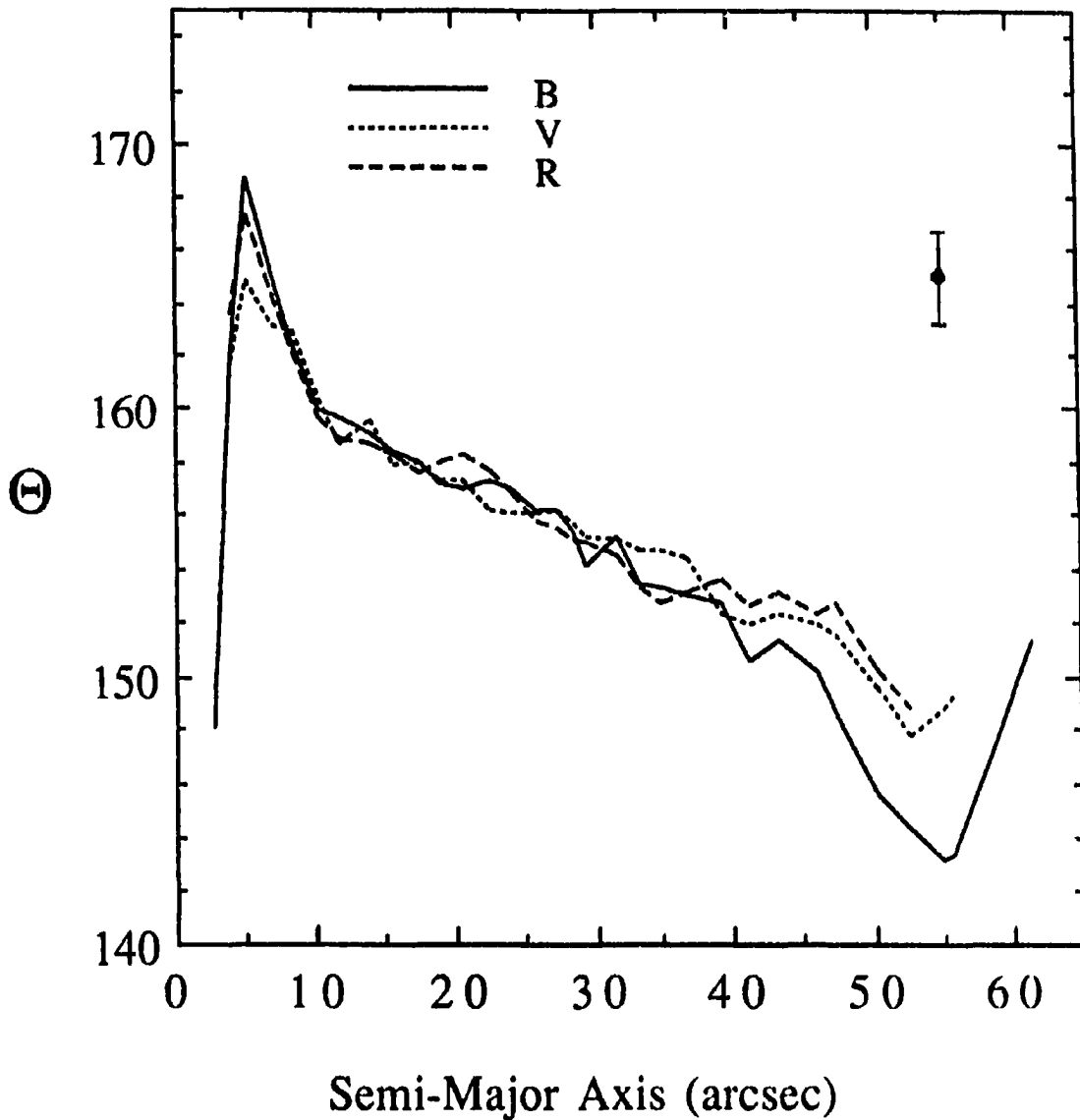


Figure III - 2. Variation of the mean B, V, and R isophotal position angle,  $\Theta$  (in degrees), with semi-major axis. The data are taken from Tables III - 1, 2, and 3. The length of the bar represents twice the average rms deviation from the mean profile derived from the four frames in each colour.

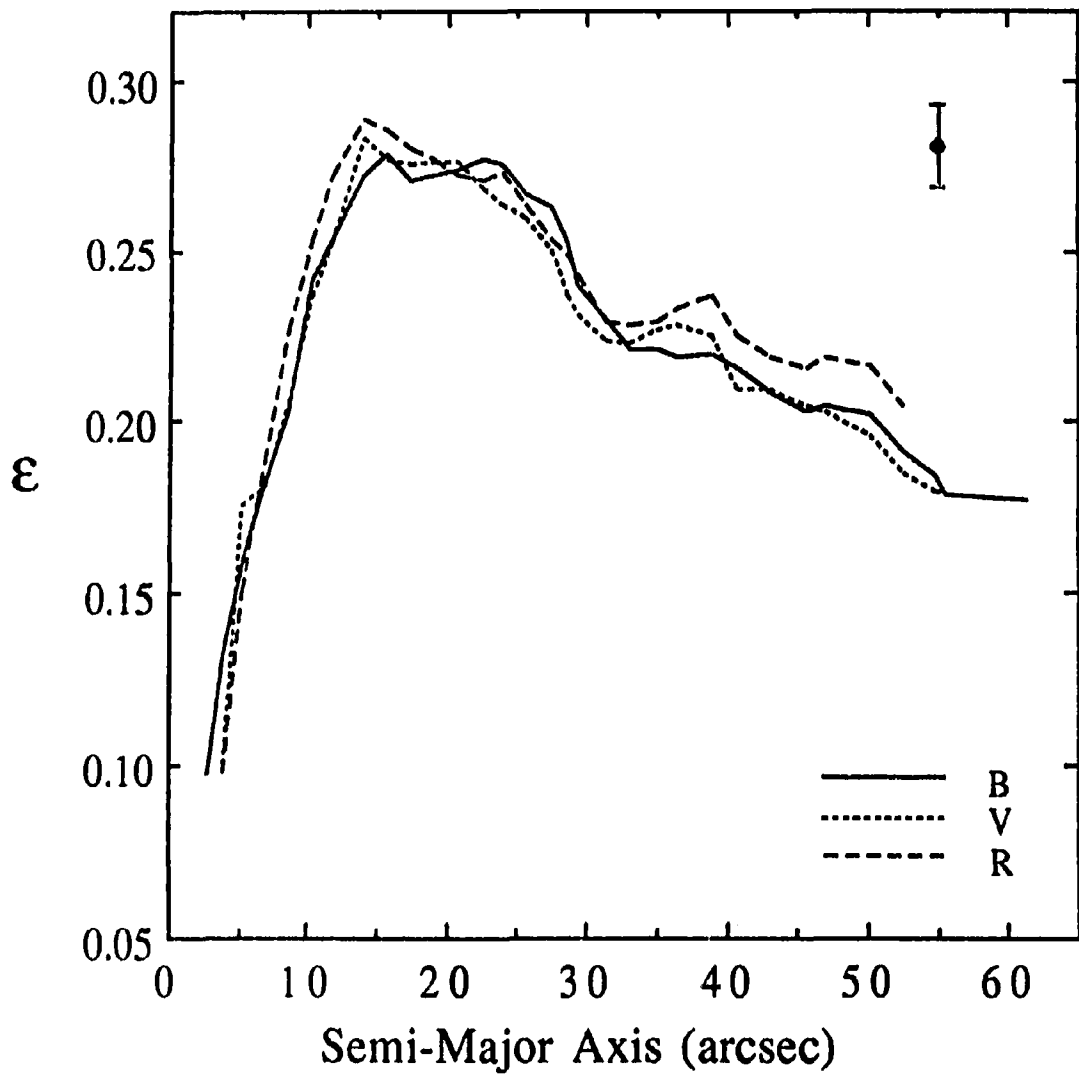


Figure III - 3. Variation of the mean isophotal ellipticity,  $\epsilon$ , in each passband with semi-major axis, where the data are taken from Tables III - 1, 2, and 3. The length of the bar represents twice the average rms deviation from the mean profile derived from the four frames in each colour.

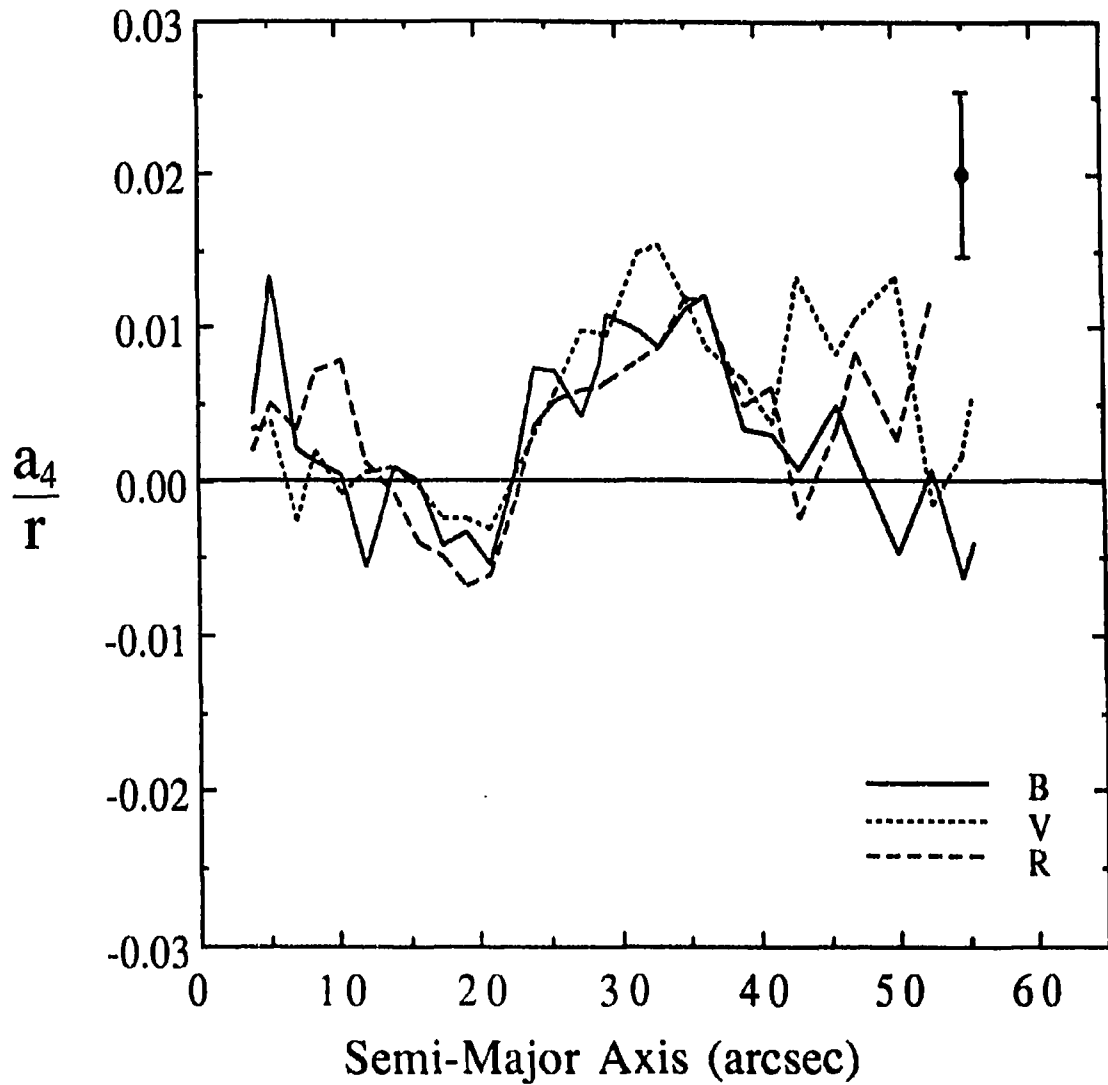


Figure III - 4. Variation of the normalized  $a_4$  term ( $a_4/r$ ) as a function of semi-major axis for NGC 2865, where the data are taken from Tables III - 1, 2, and 3. The length of the bar represents twice the average rms deviation from the mean profile derived from the four frames in each passband.

$(B_J - R_C)$  and  $(B - R)_J$ , an average offset of  $0^m24$  can be applied. Table III - 4 lists the  $(B - V)$ ,  $(B_J - R_C)$ , and transformed  $(B - R)_J$  galaxy colours as a function of semi-major axis. The  $(B - V)$  and  $(B_J - R_C)$  colours are shown graphically in Figure III - 5. No changes were made to the other parameters derived using the Cousins R passband.

The colour of an old stellar system is a complex measure of metallicity (Burstein *et al.* 1984, Aragón *et al.* 1987) and age (O'Connell 1986). Thus, measurements of radial colour gradients may reveal corresponding changes in metallicity or age in the galaxy. In addition, if the isophotal ellipses show radial gradients in ellipticity and position angle, this would suggest that NGC 2865 has a triaxial shape. This would imply that the galaxy does not possess an axis of rotational symmetry.

The logarithmic gradients in the isophotal position angle, ellipticity, and  $(B - V)$  and  $(B - R)$  colours were measured for each passband by fitting a least-squares line to each profile. The linear trends seen in all the parameter profiles are most clearly evident in the outer region of the galaxy, and so this region was used in determining the best-fit lines. This meant that a few data points near the galaxy centre were excluded from the fits because they deviated strongly from the linear trends; these data are also strongly influenced by systematic effects and noise.

For the isophotal position angle and ellipticity, the data beyond, and including, the peak values appeared to comprise the most linear section of each profile. Therefore, the best-fit line was computed using only those data points. Large departures from linearity were seen in the galaxy colours mainly at radii less than  $\sim 8''$  ( $950 h^{-1} \cdot \text{kpc}$ ), and so these points were excluded

Table III - 4. (B - V) and (B - R) Colours of NGC 2865

Semi-Major Axis (arcsec)	Mean (B - V) (mag·arcsec <sup>-2</sup> )	Mean (B <sub>J</sub> - R <sub>C</sub> ) <sup>1</sup> (mag·arcsec <sup>-2</sup> )	Mean (B - R) <sub>J</sub> (mag·arcsec <sup>-2</sup> )
3.94	0.86	1.42	1.66
5.28	0.91	1.45	1.69
6.93	0.91	1.46	1.71
8.43	0.91	1.49	1.74
10.25	0.90	1.49	1.74
11.74	0.90	1.48	1.73
13.98	0.92	1.48	1.73
15.65	0.90	1.47	1.72
17.30	0.90	1.47	1.72
18.97	0.90	1.46	1.71
20.67	0.90	1.45	1.69
22.47	0.88	1.45	1.69
23.79	0.89	1.46	1.71
25.51	0.89	1.44	1.68
27.18	0.88	1.42	1.66
28.47	0.88	1.43	1.67
29.15	0.88	1.44	1.68
31.23	0.88	1.43	1.67
32.95	0.88	1.44	1.68
34.67	0.89	1.45	1.69
36.19	0.89	1.45	1.69
38.68	0.87	1.43	1.67
40.67	0.83	1.38	1.62
42.77	0.88	1.41	1.65
45.45	0.86	1.40	1.64
46.71	0.84	1.38	1.62

Table III - 4. Continued

Semi-Major Axis (arcsec)	Mean (B - V) (mag·arcsec <sup>-2</sup> )	Mean (B <sub>J</sub> - R <sub>C</sub> ) <sup>1</sup> (mag·arcsec <sup>-2</sup> )	Mean (B - R) <sub>J</sub> (mag·arcsec <sup>-2</sup> )
49.81	0.85	1.41	1.65
52.23	0.83	1.37	1.60
54.43	0.87	— <sup>2</sup>	— <sup>2</sup>
55.21	0.88	— <sup>2</sup>	— <sup>2</sup>

<sup>1</sup> The subscripts J and C indicate Johnson and Cousins passbands respectively.

<sup>2</sup> Semi-major axis is beyond limit of R magnitudes obtained in this study.

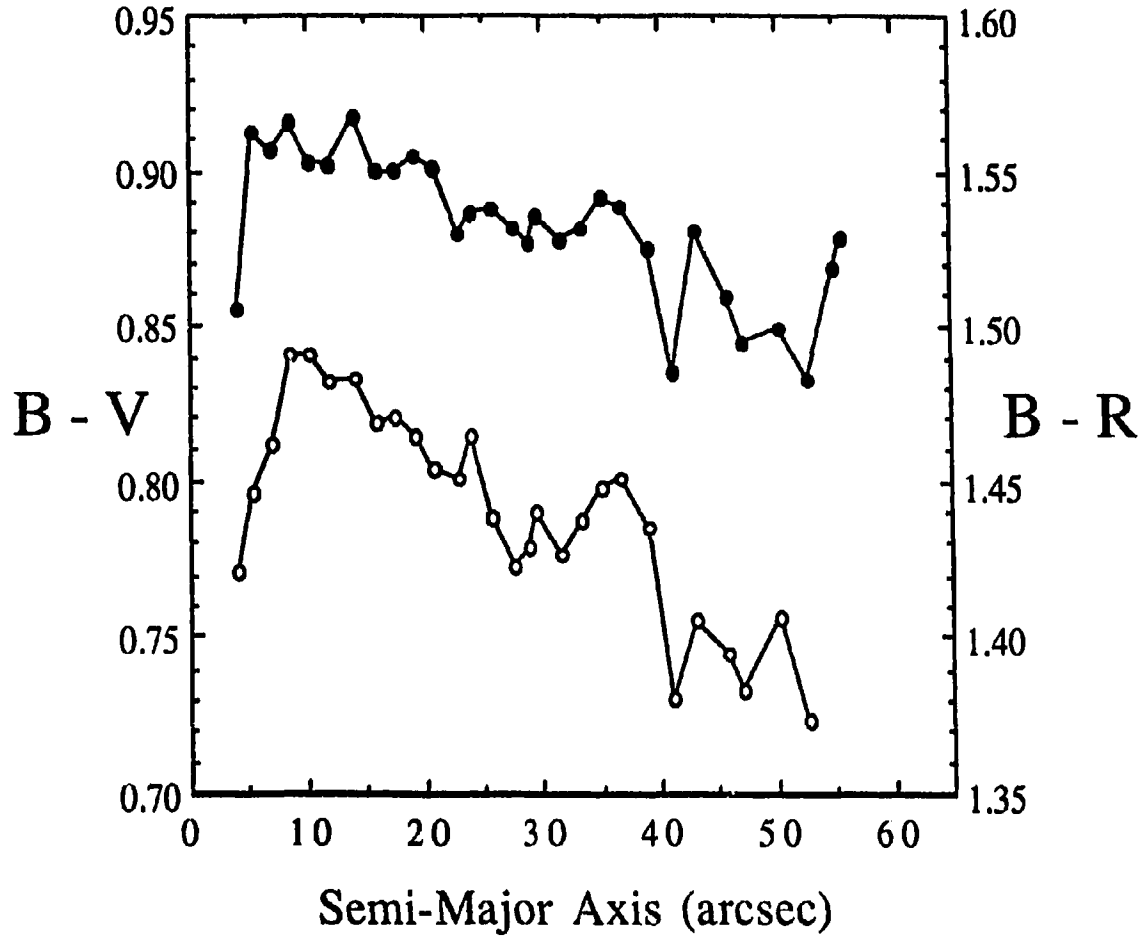


Figure III - 5. Plot of the colour variations (in mag-arcsec<sup>-2</sup>) across the galaxy as a function of semi-major axis. The data are taken from Table III - 4. The solid circles are (B - V) and the open circles are (B<sub>J</sub> - R<sub>C</sub>).

from the fits. For (B - V) the first value in Table III - 4, corresponding to the smallest radial distance, was excluded from the fit. For (B - R), the first three data points were excluded. The gradients, measured per decade change in semi-major axis, were:

Passband	$\frac{\Delta\epsilon}{\Delta\log(r)}$	$\frac{\Delta\Theta}{\Delta\log(r)}$
B	$-0.194 \pm 0.011$	$-19^{\circ}2 \pm 1^{\circ}5$
V	$-0.183 \pm 0.009$	$-14^{\circ}9 \pm 1^{\circ}1$
R	$-0.152 \pm 0.008$	$-14^{\circ}8 \pm 1^{\circ}0$

$$\frac{\Delta(B-V)}{\Delta\log(r)} = -0^m.065 \pm 0^m.009, \quad \frac{\Delta(B-R)}{\Delta\log(r)} = -0^m.139 \pm 0^m.014.$$

*b) Departures from Perfectly Elliptical Isophotes*

Departures of the isophotes from perfect ellipses may carry important implications for the structure of elliptical galaxies. Nieto and Bender (1989) suggest that galactic interactions, including mergers, may result in boxy isophotes in elliptical galaxies. If the shells of NGC 2865 are assumed to be a merger product, then the isophotes should display boxy isophotes. The radial distribution of the normalized  $a_4$  term for each passband is shown in Figure III - 5. All colours show approximately the same trend in the values of  $a_4$ , but there do not appear to be any significant ( $2\sigma$ ) departures from purely elliptical isophotes. If anything, a small positive  $a_4$  component of about 1 percent is

present between 25" and 40" (3.0 and 4.7 h<sup>-1</sup> kpc). This suggests the presence of a very weak, nearly edge-on, disk in the galaxy.

*c) Comparison with other work*

Jedrzejewski (1987) published a similar analysis of 49 galaxies including NGC 2865, and his results are compared with those found here. First, the mean values found in this study were linearly interpolated to the semi-major axis positions given by Jedrzejewski. Then the residuals were formed by subtracting Jedrzejewski's ellipse parameter values from the interpolated mean values. Figures III - 6, 7, 8, and 9 show the residuals for surface brightness, ellipticity, position angle and  $a_4$  term in both the B and R passbands. The residuals in the (B - R) colours are plotted in Figure III - 10.

Figure III - 6 is a plot of the surface brightness residuals determined by subtracting Jedrzejewski's Johnson B and R surface brightness profiles (in mag·arcs<sup>-2</sup>) from the linearly interpolated mean Johnson B and Cousins R profiles found here. The solid line at 0<sup>m</sup>24 indicates the difference expected between the Johnson and Cousins photometric R systems, as explained in section III(c). The dashed lines located at ± 0<sup>m</sup>035 from the two solid lines represent the estimated mean combined uncertainty of both this study and Jedrzejewski's work.

The B surface brightness residuals show a trend throughout the range of observations that appears approximately linear. The residuals indicate that we find the galaxy to be fainter at larger radii but brighter at smaller radii than reported by Jedrzejewski. The difference between the two values is about 0 at ~30" but deviates at the rate of about 0<sup>m</sup>005 arcsec<sup>-2</sup> per arcsec in radius. In the B passband the inner isophotes appear ~0<sup>m</sup>15 arcsec<sup>-2</sup> brighter than

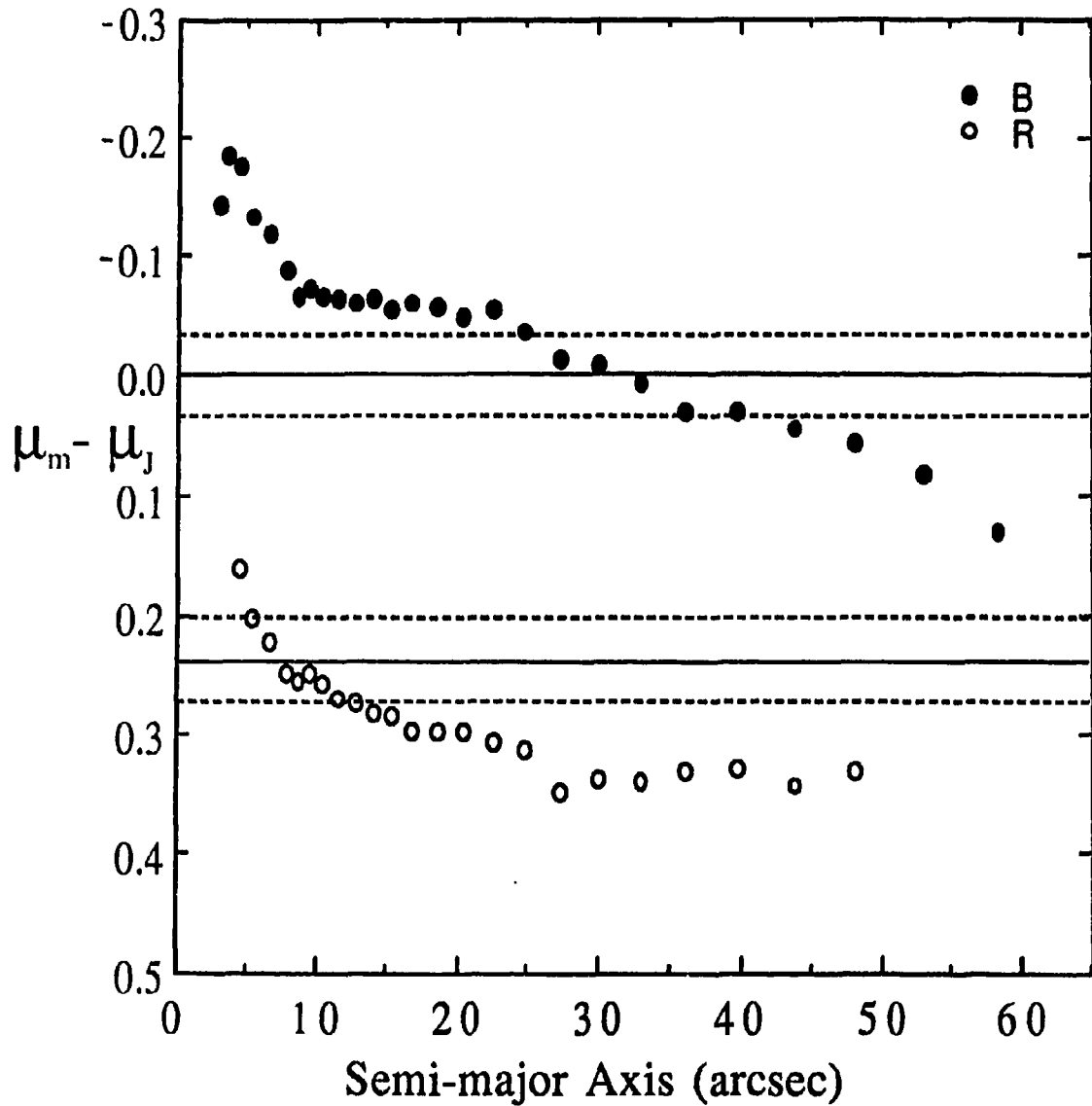


Figure III - 6. Comparison between the mean surface brightness  $\mu_m$  (in  $\text{mag}\cdot\text{arcsec}^{-2}$ ), found in this study with the  $\mu_J$  values measured by Jedrzejewski. The solid line at  $0^m24$  indicates the estimated mean difference between the Johnson and Cousins R photometric systems. The dashed lines represent the estimated combined uncertainty of both studies.

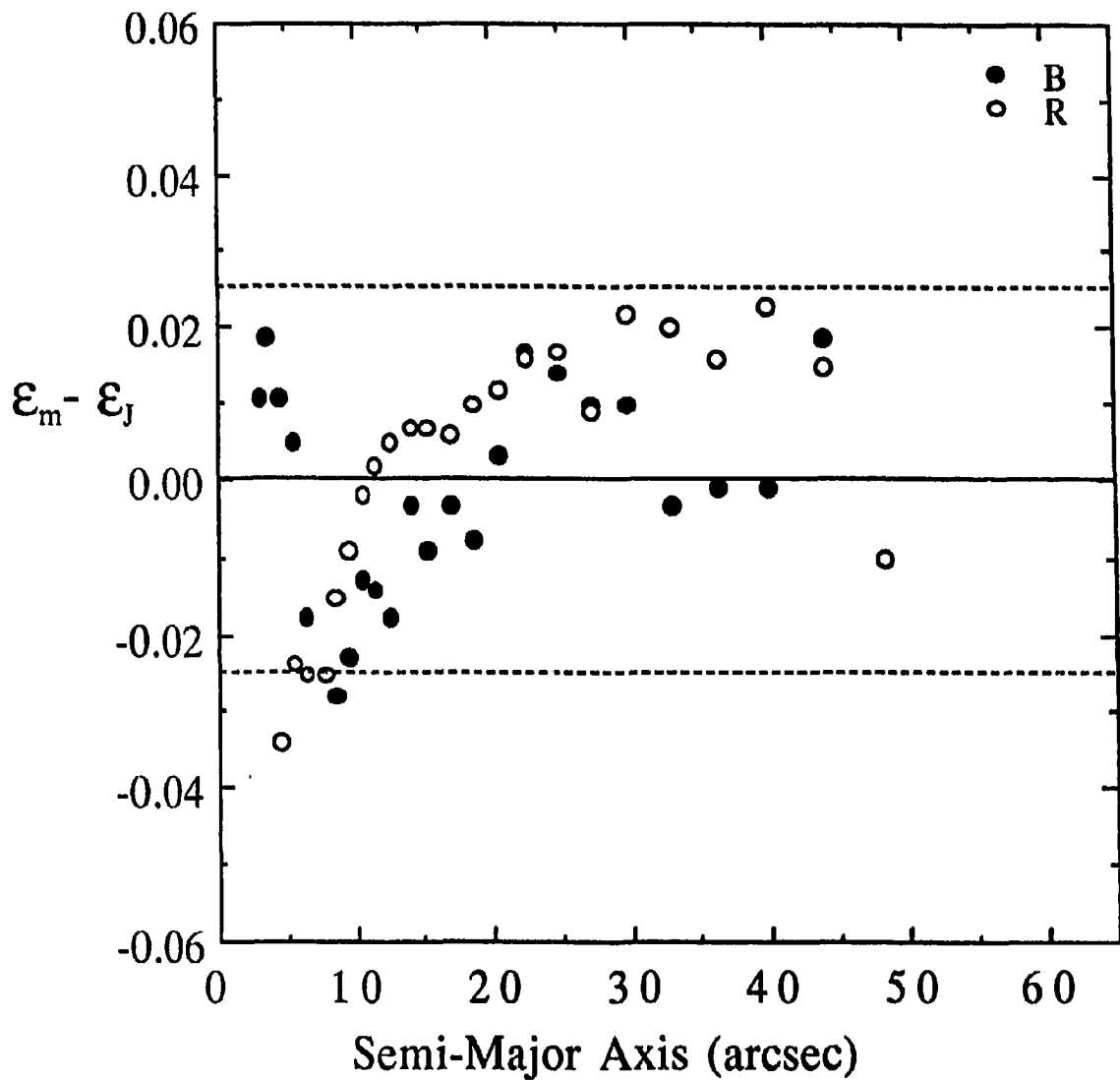


Figure III - 7. Plot of the residuals between the mean isophotal ellipticity determined in this study,  $\epsilon_m$ , and the values measured by Jedrzejewski,  $\epsilon_J$ , in the B and R passbands. The dashed lines represent the estimated combined uncertainty of both studies.

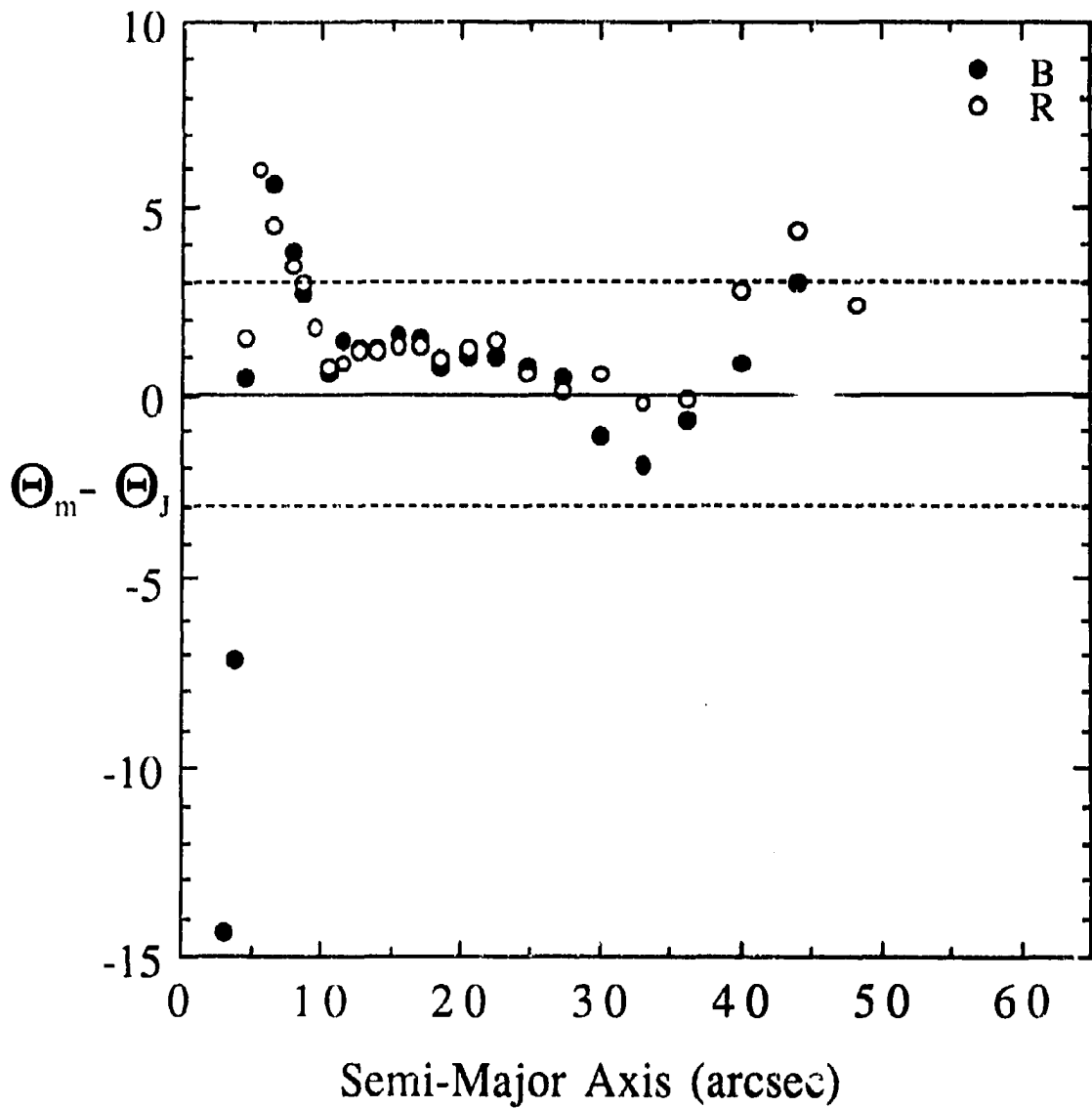


Figure III - 8. Plot of the residuals between the mean isophotal position angles,  $\Theta_m$  (in degrees), and the values measured by Jedrzejewski,  $\Theta_J$ , in the B and R passbands. The dashed lines represent the estimated combined uncertainty of both studies.

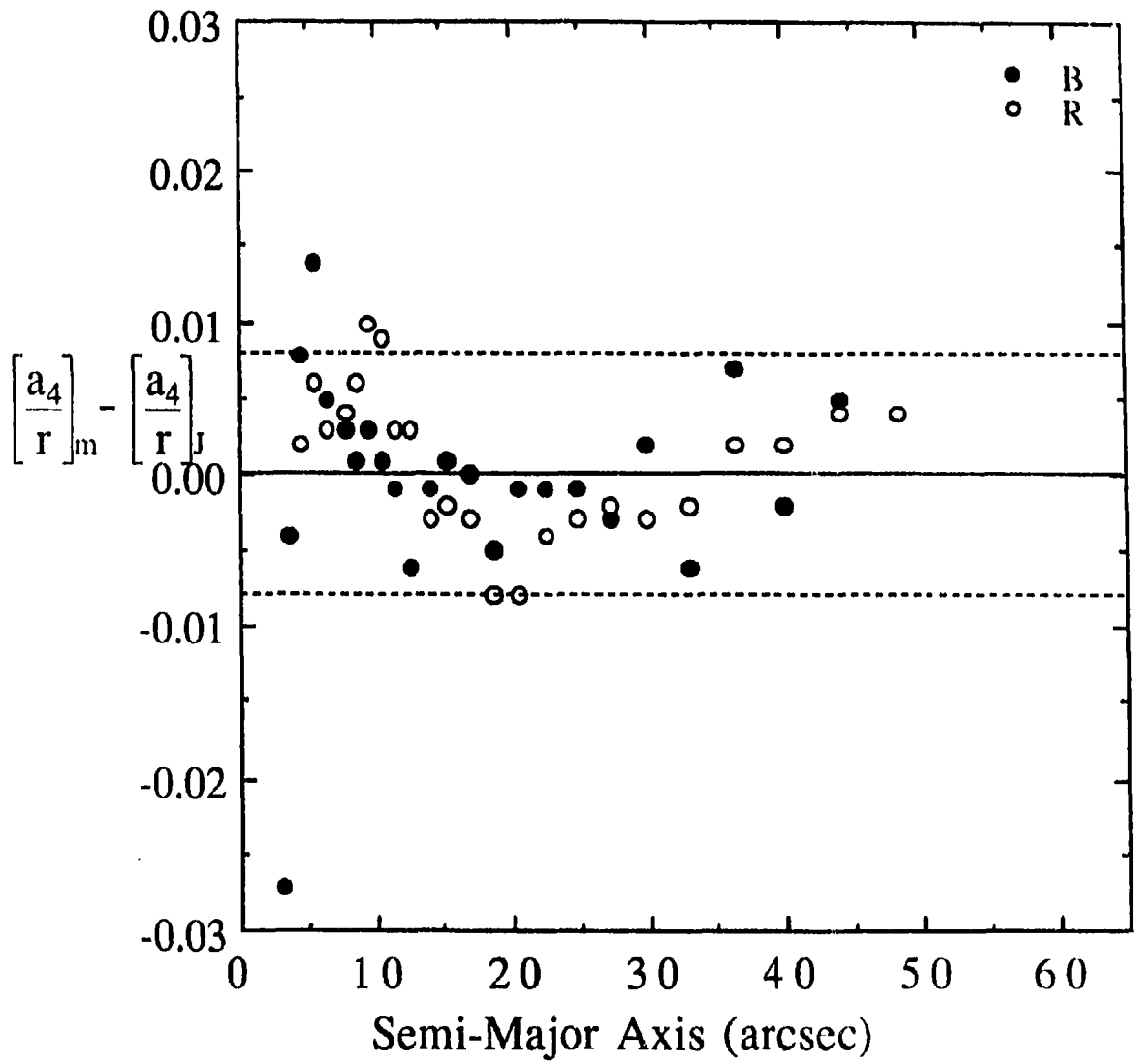


Figure III - 9. Plot of the residuals between the mean normalized  $a_4$  components of the isophotes found in this study,  $(a_4)_m$ , and the values measured by Jedrzejewski,  $(a_4)_J$ , in the B and R passbands. The dashed lines represent the estimated combined uncertainty of both studies.

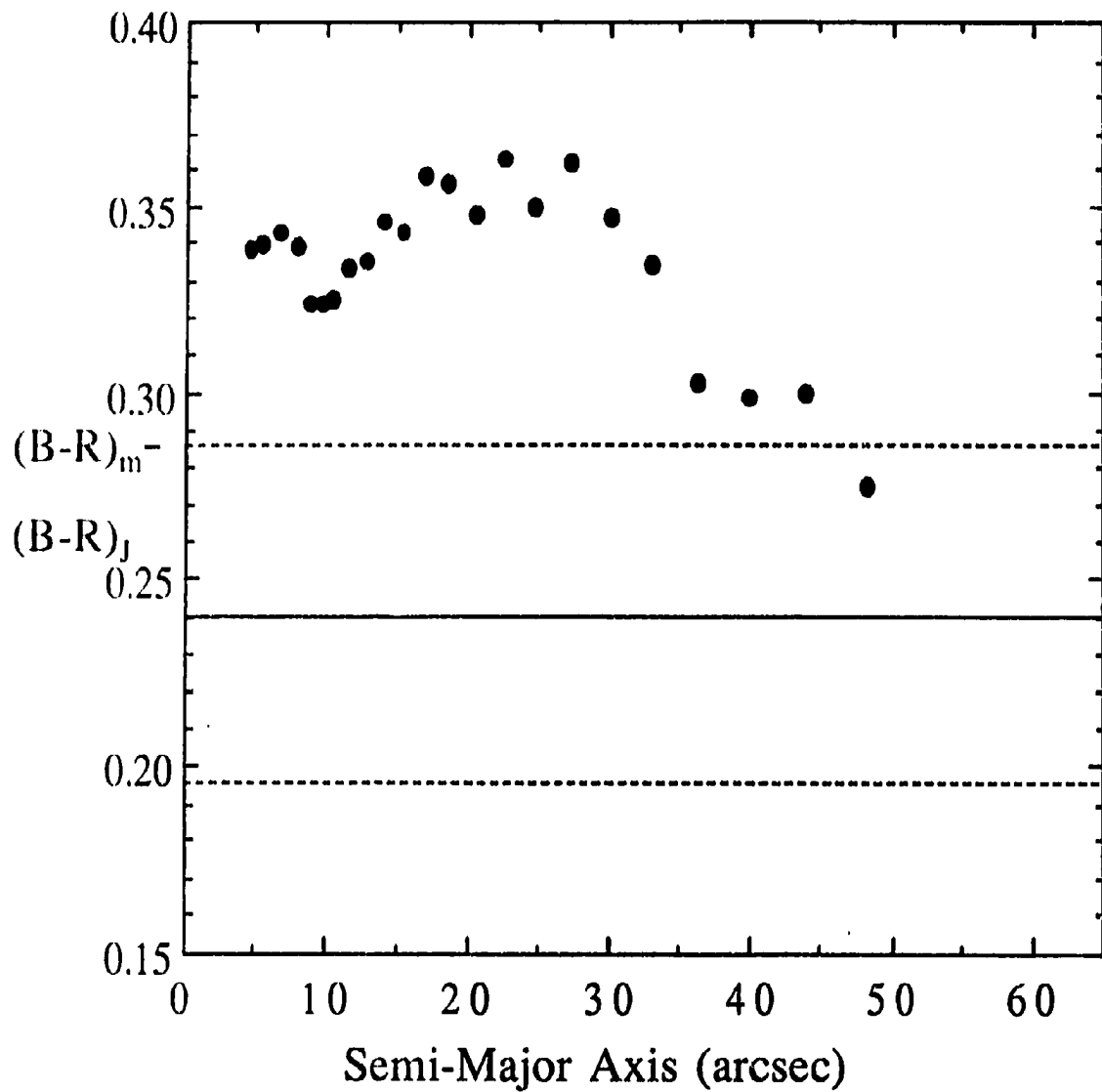


Figure III - 10. Plot of the residuals between the mean  $(B - R)_m$  colours found in this study and the  $(B - R)_J$  colours measured by Jedrzejewski, as a function of semi-major axis. The solid line at  $0^m24$  indicates the estimated mean difference between the Johnson and Cousins R photometric systems. The dashed lines represent the estimated combined uncertainty of both studies.

reported by Jedrzejewski and the largest isophotes appear about  $0^m15 \text{ arcsec}^{-2}$  fainter. The mean residual in B between the two studies was  $-0^m045$  with a rms difference from zero of  $\pm 0^m087$ .

The R surface brightness residuals (Figure III - 6) show a trend of about  $0^m005 \text{ arcsec}^{-2}$  per arcsec in radius within the inner  $\sim 25''$  of the galaxy. Beyond  $\sim 25''$ , the difference between the two profiles remains approximately constant, with our R surface brightness (converted to the Johnson system) being  $\sim 0^m11$  brighter than Jedrzejewski's R surface brightness.

It is worthwhile at this point to investigate whether the residuals seen in Figure III - 6 may be due, in part, to an inaccurate non-linear correction being applied in section II(b). Qualitatively, when the residuals show that the derived surface brightness is too bright, then this means that the k factor is too small. Conversely, when the residuals show that the mean surface brightness is too faint then the k factor is too large. The range where the k factor is the least well known is clearly in the region where the observed pixel counts are less than  $10^{1.9}$  (Figure II - 1). This region corresponds to an equivalent blue galaxy surface brightness of about  $22^m \text{ arcsec}^{-2}$  which, from Table III - 1, begins at a radial distance of about  $20''$  from the galaxy in the blue passband. As noted before, the blue surface brightness residuals appear to have a linear trend extending from about  $20''$  outward. If this trend is attributed to an incorrect k factor, then the trend is in the sense that the k factor should be smaller for fainter intensities than is currently estimated. In Figure II - 1 this would mean that the lower part of the curve should be steeper, perhaps as steep as the polynomial curve if it was extended to observed counts of less than  $10^{1.9}$ .

To determine if such a change in the k factor would reduce the trend seen in the residuals, a blue frame with a typical exposure time, LCO591, was chosen and its mean sky and contour ADU values were computed to the point before the k factor was applied. Then, new k factors were computed using only the third order polynomial fit. Finally, values for the sky levels and contour ADUs were re-computed using the new k factors, which were then compared with the previous results. It was found that the slope in the residuals was reduced by only about 30% for semi-major axes greater than 20". However, because the sky value had been altered by the use of a new k factor, the slope of the residuals in the inner region of the galaxy had increased by a factor of six over its previous value (to about  $0.^m03$  arcsec<sup>-2</sup> per arcsec). The new k factors slightly improve the residuals in the faint outer regions of the galaxy, but their effect in the bright inner regions is to make the residuals much worse than before. It does not seem possible, then, to extrapolate the correction curve from the well determined high pixel count region to the poorly determined low pixel count range. The determination of the k factor in the low pixel count range must remain somewhat uncertain, as it depends entirely on only two data points.

It is not likely that the trend in the residuals is due to incorrect sky subtraction during the preprocessing stage. Subtracting a sky level that is slightly incorrect would cause the residuals to become progressively larger as the galaxy's brightness level declines at large radii. For the bright inner regions of the galaxy, however, the residuals should remain small. Figure III - 6 shows that the residuals, especially in R, do not increase rapidly at large radii but instead change at a relatively constant rate. At very small radii the residuals do become large, but this is not expected to arise from the sky subtraction

process. This indicates that some other effect is influencing one or both of the estimates of surface brightness.

At first glance, there would seem to be no difference between the two studies. The uncertainty quoted for surface brightness by Jedrzejewski (1987) is essentially the same as the value estimated in this study. But Jedrzejewski's telescope/CCD combination produced a pixel size of  $0.49 \text{ arcsec}^{-1}$ , which is approximately 60% smaller than what was used here. That, together with seeing conditions reported to be about  $0''.85$  (FWHM) in the blue (more than twice as good than this study), allowed him to measure more accurately the isophote intensities near the galaxy centre.

However, the smaller chip scale would require separate background sky frames to be taken in order to estimate the sky intensity. These sky frames would have to be taken at a distance far enough away to prevent contamination by the galaxy and so may not be representative of the sky intensity nearer the galaxy. The short exposure images used in this study, and the averaging of four profiles in each passband, allow a more accurate measurement of the isophotes at greater distances from the galaxy. In addition, using standard star photometry produces a more accurate calibration of the galaxy's surface brightness intensities.

For the isophote ellipticity, the residuals between the mean value found in this study and the values found by Jedrzejewski (Figure III - 7) are small compared to the estimated combined uncertainty. The mean residual in ellipticity was  $-0.002$  with a rms difference from zero of  $\pm 0.014$ . There are only a couple of residuals that lie outside the mean combined uncertainty of  $\pm 0.025$

estimated for this study and Jedrzejewski's work (indicated by the dashed lines in Figure III - 7).

The mean position angles of the isophotes agree well with those found by Jedrzejewski over the radial range from about 10" - 50" (Figure III - 8) showing a mean residual of 1.95 and a rms difference from zero of  $\pm 2.94$ . Jedrzejewski's results do not show the slightly more rapid isophotal twist in the blue passband which is seen in this study at about 40" - 55". This increased twisting amounts to an offset of about 5° over the other two passbands. Within the inner ~10" of the galaxy centre, however, the residuals become as large as 15° and extend beyond the estimated mean combined uncertainty of  $\pm 3.0$  estimated for this study and Jedrzejewski's work (shown by the dashed lines in Figure III - 8). Such large residuals near the galaxy centre are probably caused by the effects of seeing and the small number of pixels in the isophotal contours.

The residuals found between the the mean  $\cos(4\theta)$  amplitude of the isophotes and Jedrzejewski's values are shown in Figure III - 9. The dashed lines at  $\pm 0.008$  represent the estimated mean combined uncertainty from both this study and Jedrzejewski's work. In general, the residuals are small except for one measurement within 5" of the galaxy centre. The residual may be large for this measurement due to the small number of pixels making up the isophotal contour. Omission of this data point produces a mean residual of 0.07 percent with a rms difference from zero of  $\pm 0.5$  percent.

Finally, the residuals between the (B - R) colours found in this study and the colours measured by Jedrzejewski are shown in Figure III-10. Included in the plot is a solid line at 0<sup>m</sup>24 showing the mean difference expected

between the Johnson and Cousins R passbands. As well, the dashed lines represent the mean combined uncertainty of  $\pm 0^m.045$  estimated for this study and Jedrzejewski's work. Essentially all the residuals in (B - R) are greater than the estimated combined uncertainty of the two studies. Out to 30" the mean colour found in this study is about  $0^m.1$  (converted to the Johnson system) redder than the values measured by Jedrzejewski. Beyond 30" the residuals decrease, approaching Jedrzejewski's values, at a rate of about  $0^m.004$  arcsec<sup>-2</sup> per arcsec.

Based on the comparison between this study and the results of Jedrzejewski, there is good agreement in all the ellipse parameters. However, the residuals in the surface brightness profiles, and in (B - R) colour profile, show a clear disagreement between the two studies. For reasons previously discussed, Jedrzejewski's surface brightness measurements were probably more accurately determined near the galaxy centre whereas measurements made further out were likely more accurately determined in this study.

## IV. DISCUSSION

### a) *Surface Brightness Profile Fits*

The surface brightness of the galaxy NGC 2865 does not show evidence for an exponential stellar disk component in any of the three passbands (see Figure III-1). The best-fit de Vaucouleurs profile in each passband has the following parameters:

$$r_o(B) = 23.''4 \pm 0.''6 \quad \mu_o(B) = 22.35 \pm 0.05 \text{ mag}\cdot\text{arcsec}^{-2}$$

$$r_o(V) = 22.''8 \pm 0.''6 \quad \mu_o(V) = 21.42 \pm 0.05 \text{ mag}\cdot\text{arcsec}^{-2}$$

$$r_o(R) = 21.''9 \pm 0.''6 \quad \mu_o(R) = 20.79 \pm 0.06 \text{ mag}\cdot\text{arcsec}^{-2}$$

where  $\mu_o$  is the effective surface brightness at the radius  $r_o$  that encloses one half of the total light of the galaxy. Within the region of the galaxy studied, the mean radial brightness profile is well fitted by the standard de Vaucouleurs law.

A tight correlation in the de Vaucouleurs law parameters was found by Kormendy (1982) for elliptical galaxies, and S0 galaxies whose disks are barely detectable and are assumed not to influence the bulge structure. The relation is

$$B_o(V) = 3.28 \log[r_o(B)] + 19.45 \quad B \text{ mag}\cdot\text{arcsec}^{-2},$$

where  $r_o(B)$  is given in kpc ( $H_o = 50 \text{ km}\cdot\text{s}^{-1}\cdot\text{Mpc}^{-1}$ ), and  $B_o(V)$  is the galaxy's blue effective surface brightness corrected for foreground extinction. Using the same galactic extinction and K correction given in the *Second Reference Catalogue* ( $0.^m46$  and  $0.^m04$  respectively), and the value of  $\mu_o(B)$  given above,

one obtains an effective surface brightness of  $B_o(V) = 21^m85$ . Under the assumption that the distance to NGC 2865 is 48 Mpc ( $H_o = 50 \text{ km s}^{-1} \text{ Mpc}^{-1}$ ),  $r_o(B)$  is found to be 5.5 kpc. With these values of  $B_o(V)$  and  $r_o(B)$ , NGC 2865 fits well into the above relation, being only  $0^m04$  brighter in  $B_o(V)$  than predicted. From these characteristic parameters, derived for radial distances of about 5" - 60", the main body of NGC 2865 appears to be a typical elliptical/S0 galaxy.

The absolute B magnitude of NGC 2865 can be estimated by combining the results of the best-fit de Vaucouleurs profiles and using the method of integrated ADU counts employed in section II(h). First, an average blue image frame was formed by registering the blue frames to one master frame, in this case LCO589. Next, the ADU values from the four frames were added pixel-by-pixel and divided by the total exposure time of 630 seconds. Then, all of the bright stars within 1' of the galaxy centre were removed by linearly interpolating the galaxy brightness profile across the stellar image. Finally, the ADU values of this mean frame were integrated within an ellipse representing the largest isophote determined in this study. This isophote had a semi-major axis of  $61''.0$  corresponding to an area of  $9\,632.4 \text{ pixel}^2$ . This gave an integrated ADU value of  $6\,377.6$ .

To estimate the contribution from the galaxy beyond  $61''$ , the best-fit  $r^{1/4}$  law was integrated from a radial distance of  $61''$  to infinity, where the parameters derived in section IV(a) were used. Under the assumption that the isophotes beyond  $61''$  have the same ellipticity as the last measured contour ( $\epsilon = 0.176$ ), the integration gives a value of  $2\,120 \pm 224 \text{ ADU}$ , where the uncertainty is based on the  $r^{1/4}$  law parameter uncertainties. This integration represents about 25 percent of the total  $r^{1/4}$  profile integration. Therefore, the

total ADU for the galaxy was 8 497, or  $m_B = 12^m35$ , which turns out to be exactly the total B magnitude listed in the *Second Reference Catalogue*. Another uncertainty associated with the integration of the  $r^{1/4}$  law beyond 61" is whether the ellipticity of the isophotes eventually drops to zero (circular isophotes). If we assume that the galaxy's isophotes beyond 60" are all circular, then  $m_B$  becomes brighter by  $0^m05$ .

With an estimated distance to NGC 2865 of 48 Mpc ( $H_0 = 50 \text{ km s}^{-1} \text{ Mpc}^{-1}$ ), and applying the same galactic extinction and K correction as given in the *Second Reference Catalogue* ( $0^m50$  total), one finds an absolute B magnitude of  $-20^m64 \pm 0^m06$ . The uncertainty is estimated by combining the rms uncertainties from the transformation equations ( $\pm 0^m02$ ), the uncertainty in the parameter values of the  $r^{1/4}$  law ( $0^m03$ ), and the uncertainty in the ellipticity of the isophotes beyond 61" ( $0^m05$ ). Compared with the mean absolute magnitude for elliptical galaxies of about -18 estimated from their observed luminosity function (Binggeli 1987), NGC 2865 is roughly  $2^m$  brighter. This absolute magnitude converts to a total luminosity of about  $2.8 \times 10^{10} \cdot L_\odot$ .

Under the assumption of a mass to light ratio (M/L) of about 10 (in solar units) for elliptical galaxies (Faber and Gallagher 1979), one finds a total mass of  $3 \times 10^{11} \cdot M_\odot$ . This gives a ratio of neutral gas mass to total galaxy luminosity of about  $0.01 M_\odot/L_\odot$ , which is similar to values found for S0 galaxies although it is somewhat high for an elliptical galaxy (Gallagher *et al.* 1975).

### *b) Deviations from the Standard Brightness Profile*

The profiles show a small scale bumpiness in the light distribution which was also noted by Jedrzejewski (1987). These bumps can be isolated by subtracting a least-squares de Vaucouleurs profile from the mean surface

brightness data in each passband. Figure IV - 1 shows the residuals when the best-fit de Vaucouleurs profile, expressed in magnitudes per arcsec<sup>2</sup>, is subtracted from the mean profile. Another way to describe this plot is that it is equivalent to the intensity ratio between the two profiles converted to units of magnitude. The largest departure found between 5" and 55" (0.6 - 6.6 h<sup>-1</sup> kpc) from the galaxy centre is only 0.<sup>m</sup>08 arcsec<sup>-2</sup> in the blue passband. The graph shows one peak in the surface brightness residuals located at approximately 20" (2.4 h<sup>-1</sup> kpc) from the galaxy centre having a radial thickness of roughly 20". The residuals begin to rise again at about 45" (4.7 h<sup>-1</sup> kpc) and continue to increase out to the limiting distance of the isophotometry without showing signs of leveling off. If these rises in surface brightness residuals are associated with the shells surrounding the galaxy, then the increase seen for radial distances greater than 45" correspond to a combination of the shells 2A and 2B investigated by Fort *et al.* (1985). In the core of elliptical galaxies the de Vaucouleurs law typically underestimates the galaxy's surface brightness. This explains the sharp rise in the residuals at very small radial distances.

### *c) Isophotal Shapes and Orientations*

The isophotal ellipticity (Figure III - 3) rises very sharply from a value of about 0.1 at a radial distance of 5" to a maximum ellipticity of 0.3 at radial distances of about 10" - 15". The ellipticity then gradually decreases at a constant rate of approximately 0.0025 arcsec<sup>-1</sup> until it reaches 0.2 at 55". All passbands follow the same trend within the 2 $\sigma$  uncertainties. The drop in ellipticity near the centre cannot be due entirely to seeing since the estimated seeing was found to be better than 2" in all passbands.

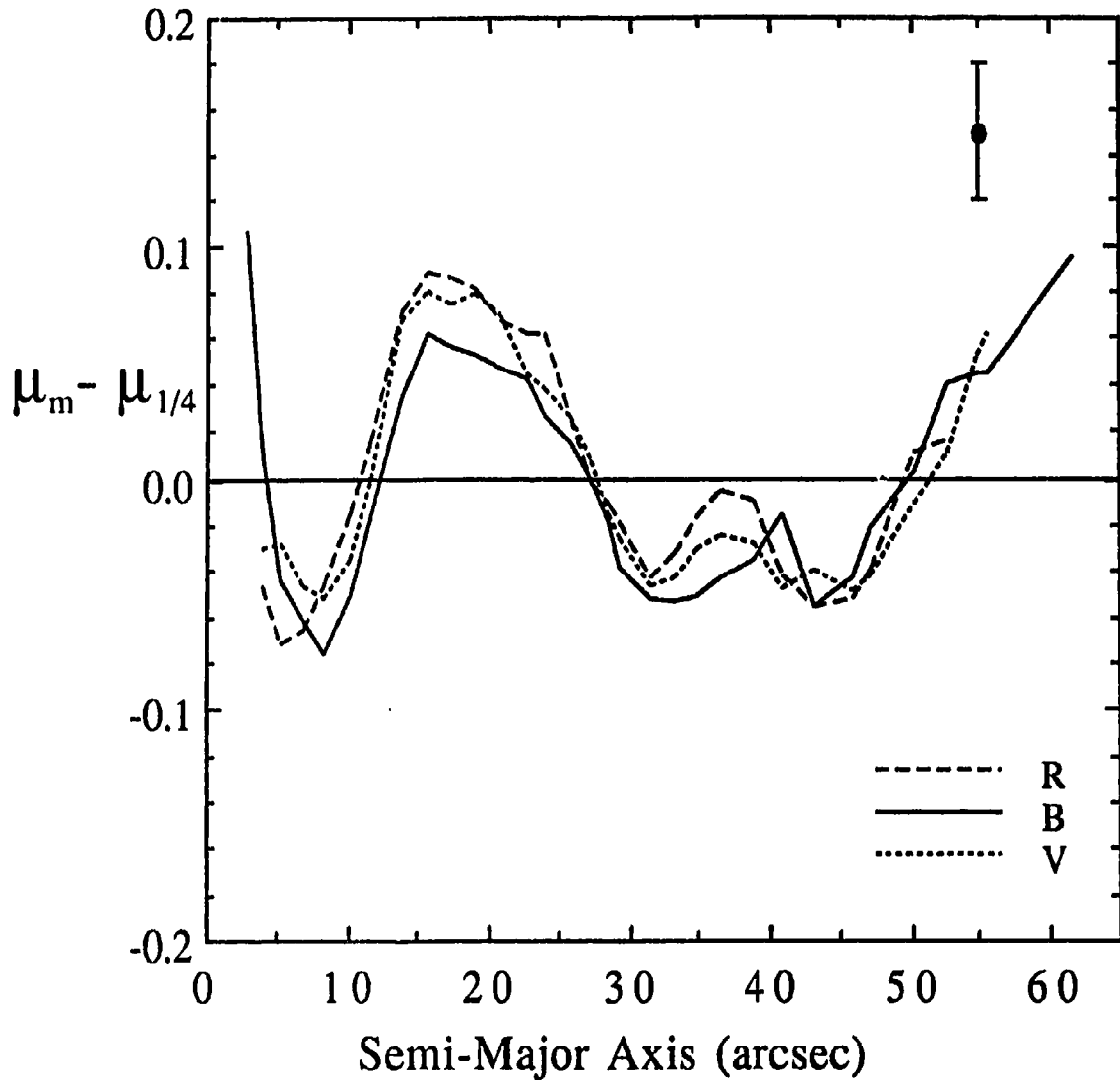


Figure IV - 1. Surface brightness residuals obtained by subtracting the best-fit  $r^{1/4}$  law,  $\mu_{1/4}$  (in mag arcsec<sup>-2</sup>), from the mean surface brightness profile,  $\mu_m$ , found in this study. Sections of the curve above the zero line indicate that the galaxy is brighter than the  $r^{1/4}$  law and vice versa. The length of the error bar represents twice the average rms difference from the mean between the four blue data frames.

In the innermost regions of the galaxy, where the ellipticity tends towards zero (circular isophotes) and where there are the fewest number of pixels to work with, the position angle of the best fit ellipse (Figure III - 2) is poorly defined. Therefore, we expect to see, and do see, a large amount of scatter in the value of the position angle for radial distances of less than  $\sim 5''$  from the centre of the galaxy. The position angle profile shows a rapid isophotal twist of about  $5^\circ - 10^\circ$  occurring over the range  $5'' - 10''$  from the galaxy centre. The greatest jump in position angle is seen in the blue passband with a slightly smaller jump ( $\sim 5^\circ$  smaller) occurring in the R passband. At a radial distance of  $\sim 10''$  the position angle is about  $160^\circ$  and begins to twist at a slower constant rate of about  $-0.25 \text{ arcsec}^{-1}$ . This appears to be independent of colour out to about  $40''$ , with a spread of less than  $5^\circ$ . This results in a  $10^\circ$  position angle twist over an interval of  $\sim 50''$ . However, beyond  $40''$  the position angle in the blue passband appears to twist slightly faster than in the other colours. This results in a position angle that is about  $5^\circ$  smaller in the blue at a radial distance of  $\sim 55''$ .

The normalized  $a_4$  components of the isophotes are shown in Figure III - 5, averaged between the four frames in each passband. In the range of about  $25''$  to  $35''$  from the galaxy centre, the  $a_4$  component reaches its furthest deviation from zero, reaching a value of about  $+1$  percent in all passbands. This very small rise (less than  $2\sigma$ ) in  $a_4$  is also seen in Jedrzejewski's R and B data at the same radial position and size, and suggests the presence of a weak disk in NGC 2865. The possible presence of a disk in NGC 2865, together with the  $100\mu\text{m}$  flux detected by *IRAS* indicating the presence of dust, may point to this galaxy being more like an S0 galaxy than an elliptical galaxy.

If the disk is real, it would be contrary to the suggestion by Nieto and Bender (1989) that a merger process leads to a high velocity dispersion in the parent galaxy which in turn produces boxy isophotes. This is because they find that a violent merger is likely to completely destroy a disk that may already be present in the parent galaxy. The results found here in this study suggest that boxy isophotes may not be an inevitable outcome of a merger process. Indeed, accreted material captured by a parent galaxy should continue to trickle in long after the merger process is complete (Kormendy and Djorgovski 1989). Enough material may be accreted to form an observable disk which would change the galaxy's morphological type resulting in secular evolution by accretion.

As illustrated in Figures III - 2, 3, and 5, the isophotes of NGC 2865 undergo large changes in both orientation and shape with radial position. Although seeing and sampling effects are likely to become important within  $\sim 5''$  of the galaxy centre, the overall trends would not be altered significantly. The significant twisting observed in the isophotal position angle ( $10^\circ - 15^\circ$  total, or  $15^\circ - 20^\circ$  per decade in radius) supports the idea that this galaxy may be triaxial and not just a simple oblate spheroid. However, isophotal twists can also reflect tidal disturbances due to a nearby companion galaxy as well as equilibrium structure. Although NGC 2865 is relatively isolated, the fact that a system of shells is present, together with its jet-like feature, strongly suggest that tidal forces are indeed at work, perhaps from a recent merger. If the tidal forces producing the shells are too weak to disturb the main body of the galaxy, then the observed isophotal twist would support the theory of a triaxial shape.

#### *d) Galaxy Colours and Their Gradients*

A comparison between this galaxy's colours and the mean colours of elliptical and S0 galaxies can be made using the results found by Visvanathan and Sandage (1977) and Sandage and Visvanathan (1987a,b). These authors present mean extinction-free colours for a sample (~50 - 100) of galaxies they observed. They measured integrated galaxy colours with an aperture half the size of the reduced galaxy diameter  $D(0)$  (taken from de Vaucouleurs and de Vaucouleurs [1964]) which is  $29''.8$  for NGC 2865. The integrated colours of NGC 2865, for a diameter of  $55''$  (an aperture about 1.85 times larger), can be found from the contour integrations used in section II(h). From Section II(h), the  $(B - V)$  and the transformed  $(B - R)_J$  observed colours of the main body of the galaxy were  $0^m.90$  and  $1^m.69$ , respectively.

In order to compare our observed colours of NGC 2865 with the mean extinction-free colours derived by Sandage and Visvanathan, the reddening corrections that they applied to NGC 2865 will be applied to the colours found in this study. They used  $(B - V)$  and  $(B - R)$  extinctions of  $0^m.13$  and  $0^m.20$ , respectively, which transforms our observed colours to  $0^m.77$  and  $1^m.49$ , respectively. Compared with a mean  $(B - V)$  colour of about  $0^m.86 \pm 0^m.10$  for field elliptical and S0 galaxies found by Sandage and Visvanathan, NGC 2865 appears about  $0^m.1$  bluer. A mean  $(B - R)_J$  colour of  $1^m.71 \pm 0^m.12$  found for a mixture of field and cluster elliptical/S0 galaxies indicates that NGC 2865 is again bluer by about  $0^m.2$ . This may be the result of NGC 2865 accreting a small bluer disk galaxy.

Colour gradients are common in elliptical galaxies (Jedrzejewski 1987, Franx *et al.* 1989), and NGC 2865 is no exception. As noted before, the

galaxy shows a mean (B - V) gradient of  $-0.065 \pm 0.009$  per decade in radius, with the mean (B - R) gradient being  $-0.139 \pm 0.014$  per decade in radius. Although the images of the galaxy show no clear signature of absorption by dust, the detection of  $100\mu\text{m}$  emission by *IRAS* suggests that the observed colour gradient may, in part, be caused by dust absorption. This would require, however, that the dust column density decreases slowly with radius, which is generally thought to be unlikely. It is therefore believed that these gradients are produced primarily by general metallicity and/or age gradients within the galaxy.

The mean (B - R) gradient found for NGC 2865 appears to be relatively large. It is about a factor of two greater than the mean gradient of  $-0.07 \pm 0.05$  per decade in radius found by Franx *et al.* (1989) in their sample of 17 elliptical galaxies. This steeper colour gradient causes NGC 2865 to appear more like the bulges of spiral galaxies (Wirth 1981, Wirth and Shaw 1983).

It is well known that the strengths of metal absorption lines also show radial gradients in elliptical galaxies (Gorgas and Efstathiou 1987, Davies and Sadler 1987). This trend is in the sense that weaker metal absorption lines are seen further from the galaxy centre. It is likely, then, that such colour gradients reflect metallicity and/or metallicity-driven population changes. A mean metallicity gradient can be estimated by using the colour-metallicity relation found by Arimoto and Yoshii (1987). They computed the chemical and photometric properties of model elliptical galaxies using evolutionary population synthesis. Based on their standard model results, one finds the following colour/metallicity gradients:

$$\frac{\Delta(B-V)}{\Delta\log(Z)} = 0^m211 \pm 0^m015 \text{ per decade change in metallicity,}$$

$$\frac{\Delta(B-R)}{\Delta\log(Z)} = 0^m385 \pm 0^m032 \text{ per decade change in metallicity,}$$

where Z is the mass fraction of all elements heavier than helium. Based on the mean (B - V) and (B - R) colour gradients measured in NGC 2865, the mean metallicity gradients, per decade change in radius, are estimated to be:

$$\frac{\Delta\log(Z)}{\Delta\log(r)} = -0.31 \pm 0.06, \text{ using (B - V),}$$

$$\frac{\Delta\log(Z)}{\Delta\log(r)} = -0.40 \pm 0.07, \text{ using (B - R),}$$

where a factor of 1.12 was applied to the (B - R) gradient to transform it to the Johnson system. Both estimates are very similar, indicating about a factor of two change in metallicity per decade in radius in the sense that the outer parts of the galaxy have a lower metallicity.

## V. SUMMARY AND CONCLUSIONS

A total of twelve B, V, and R CCD images of the shell galaxy NGC 2865 were obtained using the 1-metre Swope Telescope at the Cerro Las Campanas Observatory of the Carnegie Institution of Washington. These images were independently calibrated for the Johnson B and V, and Cousins R systems using standard star images taken during the same night on which the galaxy was observed. Isophotometry was performed by fitting ellipses by the method of least-squares to the observed isophotal contours to produce ellipticity and position angle profiles as functions of the semi-major axis length. Mean intensities of the isophotes were assigned by sampling the original image along the best-fit ellipses. Departures from perfect ellipticity were expressed in terms of a normalized  $\cos(4\theta)$  amplitude ( $a_4$  term) derived from a Fourier decomposition of the isophote/best-fit ellipse residuals. Mean values for each parameter in each passband were obtained by interpolating the values derived from each of four frames to one set of semi-major axes. The derived parameters for NGC 2865 are summarized in Table V - 1.

NGC 2865 is one of several elliptical galaxies having low surface brightness shells systems (see Figure I - 1) which are thought to result from a destructive merger with a small disk galaxy. In addition, the galaxy also possesses a faint diffuse loop and a jet-like structure, both of which may suggest a recent tidal interaction. Despite these features, NGC 2865 has two properties, at least in its main body, that are characteristic of a normal elliptical or S0 galaxy.

First, the structural parameters obtained from the de Vaucouleurs surface brightness relation indicate that the main body of NGC 2865 follows the pro-

Table V - 1. Characteristics of NGC 2865 Derived in this Study.

$$M_B = -20^m64 \pm 0^m06 \text{ (assuming } H_0 = 50 \text{ km}\cdot\text{sec}^{-1}\cdot\text{Mpc}^{-1}\text{)}$$

$$\text{Luminosity} = 2.8 \times 10^{10} \cdot L_\odot$$

$$\text{Total Mass} = 3 \times 10^{11} \cdot M_\odot \text{ (assuming } M/L = 10 M_\odot/L_\odot\text{)}$$

$$(B - V) = 0^m90 \pm 0^m03$$

$$(B_J - R_C) = 1^m45 \pm 0^m03$$

$$\mu_o(B) = 22^m35 \pm 0^m05 \cdot \text{arcsec}^{-2}, \quad r_o(B) = 23''4 \pm 0''6$$

$$\mu_o(V) = 21^m42 \pm 0^m05 \cdot \text{arcsec}^{-2}, \quad r_o(V) = 22''8 \pm 0''6$$

$$\mu_o(R) = 20^m79 \pm 0^m06 \cdot \text{arcsec}^{-2}, \quad r_o(R) = 21''9 \pm 0''6$$

$$\frac{\Delta(B-V)}{\Delta \log(r)} = -0^m065 \pm 0^m009,$$

$$\frac{\Delta(B-R)}{\Delta \log(r)} = -0^m139 \pm 0^m014,$$

$$\frac{\Delta \epsilon}{\Delta \log(r)} = \begin{array}{ccc} -0.194 \pm 0.011 & -0.183 \pm 0.009 & -0.152 \pm 0.008 \\ (B) & (V) & (R) \end{array}$$

$$\frac{\Delta \Theta}{\Delta \log(r)} = \begin{array}{ccc} -19^{\circ}2 \pm 1^{\circ}5 & -14^{\circ}9 \pm 1^{\circ}1 & -14^{\circ}8 \pm 1^{\circ}0 \\ (B) & (V) & (R) \end{array}$$

file of a normal elliptical galaxy. Its surface brightness follows closely an  $r^{1/4}$  law to within  $\pm 0.1 \text{ arcsec}^{-2}$  ( $\pm 9\%$  in intensity) in all three passbands over a radial distance of about  $5'' - 60''$ . Small deviations from the  $r^{1/4}$  law are believed to be caused by the contributions of the shells. In addition, the derived values of  $B_0(V)$  and  $r_0(B)$  satisfy the relation given by Kormendy for elliptical galaxies. The observed twisting of its isophotes suggests a triaxial shape, supporting the idea that elliptical galaxies, in general, are triaxial.

Secondly, NGC 2865 is observed to have a radial colour gradient, in the sense that the galaxy becomes bluer with increasing radial distance, a common feature of elliptical galaxies. However, the observed colour gradient is roughly twice as large as is typically seen in elliptical galaxies, and in this respect the galaxy appears similar to the bulges of spiral galaxies. By interpreting this colour gradient as a change in metallicity, one finds the metallicity decreasing by about a factor of two per decade increase in radius.

The excess  $100\mu\text{m}$  flux observed in NGC 2865 indicates the presence of dust and it suggests that this galaxy is more like an S0, rather than an elliptical, galaxy. Both the results of Jedrzejewski (1987) and those found in this study indicate a weak edge-on disk oriented along the major axis of the galaxy. However, the magnitude ( $\sim 1\%$ ) of the  $a_4$  component measured in this study used to infer the existence of the disk is only about  $2\sigma$  above the estimated uncertainty in the measurement ( $\pm 0.6\%$ ). Therefore, the existence of the disk is uncertain, but if it proves to be real it would confirm the S0 classification for the galaxy.

The strongest piece of evidence that suggests NGC 2865 has undergone a recent merger is the distinct shell system surrounding the galaxy, and the jet-

like structure emanating from it (see Figure I - 1). This idea is further supported by the observed (B - V) and (B - R) colours for the main body of NGC 2865, which are slightly bluer than the colours of typical elliptical galaxies. Sandage and Visvanathan (1978a, b) have measured a (U - B) colour for this galaxy that is also slightly bluer than the mean value found for elliptical and S0 galaxies. These bluer colours could arise if NGC 2865 accreted a small disk system.

However, if a weak disk does exist in NGC 2865, it would be contrary to the suggestion by Nieto and Bender (1989) that a merger process leads to boxy isophotes. One possible explanation for the presence of a disk in the parent galaxy after a merger is that the disk was formed from material donated by the accreted galaxy. Another explanation would be that the disk was already present in the parent galaxy before the merger occurred and has survived up to the present time. This would then imply that the accreted galaxy must have been small, compared to NGC 2865, so as not to have had a destructive effect on the disk. Since NGC 2865 shows strongly the signature of a merger process, it would appear that this galaxy is an example of where boxy isophotes are not an inevitable outcome of a merger process.

Using the available data about NGC 2865, one can construct a possible model for the hypothetical merger victim. A combination of the mean value of  $M_{\text{HI}}/L_{\text{B}} = 0.40$  (in solar units) for Sc galaxies estimated by Gallagher *et al.* (1975) and the mean value of  $M_{\text{Total}}/L_{\text{B}} = 4.7$  for Sbc-c galaxies estimated by Faber and Gallagher (1979) gives a ratio of  $M_{\text{HI}}/M_{\text{Total}}$  of about 0.09. From the same authors, the mean ratio of  $M_{\text{HI}}/M_{\text{Total}}$  turns out to be about 0.03 for Sab-bc galaxies. If we assume that all of the observed HI in NGC 2865 was donated by the merger victim, then one finds the total mass of the accreted

galaxy to be about  $4 \times 10^{10} M_{\odot}$  and  $1 \times 10^{10} M_{\odot}$  for victim Sbc-c and Sab-bc galaxies respectively. Compared to the estimated mass of the parent galaxy derived in section (a), the merger victim is about 8 to 30 times less massive. This corresponds to the high end of the range of mass ratios used in the N-body simulations of Quinn (1982,1984) and which resulted in shell structure. If we assume that most of the merger victim's mass went into forming the visible shells, then about 3 - 13% of the total mass should lie in the shell system. This agrees roughly with the lower estimate of 11% made by Fort *et al.* (1986) for the contribution of the shell system to the total mass in NGC 2865, and suggests that the merger victim may have indeed been an Sb or later type galaxy.

## REFERENCES

- Aragón, A., Gorgas, J., and Rego, M. 1987, *Astron. Astrophys.*, **185**, 97.
- Arimoto, N., and Yoshii, Y. 1987, *Astron. Astrophys.*, **173**, 23.
- Arp, H. C. 1966, *Astrophys. J. Suppl.*, **14**, 1.
- Binggeli, B. 1987, In *Nearly Normal Galaxies*, edited by S. M. Faber, p. 195. (New York:Springer-Verlag).
- Burstein, D., Faber, S. M., Gaskell, C. M., and Krumm, N. 1984, *Astrophys. J.*, **287**, 586.
- Carter, D. 1987, *Astrophys. J.*, **312**, 514.
- Carter, D., Allen, D. A., and Malin, D. F. 1982, *Nature*, **295**, 126.
- Carter, D., and Wellington, K. J. 1987, unpublished.
- Davies, R. L., and Sadler, E. M. 1987, In *Structure and Dynamics of Elliptical Galaxies*, IAU Symposium No. 127, edited by T. de Zeeuw (Reidel, Dordrecht), p.441.
- Davis, L. E., Cawson, M., Davies, R. L., and Illingworth, G. 1985, *Astron. J.*, **90**, 169.
- de Vaucouleurs, G. 1977, In *The Evolution of Galaxies and Stellar Populations*, Edited by B. M. Tinsley and R. B. Larson, (New Haven: Yale University Observatory).
- de Vaucouleurs, G., de Vaucouleurs, A., and Corwin, H. G. 1976. *Second Reference Catalogue of Bright Galaxies* (Austin: University of Texas Press).
- Dupraz, C., and Combes, F. 1985, In *New Aspects of Galaxy Photometry*, edited by J.-L. Nieto, (New York:Springer-Verlag), p.151.
- Dupraz, C., and Combes, F. 1986, *Astron. Astrophys.*, **166**, 53.

- Faber, S. M., and Gallagher, J. S. 1979, *Annu. Rev. Astron. Astrophys.*, **17**, 135.
- Fabian, A. C., Nulsen, P. E. J., and Stewart, G. C. 1980, *Nature*, **287**, 613.
- Fort, B. P., and Prieur, J.-L., Carter, D., Meatheringham, S. J., and Vigroux, L. 1986, *Astrophys. J.*, **306**, 110.
- Franx, M., Illingworth, G., and Heckman, T. 1989, *Astron. J.*, **98**, 538.
- Gallagher, J. S., Faber, S. M., and Balick, B. 1975, *Astrophys. J.*, **202**, 7.
- Gorgas, J., and Efstathiou, G. 1987, In *Structure and Dynamics of Elliptical Galaxies*, IAU Symposium No. 127, edited by T. de Zeeuw (Reidel, Dordrecht), p.189.
- Hernquist, L., and Quinn, P. 1986. Preprint.
- Hernquist, L., and Quinn, P. 1987a, *Astrophys. J.*, **312**, 1.
- Hernquist, L., and Quinn, P. 1987b. *Astrophys. J.*, **312**, 17.
- Huchtmeier, W. K., and Richter, O.-G. 1989, *A General Catalog of HI Observations of Galaxies*, (Springer-Verlag).
- Jacoby, S. L. S., Kowalik, J. S., and Pizzo, J. T. 1972, *Iterative Methods for Nonlinear Optimization Problems*, (Englewood Cliffs, N.J.: Prentice-Hall).
- Jedrzejewski, R. I. 1987, *Mon. Not. R. Astr. Soc.*, **226**, 747.
- Kormendy, J. 1982 *Morphology and Dynamics of Galaxies*, 12<sup>th</sup> Advanced Course of the Swiss Society of Astronomy and Astrophysics, edited by L. Martinet and M. Meyor. p.115.
- Kormendy, J. 1985, *Astrophys. J.*, **295**, 73.
- Kormendy, J., and Djorgovski, S. 1989, *Annu. Rev. Astron. Astrophys.*, **27**, 235.
- Kundt, W., and Krause, M. 1985, *Astron. and Astrophys.* **142**, 150.

- Landolt, A. U. 1973, *Astron. J.*, **78**, 959.
- Landolt, A. U. 1983, *Astron. J.*, **88**, 439.
- Malin, D. F. 1977, *Am. Astron. Soc. Photo. Bull.*, **16**, 10.
- Malin, D. F. 1978, *Nature*, **276**, 591.
- Malin, D. F., and Carter, D. 1980, *Nature*, **285**, 643.
- Malin, D. F., and Carter, D. 1981, *Nature*, **285**, 643.
- Malin, D. F., and Carter, D. 1983, *Astrophys. J.*, **274**, 534.
- Nieto, J.-L., and Bender, R. 1989, *Astron. and Astrophys.*, **215**, 266.
- O'Connell, R. W. 1986. In *Stellar Populations*, edited by C. A. Norman, A. Renzini, and M. Tosi (Cambridge University Press), p. 167.
- Okamura, S. 1988, *Publ. Astron. Soc. Pac.*, **100**, 524.
- Quinn, P. J. 1982, Ph.D. thesis. Aust. Natl. Univ., Canberra.
- Quinn, P. J. 1984, *Astrophys. J.*, **279**, 596.
- Sandage, A., and Visvanathan, N. 1978a, *Astrophys. J.*, **223**, 707.
- Sandage, A., and Visvanathan, N. 1978b, *Astrophys. J.*, **225**, 742.
- Schweizer, F. 1983, in *IAU Symposium 100, Internal Kinematics and Dynamics of Galaxies*, edited by E. Athanassoula (Dordrecht: Reidel), p. 347.
- Stetson, P. B., 1987, *Pub. Astr. Soc. Pac.*, **99**, 191.
- Thronson, H. A., Bally, J., and Hacking, P. 1989, *Astron. J.*, **97**, 363.
- Visvanathan, N., and Sandage, A. 1977, *Astrophys. J.*, **216**, 214.
- Vorontsov-Velyaminov, B. A. 1959, *Atlas and Catalog of Interacting Galaxies* (Sternberg State Astronomical Institute, Moscow).
- Wilkinson, A., Browne, I. W. A., Kotanyi, C., Christiansen, W. A., Williams, R., and Sparks, W. B. 1987, *Mon. Not. R. Astr. Soc.*, **224**, 895.
- Williams, R. E., and Christiansen, W. A. 1984, Preprint (ESO No. 322).

Wirth, A. 1981, *Astron. J.*, **86**, 981.

Wirth, A., and Shaw, R. 1983, *Astron. J.*, **88**, 171.

## Curriculum Vitae

Name: David Lee Wing  
Birthplace: Edmonton, Alberta  
Birthday: 23 September 1959

Education: Vancouver Community College, Langara Campus,  
Vancouver, British Columbia.  
Photographic Technician Diploma 1979

University of British Columbia,  
Vancouver, British Columbia.  
B.Sc. (Astronomy) 1988  
"Some Dynamical Properties of M71"

Saint Mary's University,  
Halifax, Nova Scotia.  
M.Sc. (Astronomy) 1990  
"Surface Photometry of the Shell Galaxy NGC 2865"

University of Waterloo, Waterloo Campus,  
Waterloo, Ontario.  
1990 -

Experience: Laboratory Demonstrator,  
Department of Astronomy,  
Saint Mary's University.  
1988 - 1989

Laboratory Demonstrator,  
Department of Physics,  
Saint Mary's University.  
1989 - 1990

Presented Papers: "Surface Photometry of the Shell Galaxy NGC 2865",  
David L. Wing and Gary A. Welch, presented at the 21<sup>st</sup>  
Annual Meeting of the Canadian Astronomical Society -  
Calgary, Alberta 1990.